# UNIVERSITÀ DEGLI STUDI DI ROMA "TOR VERGATA"

FACOLTA' DI INGEGNERIA

DOTTORATO DI RICERCA IN
MATERIALI PER L'AMBIENTE E L'ENERGIA

CICLO DEL CORSO DI DOTTORATO XIX

# PREPARATION AND CHARACTERIZATION OF CERIA AND DOPED CERIA VIA METAL ORGANIC COMPLEX METHOD FOR SOLID OXIDE FUEL CELL ELECTROLYTE MATERIALS

Chatchai Veranitisagul

A.A. 2008/2009

Tutor: Prof. Enrico Traversa

Co-Tutor: Prof. Apirat Laobuthee

Coordinatore: Prof. Enrico Traversa

## ACKNOWLEDGEMENTS

The author would like to thank his supervisor, Professor Enrico Traversa, who gave him intensive recommendation, constructive criticism, suggestions, constant encouragement, inspiration, and the opportunity to study and have more experiences in Italy.

He is deeply indebted to Assistant Professor Apirat Laobuthee and Assistant Professor Nattamon Koonsaeng who gave valuable advice and discussion on the research including a partial financial support during carrying out the experiments in Thailand.

A deep gratitude is expressed to Association Professor Sutin Kuharuangrong (School of Ceramic Engineering, Suranaree University of Technology), Dr. Sumittra Charojrochkul, and Dr. Pimpa Limthongkul (National Metal and Materials Technology Center (MTEC)) for the fruitful discussion and helps in impedance spectroscopy measurements. His deep gratitude is also extended to Assistant Professor Duangrudee Chaysuwan (Department of Materials Engineering, Faculty of Engineering, Kasetsart University) for using the high temperature furnace.

He wants to express appreciation to Association Professor Vanida Bhavakul (King Mongkut's University of Technology Thonburi), Assistance Professor Hathaikarn Manuspiya (The Petroleum and Petrochemical College, Chulalongkorn University), Assistance Professor Bussarin Ksapabutr (Faculty of Engineering and Industrial Technology, Silpakorn University), and Dr. Harittapak Kiratisaevee (Faculty of Science and Technology, Kanchanaburi Rajabhat University) for the valuable time in discussion and suggestions. He would like to thank Dr. Nungruethai Yoswathananont (Osaka Prefecture University) and Dr. Amornrat Lertworasirikul (Department of Materials Engineering, Faculty of Engineering, Kasetsart University) for the valuable time during his stay at Kasetsart University.

He would like to acknowledge Mettler-Toledo (Thailand) Limited for TGA/SDTA analysis, Thailand Institute of Scientific and Technological Research (TISTR) for Cold Isostatic Pressure (CIP) machine, and Thailand Institute of Nuclear Technology (TINT) for XRD analysis.

He wishes to express his gratitude to Ms. Wannee Srinutrakul (Thailand Institute of Nuclear Technology (TINT)) for BET measurement.

He would like to thank all Professors and friends at University of Rome “Tor Vergata” for giving him helps, good time and good memories during his stay in Italy.

Special thanks are due to Mr. Thamrong Rakthin, Mr. Attaphon Kaewvilai, Mr. Sarawut Sangngirn, and Mr. Sarute Ummartyothin, for giving him helps, good time and good memories during his stay at Kasetsart University.

Finally he wishes to express his gratitude to his family for their love, understanding, encouragement, limitless sacrifice, and for being a constant source of his inspiration.

# TABLE OF CONTENTS

# LIST OF TABLES

# LIST OF FIGURES

# CHAPTER I
# INTRODUCTION

Fuel cells are electrochemical devices that can produce electric current via redox reactions by directly transforming chemical energy into electrical energy. Therefore, this is an alternative way to produce energy with less environmental impact compared to fossil fuel combustion, if hydrogen produced from renewable sources is used as the fuel.

A fuel cell consists of 3 main elements: cathode, anode, and electrolyte. The electrolyte is placed between the two electrodes. Fuel cells can be operated by feeding hydrogen gas as fuel to the anode side and oxygen as oxidant to the cathode side. Hydrogen at the anode is ionized to proton and electron. Protons pass through the electrolyte to the cathode and react with oxygen, while electrons flow through an external circuit to react with oxygen gas to obtain water at the cathode.

Comparing between fuel cells and batteries, fuel cells cannot store the current but enable continuous electricity production whenever the reactants are fed to the electrodes. Among the various types of fuel cells, solid oxide fuel cells (SOFCs) show the best efficiency for electricity production. Therefore, many scientists are investigating SOFCs as the source for electrical current production for the future.

Yttria stabilized zirconia (YSZ) is the state-of-the-art electrolyte for SOFCs. However, one of the disadvantages of YSZ is the need for high operating temperatures (~1000˚C). Recently, alternative electrolyte materials to operate SOFCs in the intermediate temperature range (600-800˚C) are intensively investigated. Ceria based electrolytes, such as gadolinia doped ceria (GDC) and samaria doped ceria (SDC), are interesting candidates because they exhibit higher ionic conductivity at lower temperature with respect to YSZ.

There are many routes to prepare ceria based solid solutions, such as solid solid reaction, co-precipitation of hydroxides, and sol-gel formation. However, these methods show several disadvantages, such as high cost of the starting materials, presence of impurities, and high reaction temperatures. Recently, the oxide one pot synthesis (OOPS) process has been developed to synthesize magnesium aluminate spinel. This method shows various advantages, such as simple and straight-forward synthesis, and provides high purity products. Thus, aim of this work is the synthesis of doped ceria using the same procedure as the OOPS process.

It is well-known that the OOPS process requires high reaction temperature because the reaction proceeds in ethylene glycol as a solvent for the oxide compound reactants. To solve this problem, in this research work, we modified the OOPS process to prepare ceria based solid solutions. The metal organic complex used as precursor was synthesized from metal salts, such as nitrate and chloride salts, instead of oxide compounds. In addition, low boiling point solvents, such as methanol, ethanol, and n-propanol, were used to reduce the reaction temperature.

This work is divided into four chapters. The first chapter deals with the synthesis of cerium metal organic complex from cerium nitrate and triethanolamine in n-propanol as a solvent. The complex structure was analyzed by FTIR and MS. The complex was calcined to obtain cerium oxide powders. The thermal property of the complexes was studied by TG/DTA analysis. The phase identification of the complexes and the calcined powders was performed using XRD. The morphology of the calcined powders was examined by SEM and BET. Chapters 2 and 3 deal with the preparation from nitrate salts of gadolinia doped ceria and samaria doped ceria, respectively, using the same approach considering the results obtained in chapter 1. The thermal property, phase identification, and morphology of the calcined powders were examined. Moreover, the ionic conductivities of these powders were characterized by AC impedance spectroscopy measurements. In chapter 4, gadolinia doped ceria was prepared from chloride salts instead of nitrates. The powder products were studied using the same procedures described in the chapter 2.

# CHAPTER II
# LITERATURE REVIEW

## 2.1 Basic Principle of Fuel Cells

Fuel cells are electrochemical devices converting chemical energy directly into electricity, heat, and water. The fuel cell basic construction is composed of an electrolyte layer in contact with porous electrodes; an anode and a cathode, on either sides. A schematic representation of a fuel cell with the reactant/product gases and the ion conduction flow directions through the cell is shown in Figure 2.1

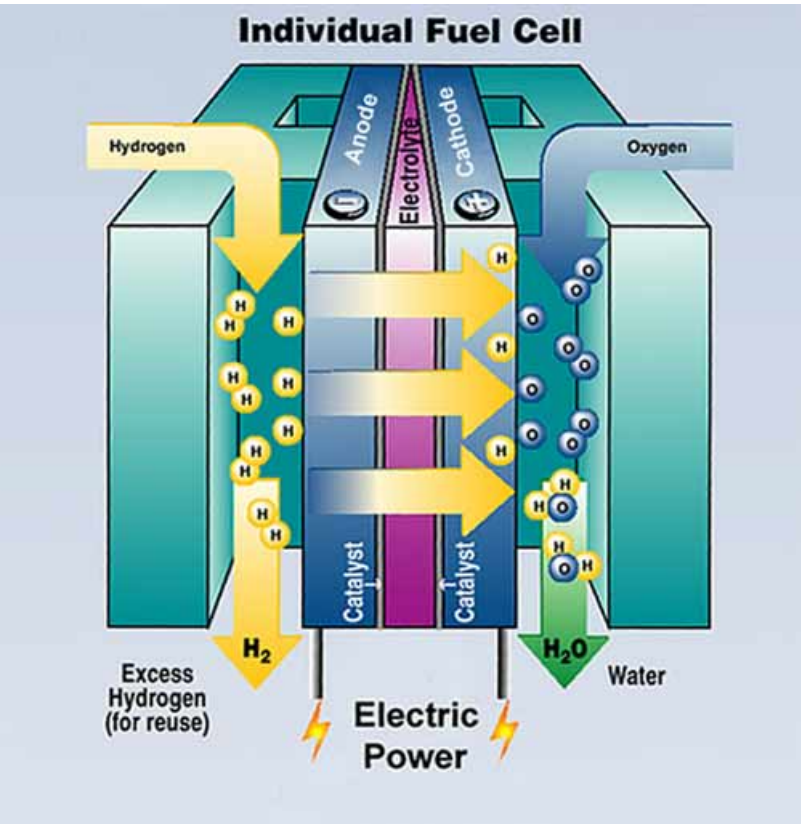


Figure 2.1 The principle and components of a fuel cell.
Taken from http://www.greenjobs.com/Public/images/fuel-cell.jpg

In a simple fuel cell, fuel (i.e. $H_2$ gas) is continuously fed to the anode (negative electrode) while an oxidant (i.e., oxygen from air) is continuously fed to the cathode (positive electrode). The electrochemical reactions occur at both electrodes and produce an electric current. Although a fuel cell has components and characteristics similar to those of a battery, several aspects make it still different from

a battery. A battery is an energy storage device. The maximum available energy depends on the amount of chemical reactants stored inside the battery itself. The battery can produce electrical energy until the chemical reactants are consumed. In a secondary battery, the reactants can be recharged by putting energy into the battery from an external source, reversing its polarity. On the other hand, a fuel cell is an energy conversion device producing electrical energy as long as fuel and oxidant are supplied to anode, and cathode, respectively. In fact, the practical operating life of fuel cells is limited by degradation, primarily corrosion, or component malfunctions.

Generally, fuel cells provide low to zero-emission power sources for various applications, such as stationary power generation systems, spacecraft, automobiles, and small electronic devices. The concerns about pollution in environment are the main factor that has influenced the fuel cell development. Because of high cost of the materials used in fuel cells, fuel cells are still not available for commercialization.

In 1839, Sir William Grove firstly reported the principles of the fuel cell operation. A $H_2/O_2$ fuel cell in acid electrolytes was demonstrated. Dilute sulfuric acid was used as the electrolyte in the fuel cell. His cell can be operated at room temperature. Fifty years later, in 1889, L. Moud and C. Langer invented the fuel cell by scaling up cell area to 700 $cm^2$, used Pt foil and platinum black electrode and sulfuric acid as electrolyte. From this origin, fuel cells are developed until present.

### 2.1.1 Classification of fuel cells

Fuel cells can be classified into different ways depending on the combination of type of fuel and oxidant, whether the fuel processed outside or inside the fuel cell, the type of electrolyte, the operation temperature, whether the reactants are fed to the cell by internal or external manifold. Typically, fuel cells are classified into 5 types based on the electrolyte and its operating temperature. There are alkaline fuel cell (AFC), phosphoric acid fuel cell (PAFC), polymer electrolyte membrane fuel cell (PEMFC), molten carbonate fuel cell (MCFC), and solid oxide fuel cell (SOFC). An overview of the fuel cell types is given in Table 2.1.

Table 2.1 Characteristics of different types of fuel cell.

| Types of fuel cell | Fuel | Charge carrier in the electrolyte | T (˚C) | Efficiency (%) | Applications | Advantages | Disadvantage |
|---|---|---|---|---|---|---|---|
| AFC | $H_2$ | $OH^-$ | 50-90 | 50-70 | Space application | High efficiency | Intolerant to $CO_2$ in impure $H_2$ and air, corrosion, expensive |
| PAFC | $H_2$ | $H^+$ | 175-220 | 40-45 | Stand alone and combined heat and power | Tolerant to impure $H_2$, commercial | Low power density, corrosion and sulfur poisoning |
| PEMFC | $H_2$ | $H^+$ | 60-100 | 40-50 | Vehicle and portable | High power density, low temperature | Intolerant to $CO_2$ in impure $H_2$ and expensive |
| MCFC | $H_2$, $CH_4$, CO | $CO_3^{2-}$ | 600-650 | 50-60 | Stand alone and combined heat and power | High efficiency, near commercial | Electrolyte instability, corrosion, and sulfur poisoning |
| SOFC | $H_2$, $CH_4$, CO | $O^{2-}$ | 800-1000 | 50-60 | Stand alone and combined heat and power | Highest efficiency and direct fossil fuel | High temperature, thermal stress failure, coking, and sulfur poisoning |

## 2.2 Solid Oxide Fuel Cells (SOFCs)

SOFCs show several advantages as compared to other types of fuel cell. For instance, all solid materials are used avoiding corrosion problems. Moreover, SOFCs require high operating temperature at 800-1000˚C, and this allows to obtain high energy conversion efficiency and the waste heat can be used for co-generation systems. The high operating temperature allows also fuel flexibility, and the use of low cost catalysts for electrode. High operating temperature is, however, a limitation for the material selection for anode, cathode and electrolyte due to thermal expansion mismatch and chemical incompatibility of each component. For these reasons, there are many scientists attempting to improve SOFC materials to operate at reduced temperatures.

### 2.2.1 Fundamental operation of SOFCs

Similar to other types of fuel cells, in SOFCs two electrochemical reactions (oxidation and reduction) take place. An oxidant gas (air, $O_2$) is reduced at the cathode and a fuel gas ($H_2$ or CO) is oxidized at the anode. The oxygen ions generated at the cathode can pass through the solid electrolyte to react with hydrogen or carbon monoxide at the anode to produce water vapor or $CO_2$. The electrons produced at the anode flow through the external circuit to maintain charge balance and consequently generate a direct current.

The reaction at the cathode is: $\frac{1}{2} O_2 + 2e^- \longrightarrow O^{2-}$

The reaction at the anode is: $H_2 + O_2^- \longrightarrow H_2O + 2e^-$

The overall reaction is: $H_2 + 1/2O_2 \longrightarrow H_2O$

Fundamental reactions in the solid oxide fuel cell are shown in Figure 2.2.

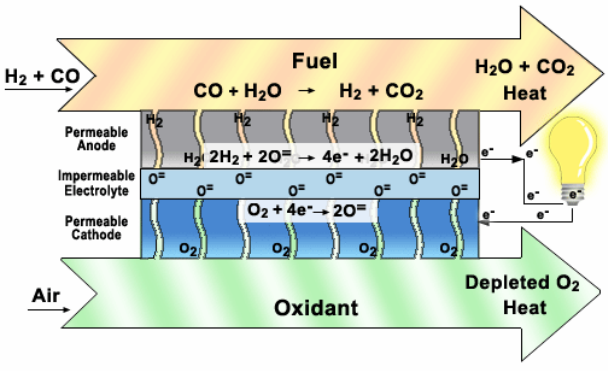


Figure 2.2 Basic operation of a solid oxide fuel cell.

Taken from http://science.nasa.gov/headlines/y2003/images/fuelcell/sofc-brochure-new.gif

2.2.2 Cell components and requirements

The principal components of a SOFC are cathode, anode, electrolyte, and interconnect. Each component must have the proper stability (chemical, phase, morphological and dimensional) in oxidizing and/or reducing atmosphere, chemical compatibility with other components, and sufficient conductivity. In addition, each component must have similar thermal expansion coefficient to avoid separation or cracking during fabrication and operation at high temperatures.

2.2.2.1 Cathode

The major function of the cathode is to provide the active sites for reduction of the oxidant. The cathode has to, therefore, operate in an oxidizing atmosphere. The requirements of the cathode are high electronic conductivity and also high ionic conductivity, chemical stability under the oxidizing atmosphere, sufficient catalytic activity for the oxidant gas reaction at the operating condition, chemical and thermal compatibility with the other components, sufficient porosity to allow air or oxygen gas transport to the reaction sites. The most common used cathode material is doped lanthanum manganite ($LaMnO_3$). Besides, there are other materials for operation at intermediate temperatures, such as doped $LaFeO_3$, doped $LaCoO_3$, and doped $PrMnO_3$. However, they exhibit some disadvantages such as thermal expansion mismatch with other components and insufficient conductivity.

2.2.2.2 Anode

The main function of the anode is to provide the active sites for oxidation of the fuel. The requirements of the anode are high electronic conductivity and also high ionic conductivity, chemical stability under reducing atmosphere, sufficient catalytic activity, chemical and thermal compatibility with the other components, tolerance of contaminants in fuel gas, and sufficient porosity to allow fuel gas transport. Due to the reducing conditions of the fuel, mostly metals can be used as the anode material, such as nickel. In general, nickel metal, a low cost material, is dispersed on the surface of the YSZ support to form a Ni-YSZ cermet to eliminate thermal mismatch with YSZ as an electrolyte and to maintain the porous structure. Recently, $CeO_2$ based materials have been also studied for intermediate temperature SOFC.

2.2.2.3 Electrolyte

The important function of the SOFC electrolyte is to conduct oxide ions between the anode and the cathode. Furthermore, the electrolyte has to separate the fuel from the oxidant in the fuel cell. The key requirements for the electrolyte in the

SOFC are adequate ionic conductivity in both reducing and oxidizing atmospheres, stable in both oxidizing and reducing atmospheres, chemically and thermally compatible with other components, dense to prevent gas cross leak and high strength.

At present, yttria stabilized zirconia (YSZ) is the typical material used as an electrolyte in SOFCs. Also, other materials have been developed, for example, doped $CeO_2$, $Bi_2O_3$, and perovskite type oxides.

2.2.2.4 Interconnect materials

The function of the SOFC interconnect is to join the anode of one cell to the cathode of the other cell. The requirements for material selection are stability in both reducing and oxidizing atmospheres, impermeability to gases, sufficient conductivity to support electron flow at the operating conditions, chemical and thermal compatibility with other components, and durability at high temperatures. The most appropriate materials are perovskite type ceramics based on $LaCrO_3$.

**2.3 Solid electrolytes**

The solid electrolyte in SOFC requires high ionic conductivity. The electrical conductivity as a function of temperature for conventional oxide ionic conductors is shown in Figure 2.3.

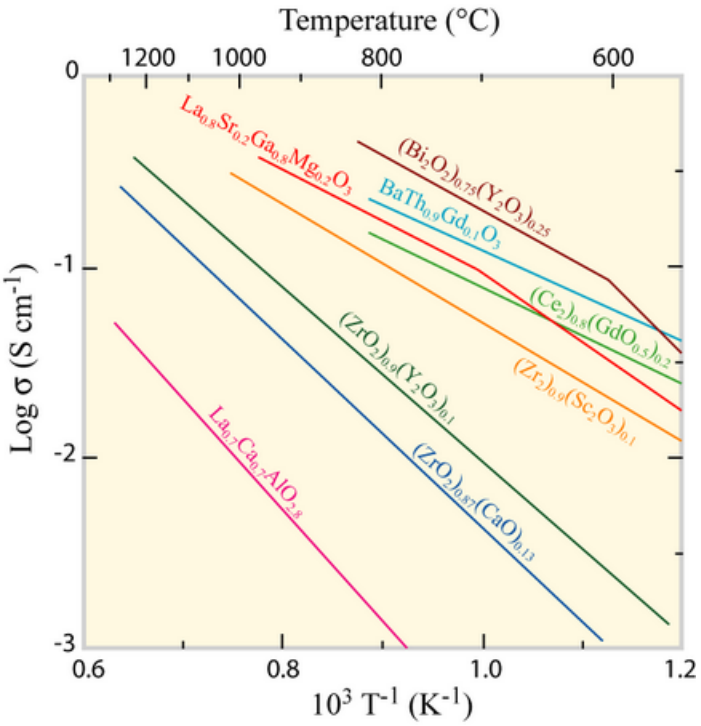


Figure 2.3 Solid electrolyte conductivity as a function of temperature. Taken from Steele, B.C.H.; and Heinzel A. Nature, 2001, 44, 345-352.

2.3.1 Zirconia based

Stabilized zirconia ($ZrO_2$), especially yttria stabilized zirconia, is extensively used as an electrolyte in SOFCs because this material has an adequate level of oxide ionic conductivity and shows the desirable stability in both oxidizing and reducing environments. In general, pure zirconia can not act as a good electrolyte because of its low ionic conductivity. At room temperature, zirconia has a monoclinic crystal structure. Above 1170˚C, the monoclinic structure changes to tetragonal structure. In addition, above 2370˚C, zirconia can be transformed into cubic fluorite structure. The tetragonal-monoclinic transformation is associated with a large volume change (3% to 5%) (contraction on heating and expansion on cooling). The cubic phase still exists up to the melting point at 2680˚C. However, the doping of certain aliovalent oxides stabilizes the cubic fluorite crystal structure of zirconia from room temperature to its melting point and simultaneously increases oxygen vacancy concentration. From

these reasons, the ionic conductivity can be enhanced, and the oxygen partial pressure range of ionic conduction can be extended, making stabilized zirconia suitable for use as an electrolyte in SOFCs. The most commonly dopants are CaO, MgO, $Y_2O_3$, $Sc_2O_3$, and certain rare earth oxides. These oxides have a relatively high solubility in zirconia and are stable to form the fluorite structure.

As shown in Figure 2.3, SOFCs based on zirconia electrolytes usually require high operating temperatures in the 800-1000˚C range, resulting in serious problems, such as chemical reaction between components, thermal degradation of materials or cracking during heating cycles, a short life of the cell, and expensive ceramic materials for interconnect. However, these problems can be solved by decreasing the operation temperature of SOFCs from 800-1000˚C to 600-800˚C. This can be obtained with YSZ electrolytes if they are manufactured having a thickness below 20 μm, therefore in film form. This solution provides the opportunity for iron based alloys (FE-Cr) for use as interconnect materials for intermediate temperature solid oxide fuel cells (IT-SOFCs).

### 2.3.2 Bismuth oxide based

At the intermediate temperature (600-800˚C), stabilized $Bi_2O_3$ exhibits higher ionic conductivity than any other oxide ion conductors. However, the main disadvantage of this material is the optimum conductivity obtained only in the short range of oxygen partial pressure. Below this range, it can be easily reduced and decomposes into bismuth metal; consequently, the ionic conductivity disappears.

### 2.3.3 Perovskite oxide based

Recently, there are many developments of other materials having adequate ionic conductivity at the intermediate temperature. Several doped perovskite oxides ($ABO_3$) can substitute YSZ as intermediate temperature solid electrolytes. Early researches have shown that $La_{1-x}Sr_xGa_{1-y}Mg_yO_{3-\delta}$ exhibited high ionic conductivity at 600-800˚C and was stable in a wide range of oxygen partial pressures.

## 2.4 Ceria based electrolytes

### 2.4.1 Ceria structure

Cerium oxide (ceria or $CeO_2$) has a fluorite type crystal structure. It has a face-centered cubic unit cell with space group Fm3m, (a=0.541134(12) nm, JCPDS 34-0394). Ceria is stable up to its melting point (2100˚C), has a large diffusion coefficient, and good corrosion resistance as comparing with other pure oxides which have oxygen ion conductivity. For this structure (Figure 2.4), each cerium cation is coordinated by eight equivalent nearest-neighbor oxygen anions at the corner of a cube while each anion is tetrahedrally coordinated by four cations.

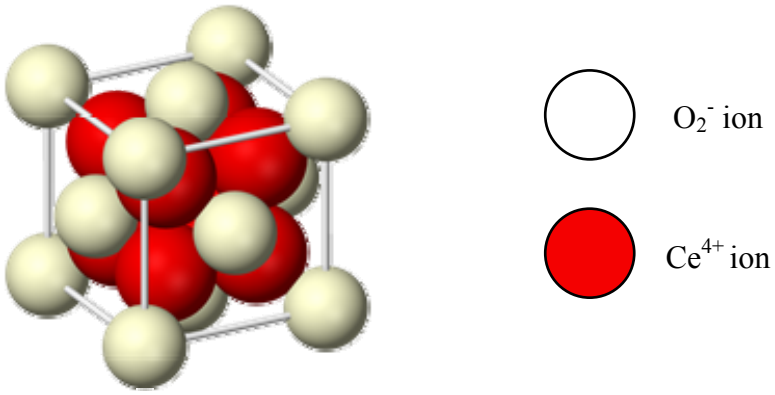


Figure 2.4 The fluorite crystal structure of $CeO_2$.
Taken from http://upload.wikimedia.org/wikipedia/commons/a/a4/Ceria-unit-cell-3D-ionic.png

Pure ceria is a mixed ionic electronic conductive material. However, the electronic conductivity of ceria can be significantly reduced upon the substitution of some trivalent cations, such as $Gd_2O_3$, $La_2O_3$, $Nd_2O_3$, $Sm_2O_3$, and $Yb_2O_3$. Ceria based electrolytes can be operated at 450-700˚C, demonstrating higher ionic conductivity than YSZ.

Although doped $CeO_2$ electrolytes has superior ionic conductivity to YSZ, their performance decreases at elevated operating temperature because of the electronic conductivity. The increase in electronic conductivity under low oxygen partial pressure (below $10^{-10}$ atm) at 800˚C is accompanied by a reduction of $Ce^{4+}$ to $Ce^{3+}$. The electronic conductivity can be neglected at temperature below 600˚C.

The electrical conductivity of doped ceria is influenced by several factors, such as the dopant ion, the dopant concentration, the oxygen vacancy concentration, and the defect association enthalpy.

2.4.2 Applications

Ceria and doped ceria powders have been considered as materials for applications in catalysts, fuel cells, ultraviolet absorbers, hydrogen storage materials, oxygen sensors, optical devices, and polishing materials or abrasive materials for chemical mechanical planarization (CMP).

## 2.5 Methods for ceria and doped ceria powder preparation

Synthesis and preparation methods have influenced some properties of ceria-based electrolyte materials, such as formed phase, particle size, surface area, catalytic activities, and oxygen storage capacity (OSC), etc. Thus, many methods have been carried out to develop the ceria-based materials with high catalytic activities, OSC, and thermal durability.

2.5.1 Solid to solid synthesis

2.5.1.1 Ceramic method or solid-state reaction

The oldest and the most typical method for preparing multi component material is a direct reaction of corresponding solid compounds at high temperatures, where reacting atoms can diffuse through solid phases to the reaction front more easily. Solid-state reactions are often very slow, and thus high temperatures are required to complete the reaction. This method is easy for the preparation of oxide materials, especially in polycrystalline powders on industrial scale.

Using small particles, cooling and regrinding of the samples, and ball-milling treatment often facilitate the solid-state reactions. These processes enhance blending and increase surface area of the reactant particles.

In the ceria based materials, the starting reactants usually used are oxides. Typically, the starting materials are mixed in an agate ball mills for several hours, as dry powders or as wet slurries using solvents (methanol). The mixed powders are subjected to repeated cycles of firing and grinding until a single phase is obtained. Temperature as high as 1800˚C might be necessary for firing.

2.5.1.2 Mechanical milling

The mechanical milling can be used for powder preparation. The obtained powders exhibit small crystallite size of a few nanometers with a high concentration of lattice defects. The mechanical milling has been used to prepare mixed oxides containing cerium oxide to enhance catalysis, for examples, $CeO_2$-$TbO_x$, $CeO_2$-$HfO_2$,

$CeO_2$-$ZrO_2$, $CeO_2$-$ZrO_2$-$MnO_x$, and $CeO_2$-$ZrO_2$-CuO.

The basic process is illustrated in Figure 2.5. The starting materials, usually oxide powders with surface area in the range of 10-50 $m^2 \cdot g^{-1}$, are placed in a high-energy vibratory ball mill in the stoichiometric amount to obtain $Ce_{1-x}M_xO_2$ ($0<x<0.9$). This mill is equipped with zirconia balls and vials made of stabilized-zirconia.

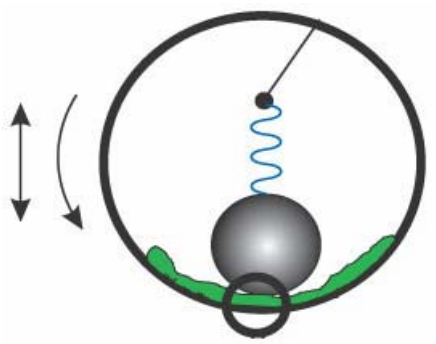

Figure 2.5 The basic mechanical milling process.
Taken from http://www.nature.com/physics/highlights/6903-2s.jpg

During the ball-milling, the particles are subjected to local high pressure and mechanical deformation during collisions with the zirconia balls. Long duration of ball milling results in formation of nanosized grains having dislocations with high density. This is a simple method for preparing $CeO_2$-based materials and the presence of structural defects in the mixed oxides promotes the increase in the oxygen strorage capacity.

2.5.2 Liquid to solid synthesis

The solid-state method needs high reaction temperatures or high mechanical energy for reactant diffusion. Synthesis in liquid phase is useful to prepare solid compounds containing the different cations in an ideally atomic dispersion.

2.5.2.1 Precursor method

Cerium oxide or ceria can be prepared by the decomposition of the precursors, such as hydroxides, nitrates, halides, sulfates, carbonates, formates, oxalates, acetates, and citrates. For example, the aqueous solution containing cerium nitrate (or oxalate) and citric acid are dissolved in a solvent. After the evaporation, the calcination of the citrate precursors can lead to the formation of nanosize or porous cerium oxide powders. Changing the stoichiometry of the precursors allows the synthesis of mixed

oxides. For instance, $CeO_2$-$Ln_2O_3$ solid solutions, where Ln = La, Pr, Sm, Gd, and Tb, have been synthesized by evaporating the mixed metal nitrate solutions to obtain the precursors. After the calcination, the doped cerium oxide powders can be obtained.

2.5.2.2 Precipitation and co-precipitation method

Chemical precipitation is an extensively used method for preparing solid materials from solutions. A liquid-phase reaction is used to prepare insoluble compounds that are amorphous or crystalline precipitates. The precipitates usually are composed of fine particles. Ceria-based fine particles can be synthesized via this process. Commonly, ceria can be prepared by calcination of the inorganic cerium salt ($Ce(NO_3)_3$,$CeCl_3$, $CeSO_4$, and $(NH_4)_2Ce(NO_3)_6$) with an alkali solution (NaOH, $NH_4OH$, and $(NH_2)_2{\cdot}H_2O$) or oxalic acid.

In a typical precipitation method, metal cations are added directly into a precipitant to obtain the oxide powders or their precursors. However, the morphology and the particle size of powders can be controlled by simply adding the solution to the precipitant due to the rapid change of solution concentration and the discontinuous nature of precipitate formation. The pH of precipitation may be different for each metal ion component. The composition at the beginning of the precipitation is different from the composition at the end. To improve this drawback, many scientists attempted to develop a homogeneous precipitation method. In this process, precipitants are generated simultaneously and uniformly throughout the solution using the controlled release of the reaction-participating ligands by another chemical source in the solution. Applying this method, ceria and doped ceria particles of spherical shape with a narrow size distribution have been obtained.

In the preparation of mixed oxides, the co-precipitation method is the most commonly used. Mixed metal salts are dissolved in the same solvent (water is the most popular one). In the ideal conditions, all cations can be simultaneously precipitated in a quantitative way without segregation of any particular constituents in the solution. However, it is very difficult in most cases if more than two metal cations are involved. Due to the differences in solubility between several precipitating phases, the precipitation kinetics of each metal ion component is affected. The homogeneous co-precipitation at an atomic level is, therefore, very difficult and the most of the obtained precipitates are considered as a homogeneous mixture of fine particles. However, this method is a very popular technique, and plenty of ceria-based mixed oxides have been prepared.

2.5.2.3 Hydrothermal and solvothermal synthesis

Hydrothermal synthesis is well known in mineralogy and geology fields for growth of minerals and ores. High temperature and high pressure water can be used as a transfer medium of heat, pressure, and mechanical energy, an adsorbate that works as a catalyst, a solvent which dissolves or reprecipitates the solid materials, and a reagent which acts as a mineralizer. This method has been used in the preparation of single crystals and particularly of fine powders with nanosized to submicron particles. Besides water (hydrothermal synthesis), ammonia water or some organic solvents are also important reaction media. Generally, this process is known as solvothermal method.

Three different processes might occur during a hydrothermal treatment: hydrothermal synthesis, hydrothermal oxidation, and hydrothermal crystallization. Hydrothermal synthesis is carried out to synthesize mixed oxides from their component oxides or hydroxides. The obtained particles are small, uniform, and well-dispersed crystallites. The size and morphology of the particles can be controlled by pressure, temperature, and mineralizer concentration. In the hydrothermal oxidation process, fine oxide particles can be directly prepared from metals, alloys, and intermetallic compounds by oxidation with a solvent at high temperature and pressure. The hydrothermal crystallization is the most popular technique for preparing ceria-based nanoparticles. Precipitation from aqueous solutions under high temperature and pressure is involved in the process. An excess amount of precipitates is added to the cerium salt solutions. Precipitate gels sealed in Teflon-lined autoclaves are quenched to obtain the crystalline powders. The particle size clearly depends on the reaction temperature and the starting materials.

2.5.2.4 Sol-gel method

Sol-gel processes are interesting to prepare many materials in various shapes and forms, and are especially appropriate for the synthesis and preparation of ultrafine oxide materials at relatively low temperatures.

A sol is a stable colloid of small particles suspended in a liquid. The particles can be amorphous or crystalline. Electrostatic repulsion is used for preventing aggregation. The particles in sols interact to form a continuous network of connected particles called a gel. In case of drying a gel by evaporating the interstitial liquid, the capillary forces cause the gel to shrink and cause the formation of cracks as a result of the differential stresses generated in the drying gel. The obtained dried gel is known

as a xerogel. When the wet gel is dried under supercritical conditions, the pore and network structure of the gel is maintained even after drying. The resulting gel in this case is called aerogel. These sol-gel materials are frequently applied to catalysts and catalyst supports because of their high surface area.

The sol can be prepared by hydrolyzing reactive metal compounds, for example alkoxides, $M(OR)_n$, where M is a metal and R is an alkyl group. In the sol-gel method, metal alkoxides are dissolved in an alcohol and addition of water causes hydrolysis of metal alkoxides.

$$M(OR)_n + n\ H_2O \longrightarrow M(OH)_n + n\ ROH$$

Then, a series of condensation reactions occurs between hydroxide groups and the overall reaction is represented by the following chemical equation:

$$M(OH)_n \longrightarrow MO_{n/2} + n/2\ H_2O$$

Based on this method, mixed oxide gels can be produced readily by mixing of their alkoxides solutions prior to hydrolysis.

2.5.2.5 Spray pyrolysis

Spray pyrolysis is an effective method for preparing homogeneous and non-agglomerated sphere particles. The particles can be generated by spraying an aqueous solution of metal salts (or liquid precursor) in a furnace. Figure 2.6 is a schematic diagram of this method. At the first step, the atomization process can be carried out by using a variety of atomizers (pressure, ultrasonic, vibration, disk rotation, electrostatic force, etc.). Then, the aerosols in air or nitrogen are converted to oxides by evaporating the solvent. The size of the obtained product is proportional to that of the aerosol droplets. This indicates that the particle size and the particle size distribution depend on the atomizer.

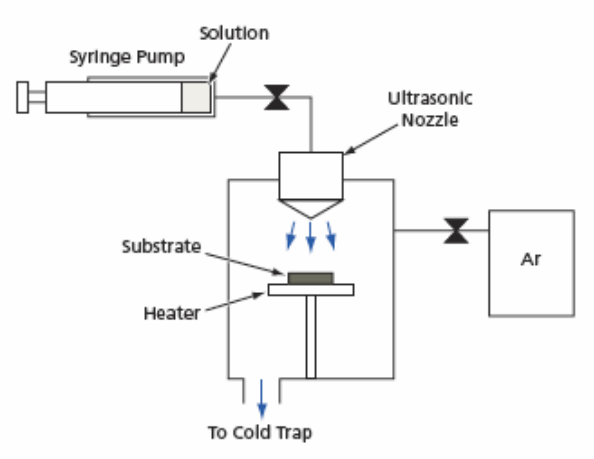


Figure 2.6 The schematic draw of the spray pyrolysis process.

Taken from http://www.techbriefs.com/images/stories/techbriefs/2007/LEW-17447-1.png

In this process, porous structures can be easily formed by controlling the precursor concentration in the droplets or by adjusting the temperature profile in the furnace. Porous particles can also be prepared when the solute concentration gradient is created during the solvent evaporation.

**2.6 The Oxide One Pot Synthesis (OOPS process)**

Among these methods, oxide one pot synthesis becomes interesting because it is a simple and straightforward process that leads to high purity products. Laobuthee A., et al. prepared magnesium aluminate spinel via OOPS process. Magnesium oxide and aluminium hydroxide are used as the starting materials while triethanolamine as a ligand is employed to react with magnesium and aluminium ions to form the complex. For this reaction, ethylene glycol (EG) is used as solvent, the reaction temperature, consequently, is high (~160-180˚C) to distill off the water and EG. The obtained complex is calcined to obtain the high purity magnesium aluminate spinel.

**2.7 Reviews of some researches from past to present**

G. Bryan Balazs and Robert S. Glass (1995) studied the structure and ionic conductivity of ceria doped with rare earth oxides. The rare earth oxides used are the entire rare earth series (except Pm). All compositions were prepared by mixing ceria with the appropriate quantity of the dopant oxide in a mixing mill with a tungsten

carbide mixing ball for several minutes. The powders were pressed and sintered at 1550°C in air. All of samples showed ionic conductivity and ceria doped with Gd, Sm and Y exhibited the highest values. The ionic conductivity of $Ce_{0.8}Sm_{0.2}O_{1.9}$ was $1.2x10^{-2}$ S/cm at 600°C. The optimized amount of Y dopant providing the maximum conductivity was 0.16 mol%.

R.S. Torrens, N.M. Sammes, and G.A. Tompsett (1998) studied the physical and electrical properties of $(CeO_2)_{0.8}(GdO_{0.15})_{0.2}$ powders prepared from different synthesis routes; a modified co-precipitaion reaction, a solid state reaction, and a commercial powder from a hydrothermal synthesis route. The modified co-precipitation reaction were produced by dissolving $Ce(NO_3)_3$ and $Gd(NO_3)_3$ in distilled water and using the oxalic acid (0.05 M) as precipitant. The pH value was adjusted in the 6.7-6.9 range, using $NH_4OH$ throughout the duration of the reaction. The precipitates were filtered, washed with distilled water and ethanol, dried at 50°C in oven and calcined at 700°C for 1 h. A solid state method was performed by mixing and milling starting oxide powders in a roller-mill and used water-free ethanol as milling solvent. The starting materials were milled for 24 h, dried at 40°C for 12 h and followed by calcining at either 1200 or 1300°C. A hydrothermal synthesis of a co-precipitated of a mixed cerium-gadolinium hydroxide gel was used to prepare commercial powders. The ceramic powder was obtained after calcination at 700°C for 1 h.

In this work, they reported that the powders prepared via solid state technique or co-precipitation had approximately the same particle size, but the particle size of the commercial powder appeared to be smaller. These powders were sintered into pellets. The pellets produced using the solid state reaction powders showed worst performance than the pellets prepared with the co-precipitated powders, although their particle size was similar. The ionic conductivity of the pellets at 800°C was $4.5x10^{-2}$ S/cm for the solid state prepared powder and $3.2x10^{-1}$ S/cm for the co-precipitated powder.

S. Dikmen, P. Shuk, M. Greenblatt, and H. Gocmez (2002) prepared $Ce_{1-x}Gd_xO_{2-\delta}$ (x = 0-0.3) solid solutions by hydrothermal synthesis method. The procedure was started by dissolving $Ce(NO_3)_3 \cdot 6H_2O$ and $Gd(NO_3)_3 \cdot 6H_2O$ separately

in water. Then, the solution were mixed and co-precipitated with $NH_4OH$ at pH = 10. The precipitate gels were placed into Teflon-line steel autoclave and hydrothermally treated at 260°C for 10 h and quenched to room temperature. The obtained crystallized powders of $Ce_{1-x}Gd_xO_{2-\delta}$ (x = 0-0.3) solid solutions were washed with deionized water and dried in air at room temperature. The particle sizes of all the compositions were in the 41-68 nm range. Highly dense ceramic pellets were obtained after sintering at only 1300-1400°C. The highest conductivity was found for 0.25 mol% Gd substitution and its activation energy was 0.58 eV. They concluded that the hydrothermal method allowed to prepare gadolinium-doped ceria with higher conductivity and lower sintering temperature with respect to GDC prepared with other synthesis methods.

A.I.Y. Tok, L.H. Luo, and F.Y.C. Boey (2004) reported the synthesis of 20 mol% $Gd_2O_3$-doped $CeO_2$ nano-particles, prepare using the carbonate co-precipitation method. Solutions of 0.3 M $Ce(NO_3)_3{\cdot}6H_2O$ and $Gd(NO_3)_3{\cdot}6H_2O$ were separately prepared in water. Both solutions were mixed and dropped very slowly into an ammonium carbonate solution maintained under mild stirring. The resulting suspension was separated into two parts; one part was aged at 70°C for 1 h and the other was aged at room temperature for 1 h. The precursor aged at 70°C for 1 h was dried with flowing $N_2$ gas for 12 h and the precursor aged at room temperature was vacuum dried for 12 h. Both precursors were then calcined at 600, 700 and 800°C in flowing $O_2$ gas for 2 h.

The room temperature aging and the air-drying allowed the formation of weakly agglomerated crystalline nano-particles, with size in the 30-50 nm range, demonstrating that this synthesis method was easy and cost-effective.

T. Mahata, G. Das, R.K. Mishra, and B.P. Sharma (2005) reported on the combustion synthesis route to prepare gadolinia doped ceria powders with different gadolinia content in the 0-15 mol% range. Firstly, the gels were prepared by mixing together 0.6457 M $Ce(NO_3)_3{\cdot}6H_2O$ and 0.1515 M $Gd(NO_3)_3{\cdot}6H_2O$ solutions with the required amounts. Citric acid monohydrate ($C_6H_8O_7{\cdot}H_2O$) was then added to the nitrate solution. Heating favored the formation of transparent gels, which then were combusted forming light yellowish powders. The powders were pressed and sintered

at 1250°C.

The results showed that GDC powders with particle size in the nanometer range were obtained using the combustion synthesis. The specific surface area ($m^2/g$) was found to increase with increasing the gadolinia content. The thermal analysis of the gel precursors containing different amount of gadolinia showed only a single step combustion reaction. The starting temperature of the combustion reaction also increased with the gadolinia content. The lattice parameters of the samples varied linearly with the gadolinia content following the Vegard's law. The pellets density was in the 94-97% of theoretical density range, achieved after sintering at 1250°C.

Cheng Peng and Zhen Zhang (2007) synthesized $Ce_{1-x}Gd_xO_{2-\delta}$ (x = 0-0.6) solid solutions by nitrate-citrate combustion method (gel-combustion). Stoichiometric ratios of $Ce(NO_3)_3$ and $Gd(NO_3)_3$ solutions were mixed. Citric acid was, then, added to the solution. The pH value of the solution was adjusted to about 8.0 by adding $NH_4OH$. The solution was vaporized at 60-70°C and became a transparent gel. The gels were first heated on a hot plate before calcining at 500°C. The obtained powders were pressed into pellets and sintered at 1300°C for 10 h. The particle size of $Ce_{1-x}Gd_xO_{2-\delta}$ obtained from this synthesis route was 11-28 nm. The sintering temperature needed to obtain a dense ceramic pellet was then reduced from 1600°C to about 1300°C because the particle size was very small. The highest conductivity was found for the x = 0.2 Gd substitution ($\sigma_{600°C} = 5.26 \times 10^{-3}$ S/cm).

Gao Ruifeng and Mao Zongqiang (2007) prepared and studied the sintering behavior of $Ce_{0.8}Sm_{0.2}O_{1.9}$ (SDC) synthesized by oxalate co-precipitation route. Nano-powders of SDC were prepared by separately dissolving $CeO_2$ and $Sm_2O_3$ in dilute nitrate acid. The solutions were mixed and dropped to a dilute oxalic acid solution (0.05 M). The pH value (~6.6-6.9) was adjusted by ammonium hydroxide. The precipitate was washed by water and ethanol, and then calcined at 750°C for 2 h with a heating rate of 3°C/min. The pellets were sintered at temperatures between 1100 and 1450°C for 4 h.

The results showed that there were several parameters affecting the sintering behavior of SDC:

1. The radial shrinkage of SDC pellets sintered at 1350°C decreased with

increasing the forming pressure from 150 to 600 MPa.

2. For forming pressures large than 400 MPa, the density increased and then decreased again with the forming pressure for the pellets sintered at 1400°C. As the forming pressure increased, the shrinkage decreased and then increased again with the forming pressure.

3. The radial shrinkages increased with increasing the sintering temperature up to 1400°C, and then decreased. It is concluded that to achieve the maximum radial shrinkage, an appropriate combination of forming pressure and sintering temperature has to be selected.

All the effects mentioned above show that the optimized parameters for achieving dense pellets are uniaxially pressing at 200-400 MPa and sintering at 1350-1400°C for 4 h. The density of the sintered pellets was more than 90% of the theoretical density and their shrinkage was less than 0.5%.

Jian-dong Hu, Yong-xiu Li, Xue-zhen Zhou, and Ming-xia Cai (2007) synthesized ceria ($CeO_2$) nanoparticles by pyrolysis method using hydrate cerium propionate as precursor. The preparation of hydrate cerium propionate was started by dissolving hydrate cerium carbonate in a slightly excess amount of propionic acid solution, maintained under stirring and heating. The white suspension was evaporated, cooled to room temperature, filtered and dried at 80°C for 10 h. The crystalline cerium propionate was then converted to ceria by calcining at given temperatures for 90 min.

The results showed that the calcination temperature affected the physical properties of ceria particles. Increasing the calcination temperature, the ceria particle became larger and densified with clear spherical shape. The particle sizes of ceria were in the 20 to 50 nm range. The specific surface area and the negative value of zeta potential decreased with increasing the calcination temperature. They concluded that this method is very simple and economically feasible for preparing ceria because the crystalline precursor has a low molecular weight.

Snezana B. Bošković, Branko Z. Matovic, Milan D. Vlajić, and Vladimir D. Kristić (2007) investigated the synthesis method and properties of fluorite type pure ceria powder, doped ceria powders with rare earth cation in the 0-0.25 concentration range, as well as co-doped powders. The synthesis started by mixing the required

portions of glycine, cerium acetate hydrate and rare earth nitrate hexahydrate (Gd, Sm, Nd and Y) with approximately a 100 mL of distilled water in a stainless steel beaker. Cerium acetate hydrate was used because it is less expensive when compared with the cerium nitrate hexahydrate. The solutions were heated up to 450°C in air to obtain the ash powders. The ashes were then calcined at 600°C for 4 h to achieve the ceramic powders. The particle size of all those samples prepared using this method was in the nanometer range. The results showed that the dopants used in the mentioned concentration range formed solid solutions with the host ceria.

They concluded that the glycine/nitrate process which used Ce-acetate to replace Ce-nitrate for preparing single and multiple doped ceria solid solutions has several advantages as follows:

1. Producing large amount of powders in a very short time.

2. The obtained particles exhibited a single phase nanopowder with high specific surface area.

3. There was no formation of intermediate phases.

4. The materials used for the preparation are readily available and low cost.

5. The method is flexible for preparing complex compositions.

M.L. Dos Santos, R.C. Lima, C.S. Riccardi, R.L. Tranquilin, P.R. Bueno, J.A. Varela, and E. Longo (2008) have been successfully prepared crystalline ceria ($CeO_2$) nanoparticles by microwave-hydrothermal method. The method was started by dissolving $5x10^{-2}$ mol/L $(NH_4)_2Ce(NO_3)_6$ and 0.1 g PEG (surfactant) in water. $NH_4OH$ was then added to the solution until the pH = 9 was reached. The solution was put into a sealed autoclave and placed in a domestic microwave oven, and heated up to 130°C for 20 min to obtain $CeO_2$ powders. The obtained $CeO_2$ powders were washed with deionized water, dried at 80°C and calcined at 500°C for 1, 2 and 4 h. The result from field-emission scanning electron microscopy showed that synthesized ceria powders have a spherical shape with particle size below 10 nm, a narrow distribution, and exhibit weak agglomeration. The FTIR result showed a strong broad band below 700 $cm^{-1}$, which is characteristic of the Ce-O-C stretching mode, while the Raman spectrum presented a very strong band at 464.5 $cm^{-1}$. The microwave-hydrothermal method is very interesting because this method can be used to prepare $CeO_2$ powders at low temperature and for short treatment times, controlling morphological and structural properties.

R.O. Fuentes and R.T. Baker (2008) used a variation of the sol-gel technique known as cation complexation for preparing gadolinium-doped ceria solid solution at 0.1 mol% gadolinium substitution. This technique produced highly sinterable ceramic powders, due to the small amount of char formed during calcinations. Cerium and gadolinium nitrate hexahydrates were dissolved separately in water and then the solutions were mixed. After adding citric acid, the solution was heated up to 80°C under stirring until a transparent gel was formed. The product was calcined at 500°C for 1 h.

The obtained powders showed cubic fluorite structure single phase with good crystallinity. The sample calcined at 500°C was found to have an average crystallite size of 10 nm. The powder was sintered at 1300°C for 30 h and 1400°C for 8 h into pellets and their electrical conductivity was measured. It was found that the sintering conditions did not affect total conductivity, but the lower temperature and longer time condition (sintered at 1300°C for 30 h) gave higher grain boundary resistivity. Impedance measurements performed on etched samples and compared with samples before the etching treatment showed that grain boundary resistivity decreased over time for both pellets.

# CHAPTER III
# CERIA NANOPARTICLES WITH FOAM-LIKE STRUCTURE DERIVED FROM METAL ORGANIC COMPLEX METHOD


## Abstract

Nanocrystalline ceria ($CeO_2$) was successfully prepared by the thermal decomposition of Ce-triethanolamine (TEA) complex. Effect of calcination temperature on the physical properties of the as prepared $CeO_2$ powder was investigated. The XRD patterns showed that single phase $CeO_2$ was obtained after calcination at 600°C, 800°C, and 1000°C for 2 h. BET specific surface area decreased with increasing the calcination temperature, corresponding to an increase in the crystallite size determined from XRD. In addition, SEM micrographs of the ceria powder obtained at 600°C exhibited a foam-like structure.


## 3.1 Introduction

Ceria ($CeO_2$) has a fluorite structure with a space group *Fm3m* that does not show any known crystallographic change from room temperature up to its melting point (~2700°C). The properties of ceria make it an interesting material for numerous technological applications, such as automotive exhaust catalyst [1,2], polishing materials [3], reforming reaction catalyst [4-6], and fuel cells [7-9]. The success of the technological applications strongly depends on the development of powder synthesis routes. Therefore, many synthesis routes for ceria ($CeO_2$) have been proposed in the relevant literatures, such as co-precipitation of hydroxides [10,11], sol-gel method [12], and solid-solid reaction [13]. However, each synthesis routes has some disadvantages, such as the high cost of starting materials, lack of homogeneity and purity, or high processing temperatures. Laobuthee *et al.* successfully prepared magnesium aluminate ($MgAl_2O_4$) by the one pot process [14]. This method offers a very simple and low cost route to provide high purity and homogeneity products. In addition, the obtained $MgAl_2O_4$ exhibited good humidity sensitivity as compared to that prepared via other methods. Based on the basic of this process, simple and effective method for the preparation of ceria nanoparticles based on metal organic complex is here presented.

### 3.2 Experimental procedure

Cerium(III) nitrate hexahydrate [$Ce(NO_3)_3 \cdot 6H_2O$, 99.5% purity] was purchased from Acros Organics. Triethanolamine [TEA, $N(CH_2CH_2OH)_3$, 98.0% purity] and n-propanol [$CH_3CH_2CH_2OH$, 99.5% purity] were obtained from Carlo Erba (Barcelona). All chemicals were used as received.

Cerium(III) nitrate hexahydrate was dissolved in n-propanol. TEA was added to the solution in the molar ratio of TEA to cerium(III) nitrate of 1:1. The solution was distilled for 3 h to obtain the precipitate. The precipitate was filtered and washed by n-propanol to obtain the light-yellowish powder of Ce-TEA complex.

Simultaneous thermogravimetric and differential thermal analysis (TG/DTA) of the complex was carried out using TGA/SDTA analyzer (Model TGA/SDTA 851e, Mettler Toledo) in flowing air with a heating rate of 5°C/min, in the 50 to 1000°C temperature range. X-ray diffraction (XRD) analysis was carried out at room temperature in an X-ray diffractometer (D8 Advance, Bruker-AXS) operating at 40 KV and 40 mA using a Ni filter and CuKα radiation. Diffraction patterns were recorded in the range of $2\theta$ = 20-90° by step scanning with a step interval of 0.02° and a scanning time of 2 s on each step. The crystallite size (D) of the calcined products was determined by using the Scherrer equation: $D = 0.9\lambda/\beta\cos\theta$, where $\lambda$ is the X-ray wavelength (1.5406 Å for CuKα), $\theta$ is the scattering angle of the main reflection (111), and $\beta$ is the corrected peak at full width at half-maximum (FWHM) intensity. The specific surface area ($S_{BET}$) of the calcined powders was measured by using a surface area analyzer (Autosorb 1c, Quantachrome) based on BET (Brunauer-Emmett-Teller) principle with nitrogen adsorption. From the specific surface area data, the particle size was calculated using the equation: $D_{BET}=6000/\rho S_{BET}$, where the $D_{BET}$ is the average diameter of the spherical particle, $S_{BET}$ is the specific surface area of the powder, and $\rho$ is the theoretical density of $CeO_2$ (7.211 $g/cm^3$). The morphology of the calcined powders was observed by using scanning electron microscope (SEM, JEOL-JSM-6301F).

### 3.3 Results and discussion

The clear mixture solution of cerium(III) nitrate and triethanolamine in n-propanol solvent was prepared. Cerium complex precipitated during continuous distillation. The light yellowish Ce-TEA complex was collected by filtration.

The TG/DTA curves of the Ce-TEA complex are shown in Figure 3.1. The decomposition of the complex on heating showed a three-step weight loss pattern. The first weight loss on the TGA curve, accompanied by a small endothermic peak with its maximum at ~100°C in the DTA curve, was mainly caused by the loss of physisorbed moisture and n-propanol. An intense exothermic peak with its maximum at 250°C, accompanied by a sharp weight loss of about 45 wt%, was attributed to the decomposition of the organic ligand and generated char as a by-product. A broad exothermic region observed in the 300-600°C temperature range together with a slight weight loss at the same temperatures was attributed to the burning of the residual organic components. Above 600°C, the weight remained constant, indicating that 600°C is the appropriate calcination temperature for preparing the ceramic powder. TGA curve showed that the total weight loss for the complex was 35.5 wt%.

Figure 3.2 shows the XRD patterns of the ceria powders obtained after calcining the complex at different temperatures in air for 2 h. The characteristic peaks corresponding to (111), (200), (220), (311), (222), (400), (331), (420), (422) planes located at $2\theta$ = 28.535°, 33.080°, 47.495°, 56.348°, 59.102°, 69.427°, 76.710°, 79.073°, and 88.447°, respectively are in agreement to the peaks of the face-centered cubic $CeO_2$ (JCPDS No. 34-0394), indicating that all the samples can be identified to ceria with the cubic fluorite structure. In addition, all the peaks became stronger and sharper with increasing the calcination temperature.

Some physical characteristics of the as prepared ceria powders are listed in Table 3.1. It is clear that with increasing the calcination temperature, the specific surface area ($S_{BET}$) decreased, while the particle size ($D_{BET}$) increased. Furthermore, the crystallite size, determined by the Scherrer equation, increased because of the increase in the XRD peak intensities.

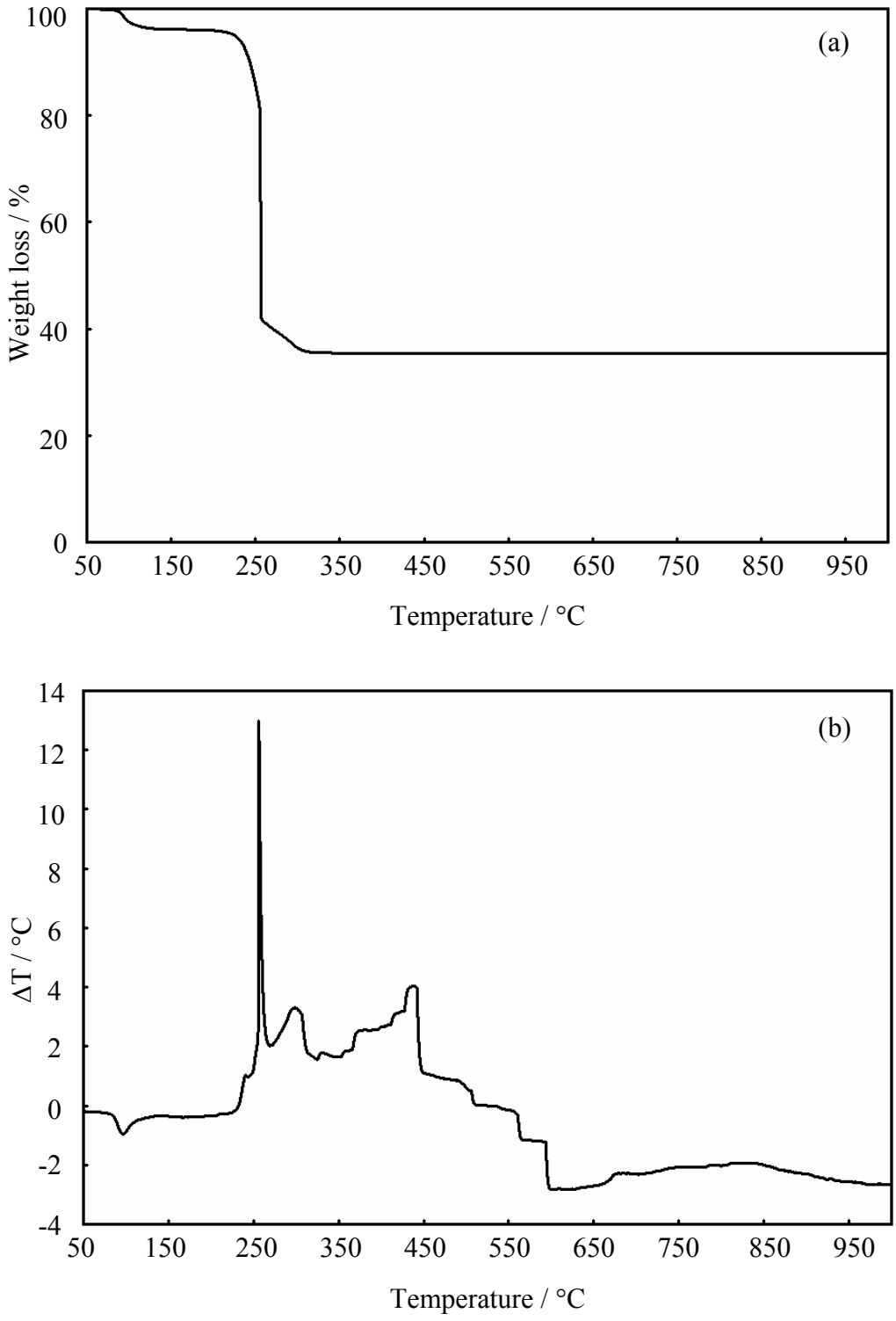


Figure 3.1 Thermograms of the Ce-TEA complex: (a) TGA, and (b) DTA.

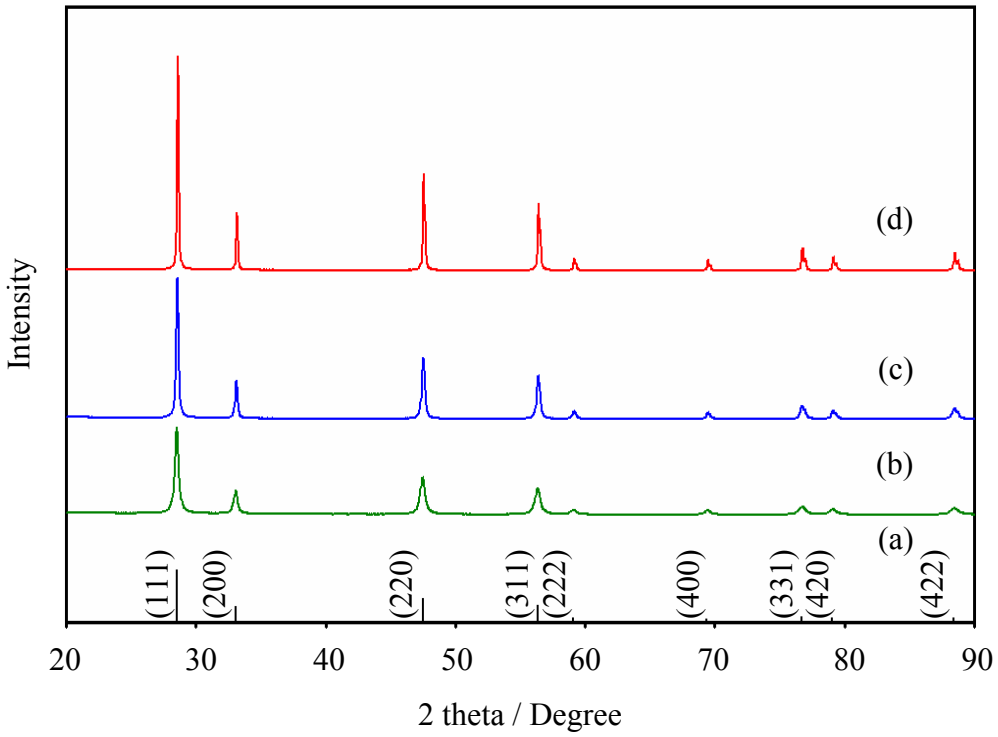


Figure 3.2 XRD patterns of (a) standard $CeO_2$ No. 34-0394 (cubic fluorite structure), and ceria powders obtained from Ce-TEA complex calcined at (b) 600°C, (c) 800°C, and (d) 1000°C.

Table 3.1 Effect of calcination temperature on the physical characteristics of ceria

| Calcination temperature (°C) | $S_{BET}$ ($m^2/g$) | $D_{BET}$ (nm) | Crystallite size (Å) |
|---|---|---|---|
| 600 | 24.8 | 34 | 254 |
| 800 | 11.6 | 72 | 397 |
| 1000 | 6.2 | 134 | 682 |

Figure 3.3 shows the SEM micrographs of the ceria particles obtained after calcining the Ce-TEA complex at different temperatures for 2 h. It can be seen that the ceria particles calcined at 600°C and 800°C displayed a foam-like morphology (Figure 3.3(a and b)), while the ceria calcined at 1000°C (Figure 3.3(c)) exhibited blocky particles with an irregular shape due to the agglomeration and sintering.

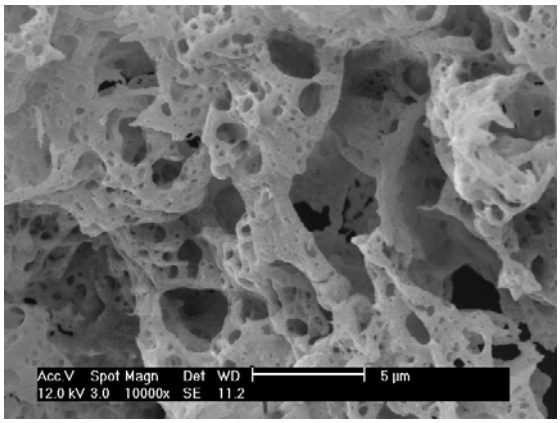


(a)

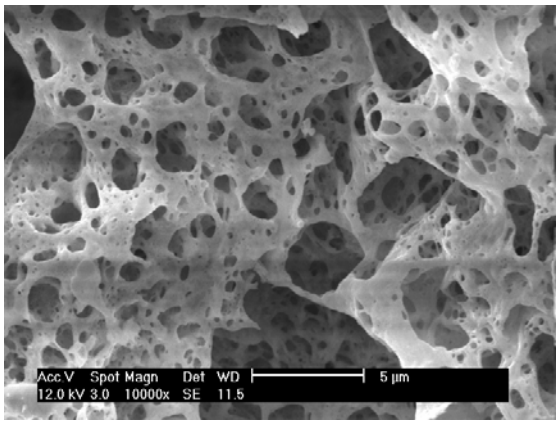


(b)

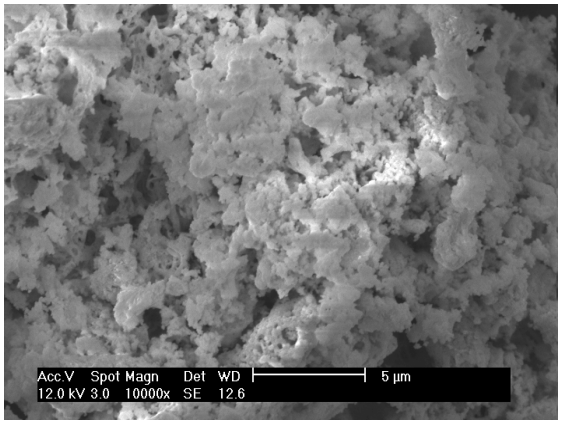


(c)

Figure 3.3 SEM micrographs of the ceria particles obtained by calcining the complex at (a) 600°C, (b) 800°C, and (c) 1000°C.

### 3.4 Conclusions

Ceria nanoparticles were successfully prepared by metal organic complex method. Ceria powders with a foam-like structure were obtained after heating the Ce-TEA complex to 600°C for 2 h. The higher the calcination temperature, the larger the crystallite size based on XRD analysis, and the larger the $D_{BET}$ calculated from BET. On the other hand, the specific surface area decreased. Thus, this method is an easy, inexpensive, straightforward alternative to solid-solid reaction, co-precipitation and other chemical techniques for the synthesis of ceria nanoparticles.

### References

[1] Gandhi HS, Graham GW, McCabe RW. J Catal 2003;216:433-442.

[2] Shinjoh H, J. Alloys Compd 2006;408-412:1061-1064.

[3] Wang L, Zhang K, Song Z, Feng S. Appl Surf Sci 2007;253:4951-4954.

[4] Ramirez-Cabrera E, Atkinson A, Chadwick D. Appl Catal, B 2004;47:127-131.

[5] Hennings U, Reimert R. Appl Catal, A 2007;325:41-49.

[6] Cai W, Zhang B, Li Y, Xu Y, Shen W. Catal Commun 2007;8:1588-1594.

[7] Dudek M. J Eur Ceram Soc 2008;28:965-971.

[8] Ruiz-Trejo E, Santoyo-Salazar J, Vilchis-Morales R, Benítez-Rico A, Gómez-García F, Flores-Morales C, Chávez-Carvayar J, Tavizón G, J Solid State Chem 2007;180:3093-3100.

[9] Jo SH, Muralidharan P, Kim DK. Solid State Ionics 2008;178:1990-1997.

[10] Thangadurai V, Kopp P, J Power Sources 2007;168:178-183.

[11] Ding D, Liu B, Zhu Z, Zhou S, Xia C. Solid State Ionics 2008;179:896-899.

[12] Fuentes RO, Baker RT. Int J Hydrogen Energy 2008;33:3480-3484.

[13] Ma J, Zhang TS, Kong LB, Hing P, Chan SH. J Power Sources 2004;132:71-76.

[14] Laobuthee A, Wongkasemjit S, Traversa E, Laine RM. J Eur Ceram Soc 2000;20:91-97.

# CHAPTER IV
# PREPARATION OF GADOLINIA DOPED CERIA (GDC) POWDER FROM A SIMPLE AND EFFECTIVE COMPLEX FOR ELECTROLTYE MEMBRANE IN SOLID OXIDE FUEL CELLS


## Abstract

Gadolinia doped ceria (GDC) powders with different gadolinium contents have been prepared from the thermal decomposition of metal organic complexes. The calcination temperatures for complexes were determined by TG/DTA analysis. The obtained powders have been characterized by XRD, SEM, and BET. All samples were found to be ceria based solid solutions of fluorite type structures. The powder, when cold pressed and sintered in air at 1500°C for 5 h, attained the sintered density ~90% of its theoretical value. The electrical conductivity of GDC pellets in air was studied as a function of temperature between 225 and 700°C by using two-probe AC impedance spectroscopy measurement. The highest total conductivity was found for the x = 0.15 Gd substituted ceria ($\sigma_{600°C}$ = 0.0249 S/cm).


## 4.1 Introduction

Solid oxide fuel cells (SOFCs), based on oxide-ion conducting electrolytes, offer a clean, low-pollution technology to electrochemically generate electricity at high efficiencies. Various advantages of SOFCs over other traditional energy conversion systems are high efficiency, reliability, modularity, fuel adaptability, very low levels of $SO_x$ and $NO_x$ emissions, and long-term stability [1,2]. However, the high operating temperatures of SOFCs affect durability due to sintering of electrodes and interfacial reactions. Reducing the operating temperature provides better durability, a wider choice for interconnect material selection, and lower costs [3].

Electrolytes providing high oxide ion conductivity being operated at low temperatures are under investigation. Additionally, reducing the thickness of the electrolyte decreases electrolyte ohmic resistance. Gadolinia doped ceria (GDC) becomes attractive because it has superior oxide ion conductivity at low temperature around 500°C [4]. Thin layers of doped ceria on the YSZ can be deposited on YSZ to avoid chemical reaction with cathode materials, such as doped lanthanum cobalto-

ferrites (LSCF), yielding reduced interfacial resistance at the cathode, thereby resulting in higher fuel cell power densities.

Among the various dopants studied for ceria, $Gd^{3+}$ and $Sm^{3+}$ singly doped ceria (GDC and SDC) were reported to have the highest conductivity [4,5]. Besides, many studies have been carried out on co-doped ceria [6-9].

In the previous chapter, the synthesis of pure ceria has been reported, using the oxide one pot synthesis (OOPS) process, which has been previously proposed for the synthesis of magnesium aluminate ($MgAl_2O_4$) by Laobuthee *et al.* [10,11]. Based on this process, the synthesis of GDC powders from nitrate salts instead of hydroxide is presented. In addition, various low boiling point solvents were used to replace a high boiling point solvent as ethylene glycol used previously. The simple and effective complexes prepared were expected to be the starting materials to produce high quality powders to be used in electrolyte membranes for SOFCs. The present work consists of two parts: (i) preparation of gadolinia doped ceria powders from the complexes and (ii) study on the electrical property of the obtained powders.

## 4.2 Experimental procedure

### 4.2.1 Complex preparation

The starting materials were cerium(III) nitrate hexahydrate [$Ce(NO_3)_3 \cdot 6H_2O$, 99.5% purity] and gadolinium(III) nitrate pentahydrate [$Gd(NO_3)_3 \cdot 5H_2O$, 99.9% purity]. These chemical were purchased from Acros Organics. Triethanolamine [TEA, $N(CH_2CH_2OH)_3$, 98% purity] and n-propanol [$CH_3CH_2CH_2OH$, 99.5% purity] were obtained from Carlo Erba (Barcelona). All chemicals were used as received.

The complexes were prepared by mixing $Ce(NO_3)_3 \cdot 6H_2O$ and $Gd(NO_3)_3 \cdot 5H_2O$, with molar ratios as Ce:Gd = 1.0:0, 0.9:0.1, 0.85:0.15, and 0.8:0.2, denoted 0GDC, 10GDC, 15GDC, and 20GDC, respectively, with 80 mL of n-propanol. TEA was added in the 1:1 molar ratio of metal ions to TEA. After mixing, the as-prepared transparent solution was distilled for 3 h to obtain the precipitates. The precipitates were collected by filtration and then washed by n-propanol. The obtained complexes were characterized by FTIR, MS, and TG/DTA. Fourier transform infrared spectra of the complexes were recorded on a Perkin-Elmer system 2000 FTIR with a spectral resolution of 4 $cm^{-1}$ using transparent potassium bromide (KBr) pellet. The complexes were thoroughly crushed and mixed with KBr with an

agate mortar and pestle at an approximate ratio by weight of complex: KBr of 1 to 20 to prepare a pellet specimen for identifying the functional groups of the complexes. Mass spectra were recorded on ESI-MS mode (Bruker Esquire mass spectrometer). Methanol was used as a solvent to prepare complexes and was used as a carrier phase. The mass ranges of the calcined powders were set from 100 to 1000. Simultaneous thermogravimetric/differential thermal analysis (TG/DTA) of the complexes was carried out in a TGA/SDTA analyzer (Model TGA/SDTA 851e, Mettler Toledo), in flowing air with a heating rate 5°C/min in the range 50 to 1000°C.

4.2.2. Powder preparation and characterization

The complexes were pyrolyzed in an alumina crucible at various temperatures: 400, 600, 800, 1000, and 1200°C for 2 h. Phase identification was determined via X-ray diffraction analysis (XRD; Philips X-Pert-MPD X-ray diffractometer) operating at 40kV/30mA, using monochromated CuKα radiation. Diffraction patterns were recorded in the range of 2θ = 20-90° by step-scanning, with a step interval of 0.02° and a scanning time of 2 s on each step.

The specific surface areas of the powders, $S_{BET}$ were measured by Brunauer-Emmett-Teller (BET) nitrogen-gas absorption method. These values were calculated from the nitrogen adsorption isotherms at 77 K using a Micromeritics ASAP 2020 surface analyzer and a value of 0.162 $nm^2$ for the cross-section of the nitrogen molecule. Samples were degassed at 350°C under high vacuum for 20 h before measurements. The specific surface area was converted to particle size ($D_{BET}$) according to Eq. (1), assuming that the particles were closed spheres with smooth surface and uniform size.

$$D_{BET} = 6 \times 10^3/d_{th}\, S_{BET} \quad (1)$$

Here, $d_{th}$ was the theoretical density of the material ($g/cm^3$). $D_{BET}$ was the average particle size (nm). The specific surface area, $S_{BET,}$ was expressed in $m^2/g$.

Scanning electron micrographs were obtained with a JEOL JSM-6301F scanning microscope operating at an acceleration voltage of 12 KV, and magnification values in 10,000x to identify the powder sample microstructures. Samples were mounted on alumina stubs using a liquid carbon paste and then sputter coated with Au to avoid particle charging.

4.2.3 Study of the electrochemical properties of pellets

The obtained powders were uniaxaially pressed into green pellets (~30 MPa) in a stainless steel die with 10 mm diameter and isostatically pressed at ~200 MPa. The dense pellets were prepared by sintering the green pellets at 1500°C for 5 h with a ramp rate 3°C/min and naturally cooled in furnace. The relative densities of these sintered pellets were determined using the Archimedes' principle. Powder X-ray diffraction analysis was carried out on polished samples.

Gold electrodes were painted using a gold paste onto both sides of the pellets, and fired at 800°C for 2 h. The pellet was placed in an alumina holder using a spring-clip arrangement between Pt current collectors. The AC conductivity measurements were performed from 0.1 Hz to 10 MHz, using a Solartron 1260 impedance/ gain phase analyzer, interfaced to a personal computer, and run through a ZPlot$^{TM}$ (National Instruments) software; 10 points were taken per decade of frequency. The amplitude of the ac signal imposed on the samples was 10 mV. The impedance spectroscopy measurements were performed from 225 to 700°C in air, using a tube furnace, with controlled heating rate (3°C/min).

**4.3 Results and discussion**

4.3.1 Complex preparation

The ceria complex was firstly prepared from $Ce(NO_3)_3$ and TEA in various solvents, such as methanol, ethanol, iso-propanol, and n-propanol. The reactants were easily dissolved in each solvent to obtain homogeneous solutions. It was found that when the reaction was completed, the yellowish powder was precipitated in the solution only when n-propanol was used as solvent. In this case, the separation of the product from the remaining starting materials and by-products was easy. Therefore n-propanol was chosen as the appropriate solvent for the complex preparation.

The structure of the yellowish products was studied using FTIR. It was found that the product showed the pattern in the FTIR spectrum, as shown in Figure 4.1. The band located at 3355 $cm^{-1}$, assigned to the O-H stretching, might be due to water adsorbed by product. The C-H stretching bands, observed in the region 2928 and 2890 $cm^{-1}$, were assigned for $-CH_2-$ group in product. The C-H bending bands were shown at 1450-1200 $cm^{-1}$. The band at 1631 $cm^{-1}$ was attributed to O-H overtone. In

addition, the resonance at 1080 $cm^{-1}$ was ascribed to the Ce-O-C stretching vibration, and the band at 550 $cm^{-1}$ was from the Ce-O stretching [12].

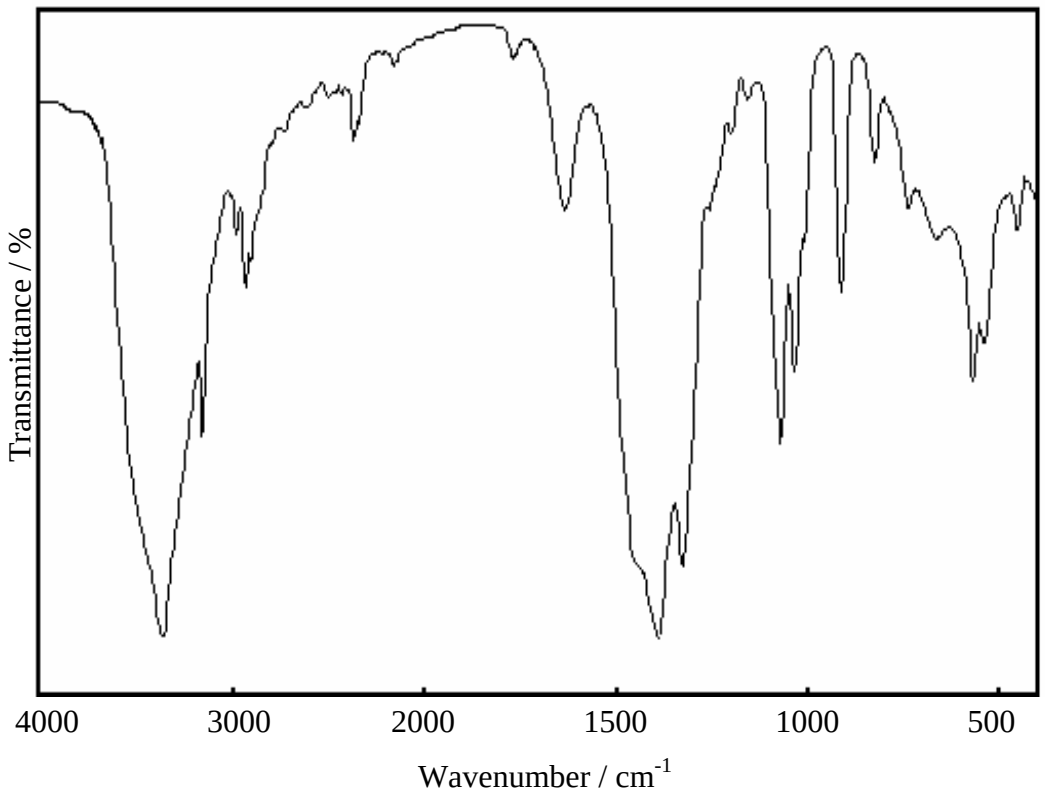


Figure 4.1 FTIR spectrum of a metal organic complex of $CeO_2$.

Since cerium is paramagnetic, NMR results on the product cannot be obtained.

The complex was also analyzed using electrospray ionization (ESI) mass spectroscopy. Since this method is a soft ionization, a few fragmentation peaks are generated (Figure 4.2). Two significant peaks were generated at m/z = 286 and 348, respectively. However, these two peaks exhibited different intensity. Two possible structures might be proposed for the product (Figure 4.3): a monometallic species consisting of one TEA group per metal ion (Structure I) and a monometallic species consisting of one TEA group per metal ion and a nitrate group (Structure II).

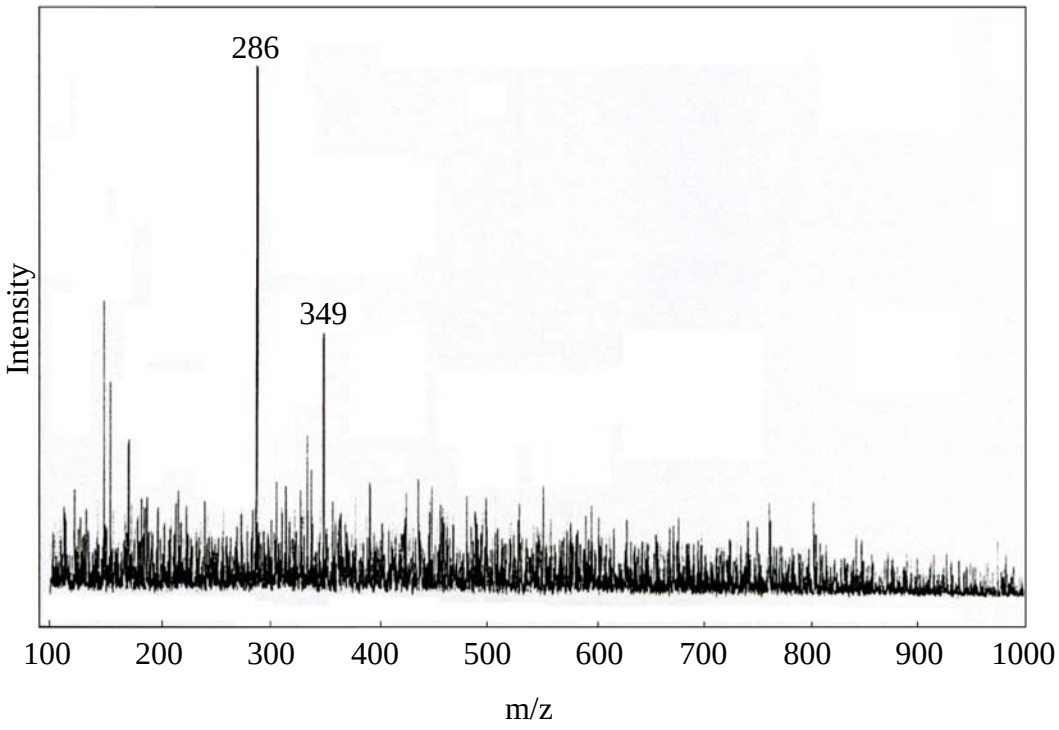


Figure 4.2 Mass spectrum of a metal organic complex of $CeO_2$.


Structure I Structure II

Figure 4.3 The possible structures of a metal organic complex of $CeO_2$.

The various complexes between $Ce(NO_3)_3$, $Gd(NO_3)_3$, and TEA were consequently prepared in n-propanol. The yellowish powders were obtained, although the compositions of $Ce^{3+}$ and $Gd^{3+}$ were varied. The yellowish powders were precipitated when the reactants completely reacted in n-propanol for 3 h.

The doped gadolinium powders were characterized by FTIR. The FTIR spectra of the as-synthesized complexes are shown in Figure 4.4. The doped gadolinium complexes showed the same FTIR peaks observed for the undoped gadolinium complex (Figure 4.1). The bands located at 3355 and 1631 $cm^{-1}$ assigned to the O-H stretching and O-H overtone, respectively, might be due to water adsorbed by product. The peaks at 2928 and 2890 $cm^{-1}$ were assigned as C-H stretching bands

while band at 1450-1200 $cm^{-1}$ are C-H bending bands for -$CH_2$- group. In addition, the peak at 1080 $cm^{-1}$ was ascribed to the Ce-O-C or Gd-O-C stretching vibration, and the band at 550 $cm^{-1}$ is from the Ce-O or Gd-O stretching. In addition, the mass spectra of doped complexes were too complicate to assign due to various types of complexes generated by $Ce^{3+}$ and $Gd^{3+}$ ions. All peaks in mass spectra might be due to the complex peaks and fragmentations from the complexes.

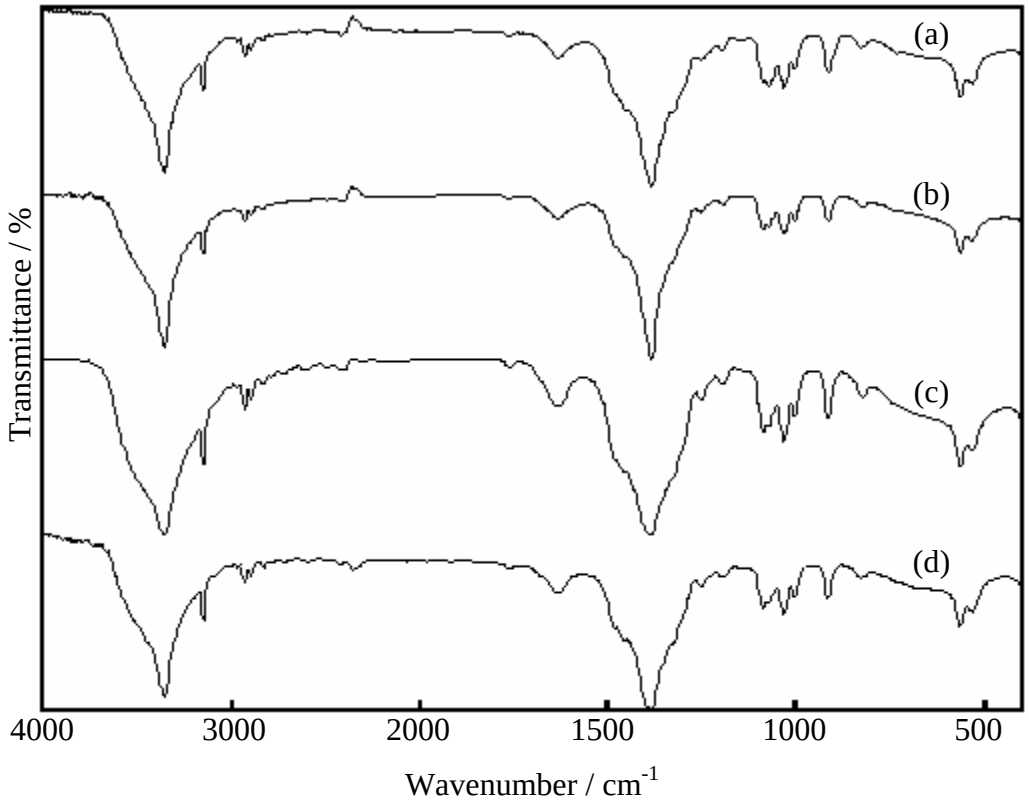


Figure 4.4 FTIR spectra of a $CeO_2$ complex: (a) without doping, (b) 10 mole % doped gadolinium, (c) 15 mole % doped gadolinium, and (d) 20 mole % doped gadolinium.

To obtain the ceramic powders, the complexes were pyrolyzed to remove the organic contents. The appropriate temperature for calcination was then studied by TG/DTA. Figures 4.5-4.8 show the TG/DTA thermograms of the obtained complexes. The broad endothermic peak centered at ~100°C on the DTA curve was mainly caused by the loss of physisorbed moisture and n-propanol, while the sharp exothermic peak with its maximum at 250°C, accompanied by an abrupt weight loss in the TGA curve, was caused by the decomposition of the organic ligand and generated char as a by-product. A slight weigh loss together with broad exothermic

effects was observed in the 300-600°C temperature range, which was ascribed to the burning of the residual organic components. Above 600°C, no weight loss was observed, showing that the appropriate calcination temperature for the preparation of the ceramic powders might be 600°C. The complexes exhibited a final weight loss ranging from ~28 to 34 wt%, as shown in the TGA curves (Figures 4.5-4.8).

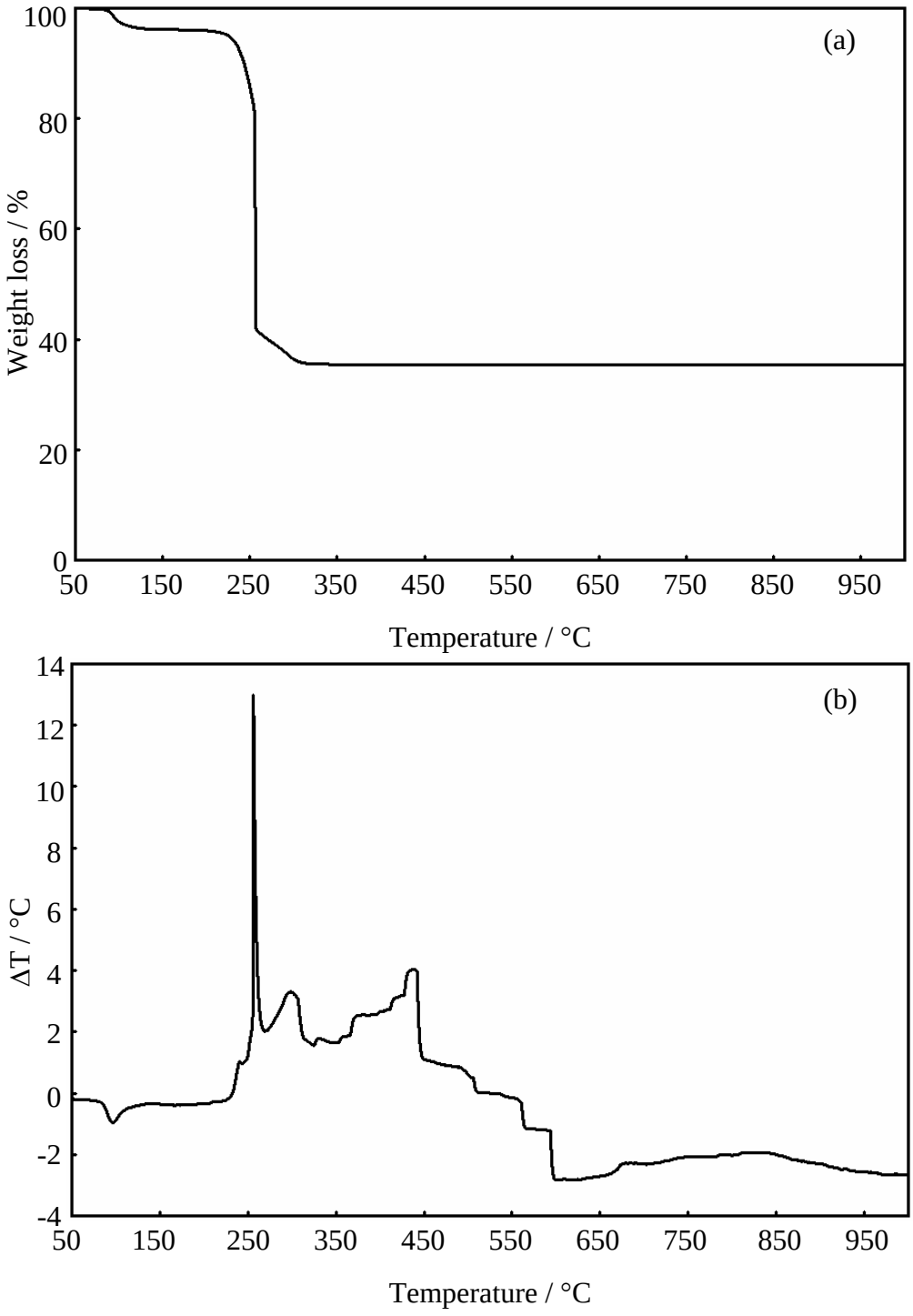


Figure 4.5 Thermogram of a metal organic complex of $CeO_2$: (a) TGA, and (b) DTA.

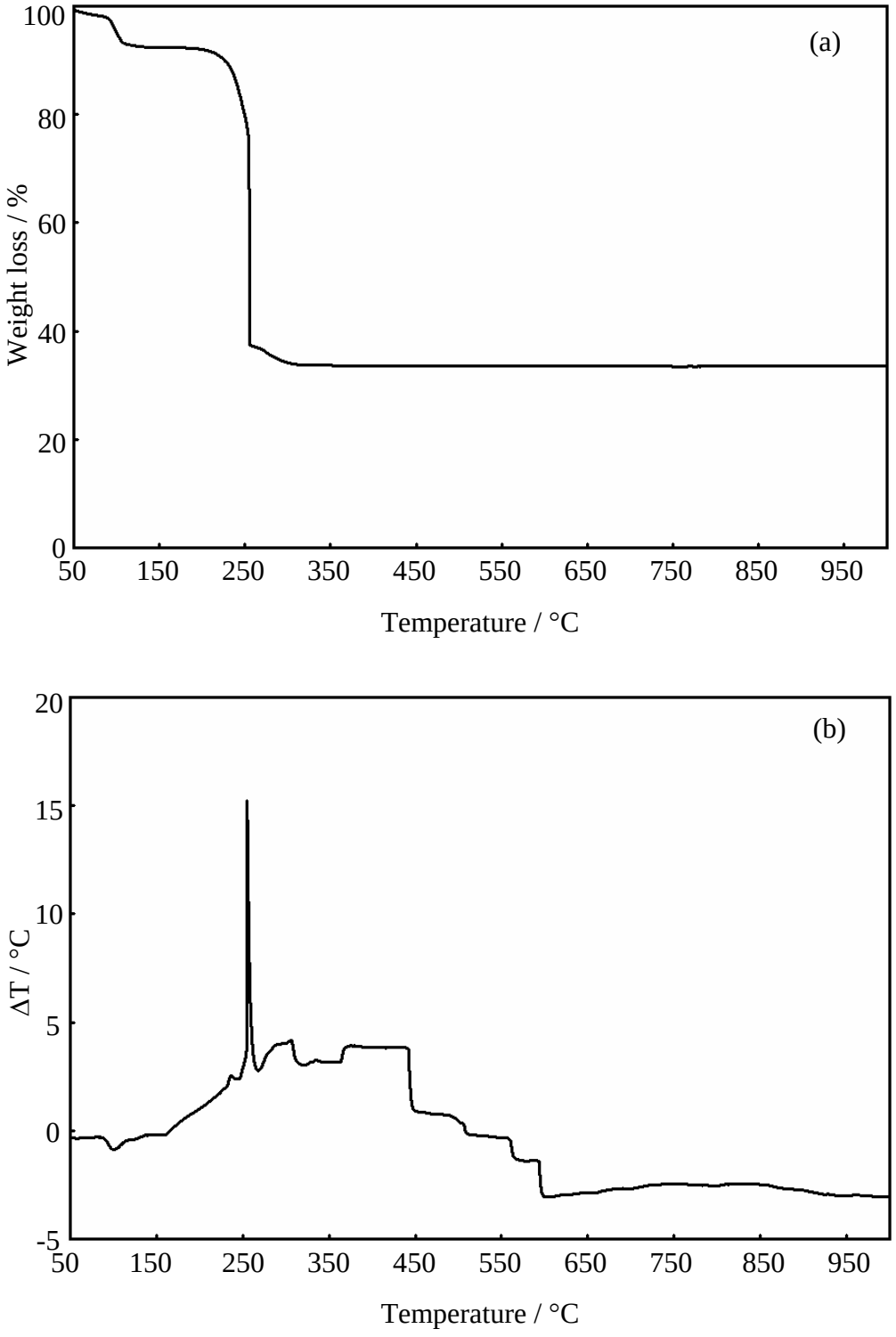


Figure 4.6 Thermogram of a 10 mole % doped gadolinium $CeO_2$ complex: (a) TGA, and (b) DTA.

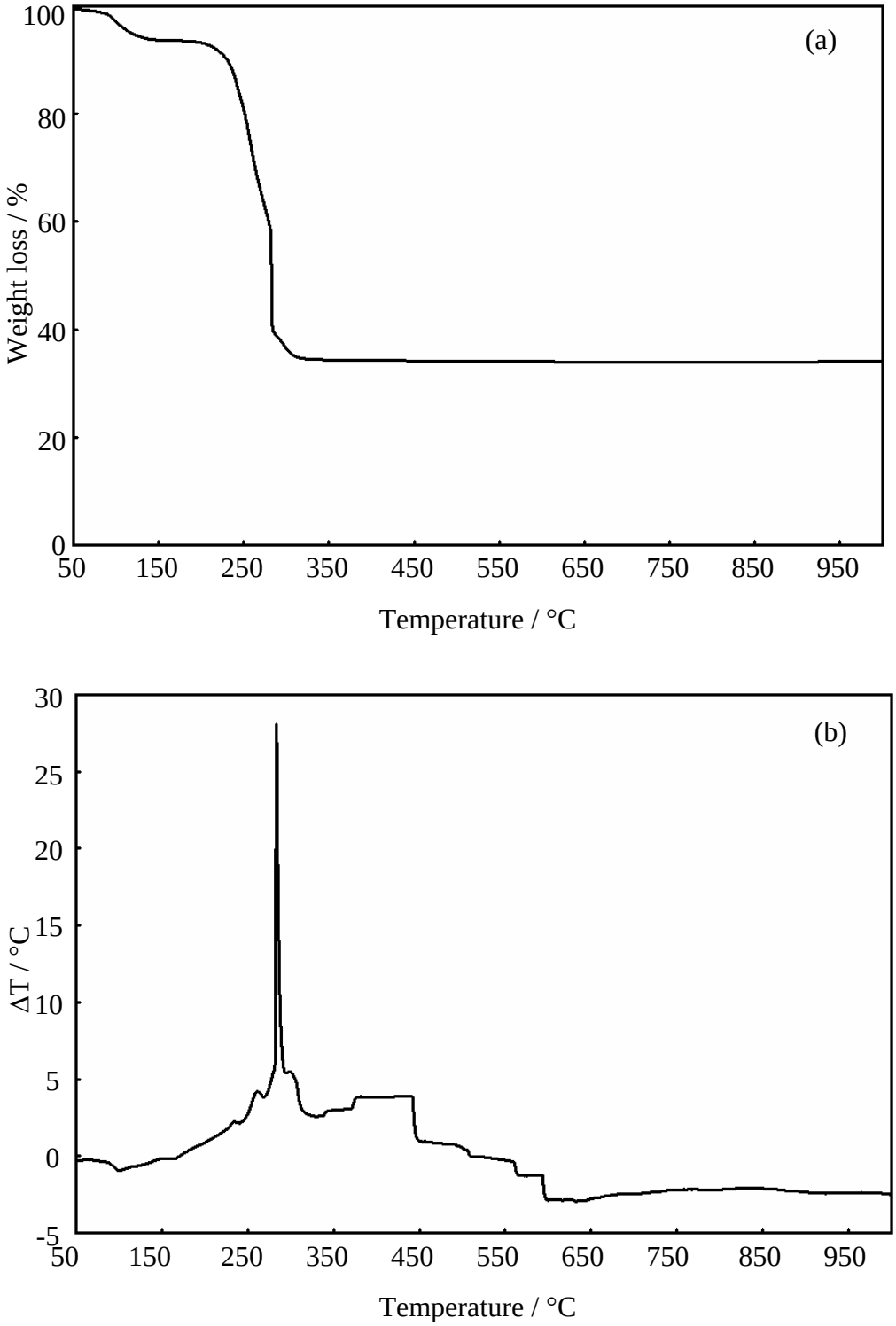


Figure 4.7 Thermogram of a 15 mole % doped gadolinium $CeO_2$ complex: (a) TGA, and (b) DTA.

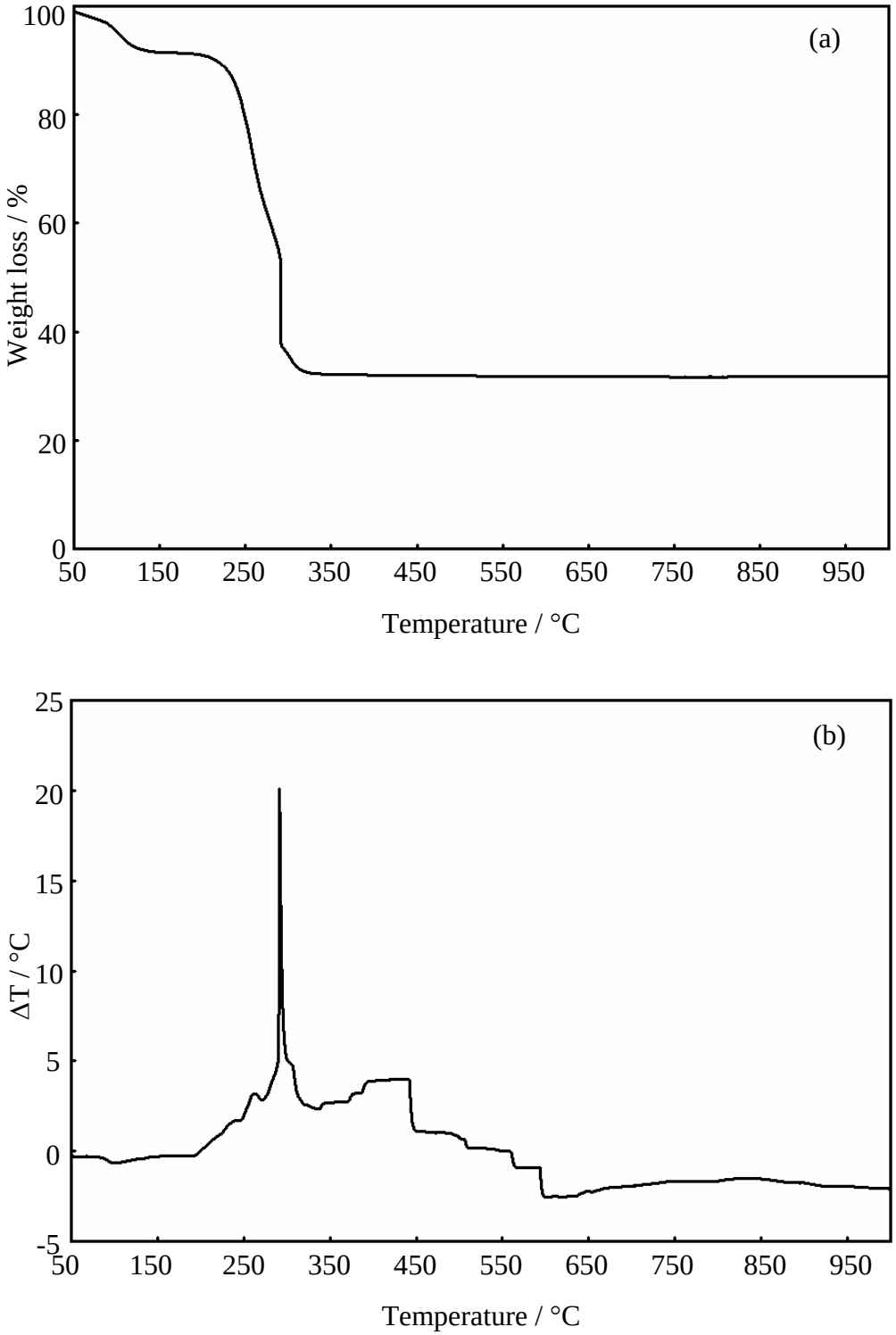


Figure 4.8 Thermogram of a 20 mole % doped gadolinium $CeO_2$ complex: (a) TGA, and (b) DTA.

4.3.2 Powder preparation and characterization

Based on the TG/DTA analysis, the complexes were calcined at 400, 600, 800, 1000 and 1200°C for 2 h in air. The obtained products were light-yellowish colored powders. Because of the organic contents in the complexes, the decomposition products, such as CO, $CO_2$, $H_2O$ and volatile hydrocarbon produced during the calcination of the complexes were difficult to escape and were retained in the resulting powders. Consequently, a gas-filled and foam-like structure was obtained.

XRD was used to characterize the powders. Figure 4.9 shows the XRD patterns of the 0GDC, 10GDC, 15GDC, and 20GDC powders at various calcination temperatures. Before calcination, all the complexes exhibited low crystallinity, as shown in Figure 4.9. In agreement with the results of TG/DTA analysis, the calcined powders of each complex at 600°C for 2 h displayed only reflections corresponding to the fluorite structure of $CeO_2$ (JCPDS Powder Diffraction File No. 34-0394). The diffraction peaks of each powder sample became sharper and narrower with increasing the calcination temperature, indicating an increase in the crystallite size. Comparing the XRD patterns of $CeO_2$ (Figures 4.9) with those of Gd-doped ceria (Figures 4.10-4.12), it was found that the XRD patterns followed the same trend. No crystalline phases corresponding to $Gd_2O_3$ could be found at any calcination temperatures for the Gd-doped complexes, indicating the direct formation of solid solutions.

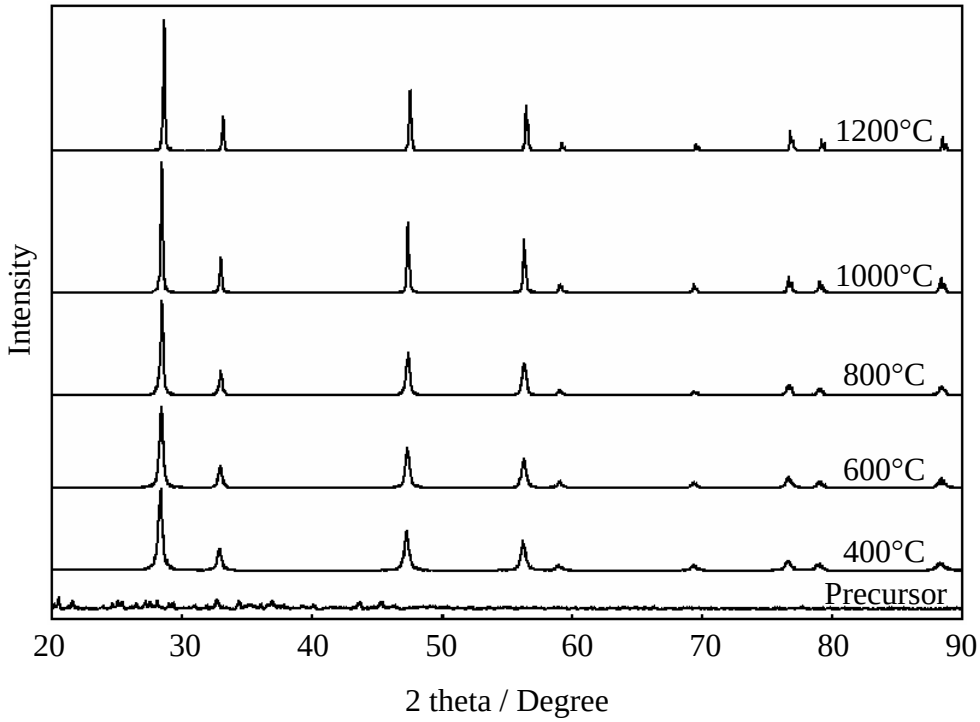


Figure 4.9 XRD patterns of 0GDC complex and 0GDC powder which calcined at 400-1200°C.

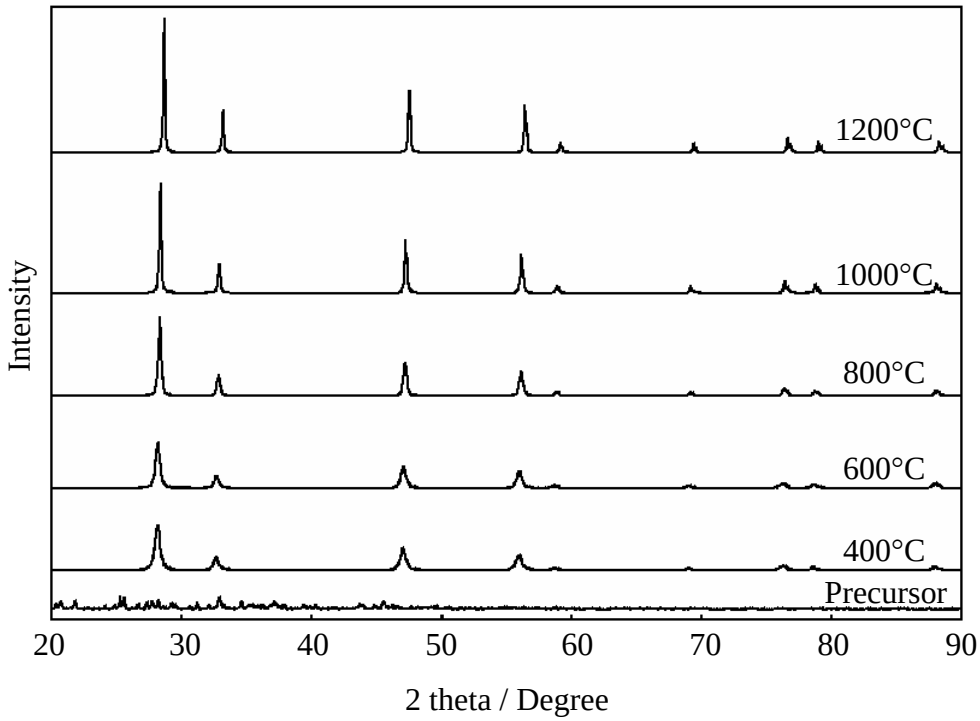


Figure 4.10 XRD patterns of 10GDC complex and 10GDC powder which calcined at 400-1200°C.

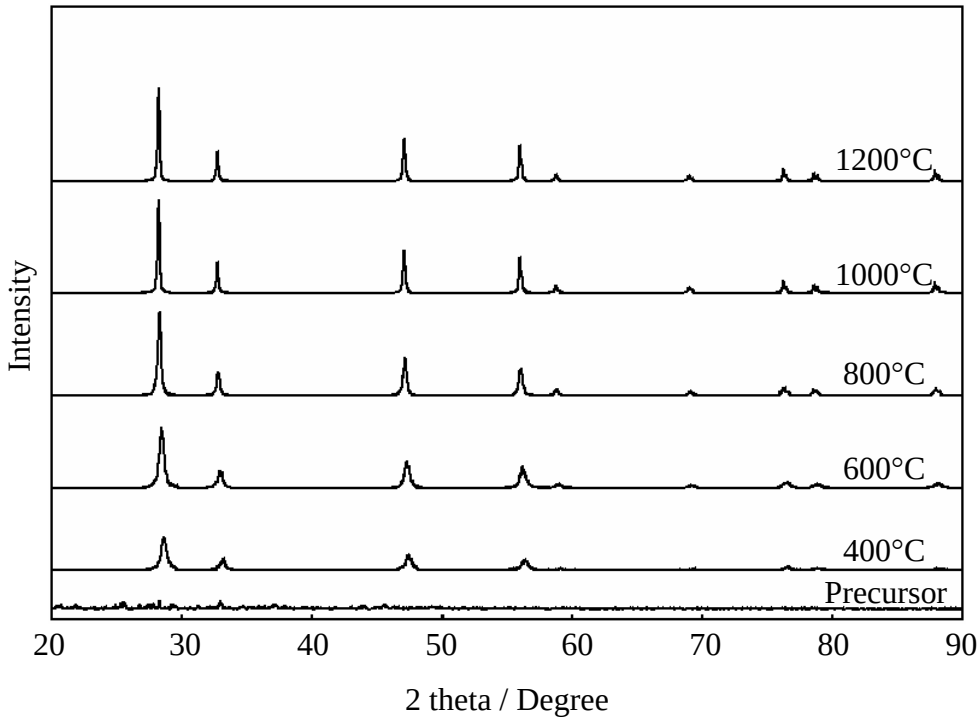


Figure 4.11 XRD patterns of 15GDC complex and 15GDC powder which calcined at 400-1200 ° C.

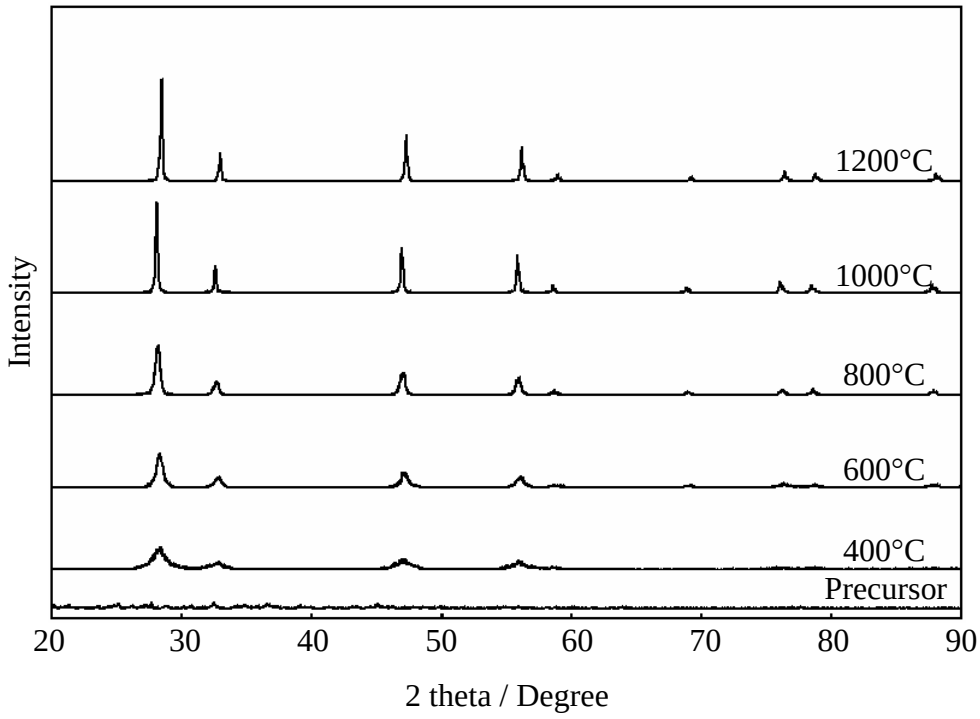


Figure 4.12 XRD patterns of 20GDC complex and 20GDC powder which calcined at 400-1200 ° C.

The specific surface area of the calcined powders is reported in Table 4.1. It was found that the surface area decreased with increasing the calcination temperature. The average particle sizes ($D_{BET}$) of the powders calcined at 600, 800, and 1000°C were calculated to be in the nanometer scale and are reported in Table 4.1. In addition, the particle size of each powder sample increased with increasing the calcination temperature.

Table 4.1 Specific surface areas and average particle sizes of 0GDC, 10GDC, 15GDC, and 20GDC powders calcined at various temperatures.

| Sample | T (°C) | Specific surface area ($m^2/g$) | $D_{BET}$(nm) |
|---|---|---|---|
| 0GDC | 600°C | 24.8 | 34 |
| | 800°C | 11.6 | 72 |
| | 1000°C | 6.2 | 134 |
| 10GDC | 600°C | 23.6 | 35 |
| | 800°C | 19.2 | 43 |
| | 1000°C | 7.5 | 111 |
| 15GDC | 600°C | 28.6 | 29 |
| | 800°C | 15.0 | 55 |
| | 1000°C | 7.8 | 106 |
| 20GDC | 600°C | 22.1 | 38 |
| | 800°C | 12.9 | 65 |
| | 1000°C | 8.6 | 97 |

The SEM micrographs of the calcined powders are shown in Figures 4.13-4.16. The powders showed a foam-like morphology at 600°C. With increasing the calcination temperature up to 1000°C, the powders exhibited blocky particles with an irregular shape, due to agglomeration occurring during calcination. The particle size ranged from submicron to larger than μm.

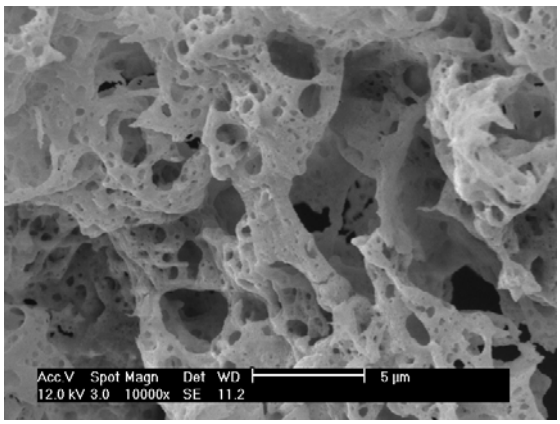


(a)

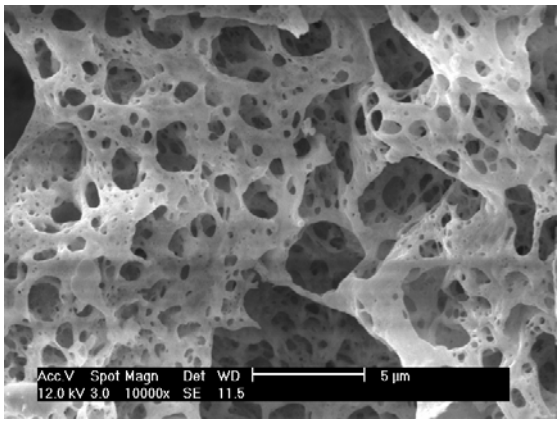


(b)

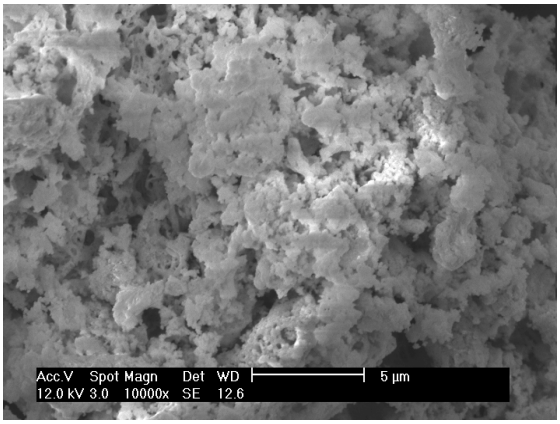


(c)

Figure 4.13 SEM micrographs of 0GDC powder calcined at: (a) 600°C, (b) 800°C, and (c) 1000°C.

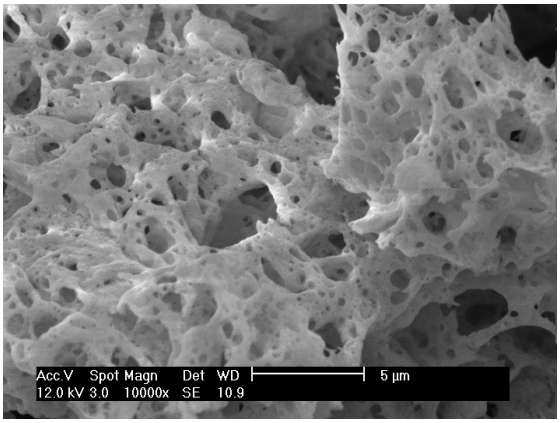


(a)

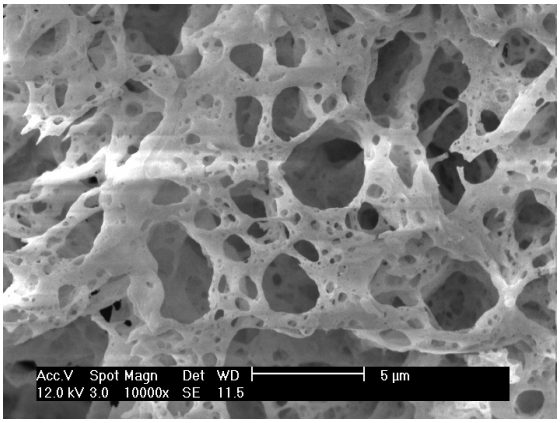


(b)

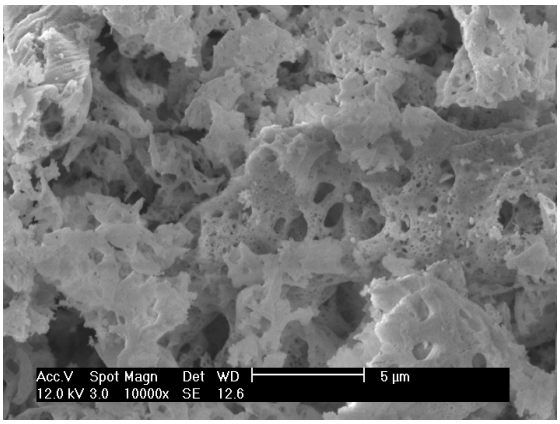


(c)

Figure 4.14 SEM micrographs of 10GDC powder calcined at: (a) 600°C, (b) 800°C, and (c) 1000°C.

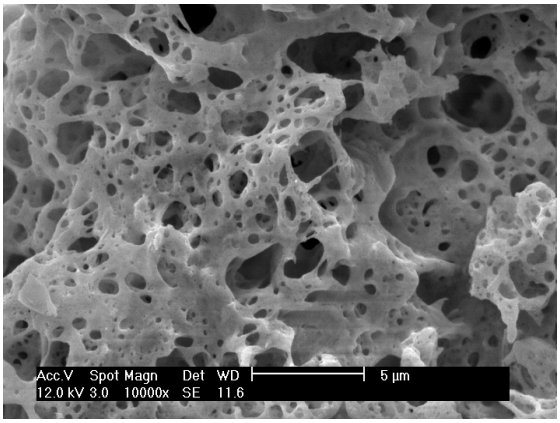


(a)

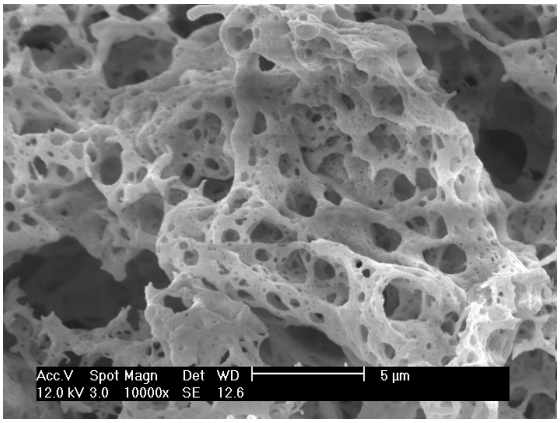


(b)

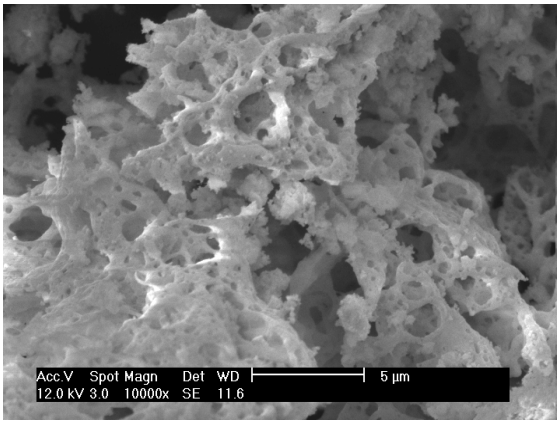


(c)

Figure 4.15 SEM micrographs of 15GDC powder calcined at: (a) 600°C, (b) 800°C, and (c) 1000°C.

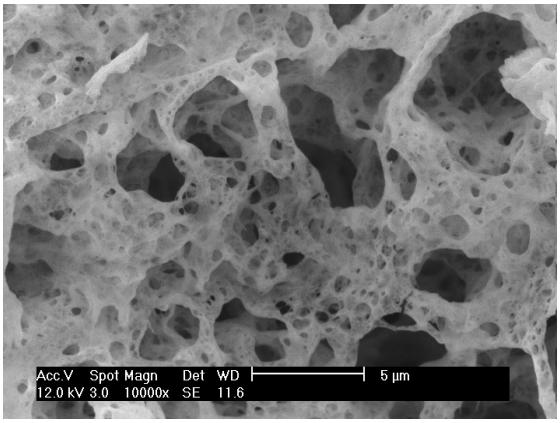


(a)

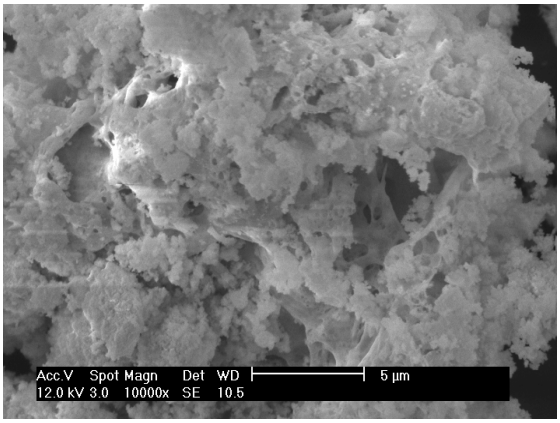


(b)

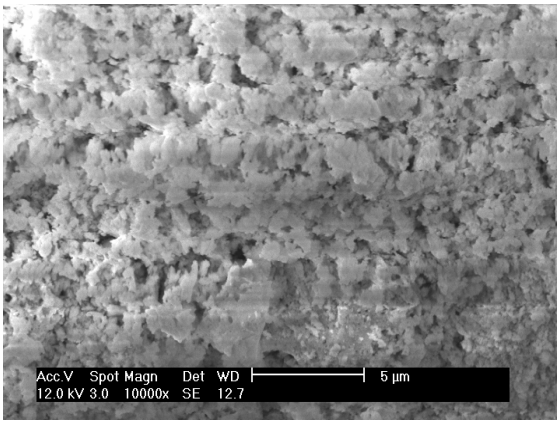


(c)

Figure 4.16 SEM micrographs of 20GDC powder calcined at: (a) 600°C, (b) 800°C, and (c) 1000°C.

4.3.3 Study of the electrochemical properties of pellets

It has been documented that oxygen ion conductivity is the main contribution to ceria based compound conductivity in air (>99.5%), being electronic conductivity negligible [4,6,13]. The samples for electrical measurement were sintered at 1500°C for 5 h to ensure a high sintered density. Moreover, phase identification was confirmed by XRD and the density of the pellets was more than 90% before measurement as shown in Table 4.2.

Table 4.2 % Theoretical density of 10GDC, 15GDC, and 20GDC pellets sintered at 1500°C

| Samples | % Theoretical density |
|---|---|
| 10GDC | 93 |
| 15GDC | 94 |
| 20GDC | 94 |

Figure 4.17 shows the typical impedance spectra of the 15GDC pellet measured at (a) 250°C, (b) 300°C, (c) 400°C, and (d) 600°C. As a general trend, two well defined semicircular arcs were observed in the complex impedance plane plots below 300°C, and two semicircles below 400°C, accompanied by a spike at low frequencies. At higher temperatures, only a spike was observed. The same trend was observed for all the samples. The features in the impedance plots can be attributed to the contribution of the bulk (B) at high frequencies, grain boundary (GB) at intermediate frequencies, and electrode polarization (E) at low frequencies, based on different relaxation frequencies and capacitances. The impedance behavior of $Ce_{1-x}Gd_xO_{2-\delta}$ ceramic pellets was similar to the trend usually observed for polycrystalline ceramic materials, as well documented in the literature [14].

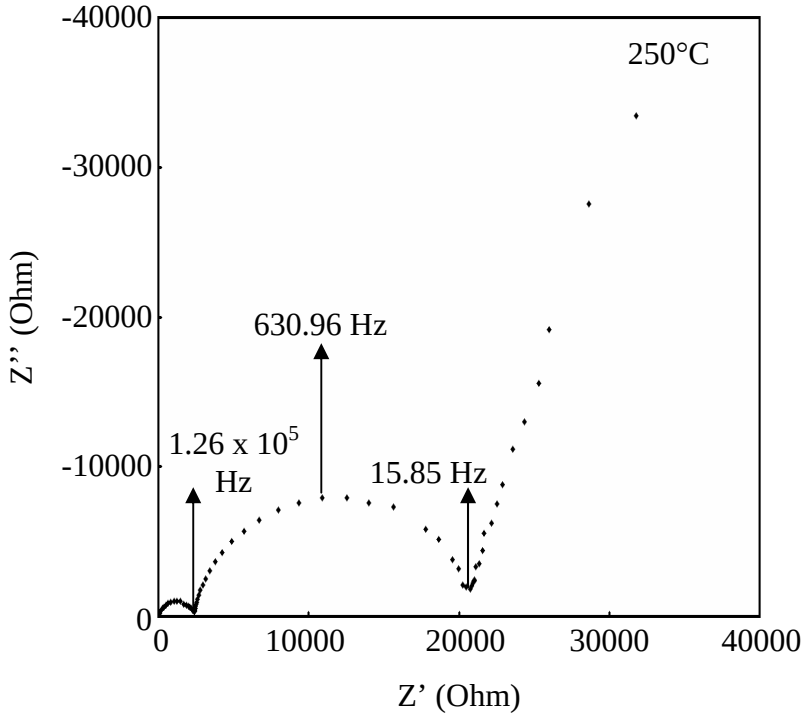
250°C
630.96 Hz
1.26 x 10^5 Hz
15.85 Hz
Z'' (Ohm)
Z' (Ohm)
-40000
-30000
-20000
-10000
0
0
10000
20000
30000
40000

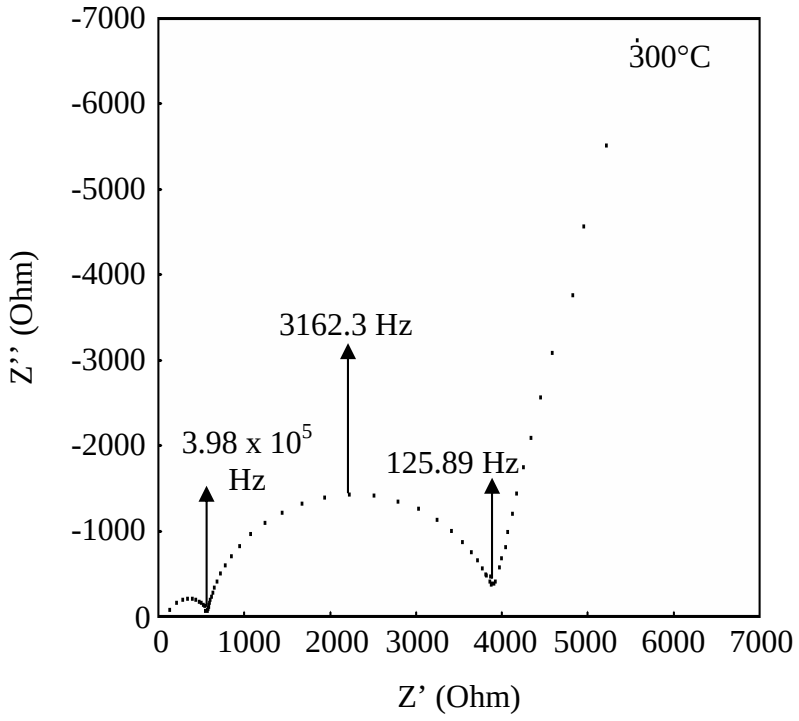
300°C
3162.3 Hz
3.98 x 10^5 Hz
125.89 Hz
Z'' (Ohm)
Z' (Ohm)
-7000
-6000
-5000
-4000
-3000
-2000
-1000
0
0
1000
2000
3000
4000
5000
6000
7000

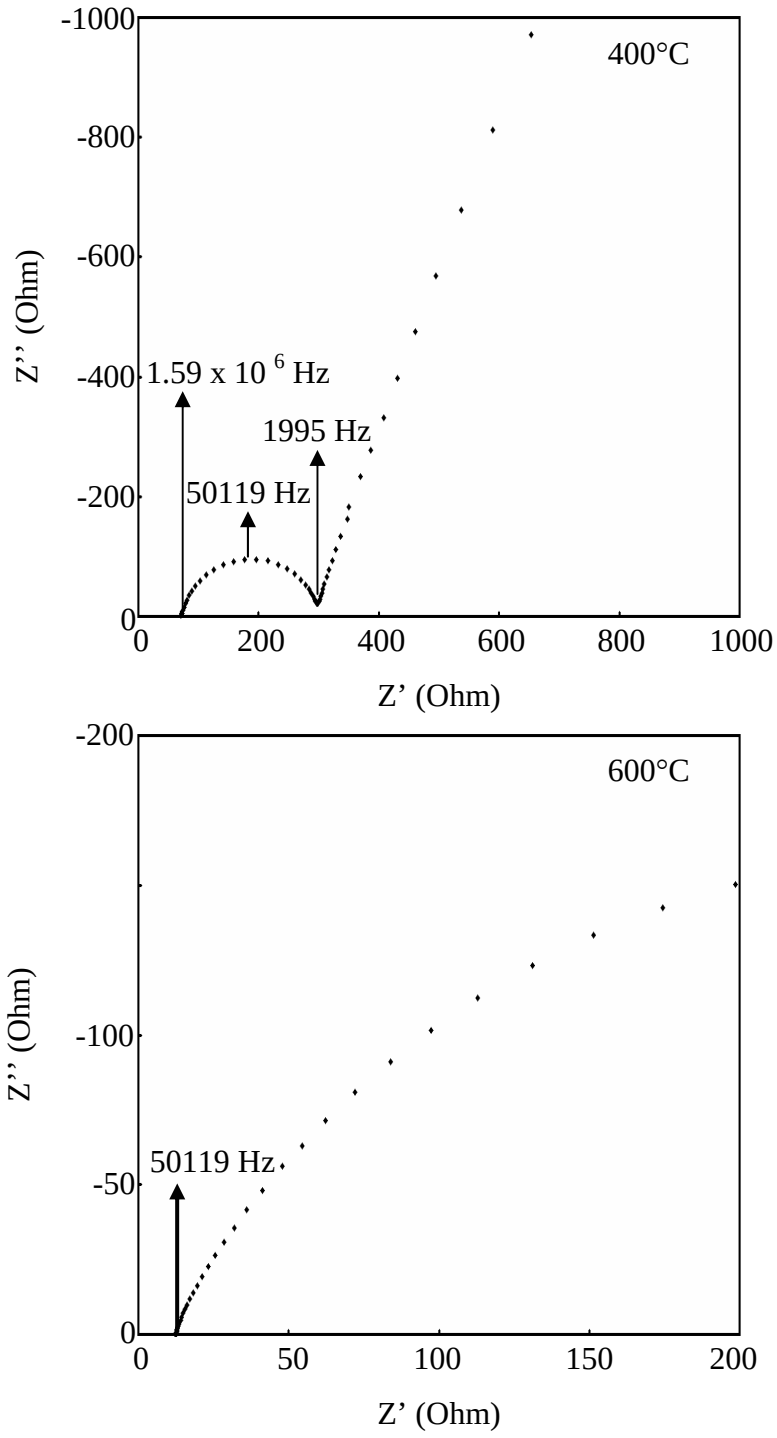


Figure 4.17 Impedance spectra of 15GDC powder which calcined at 600°C and sintered at 1500° C.

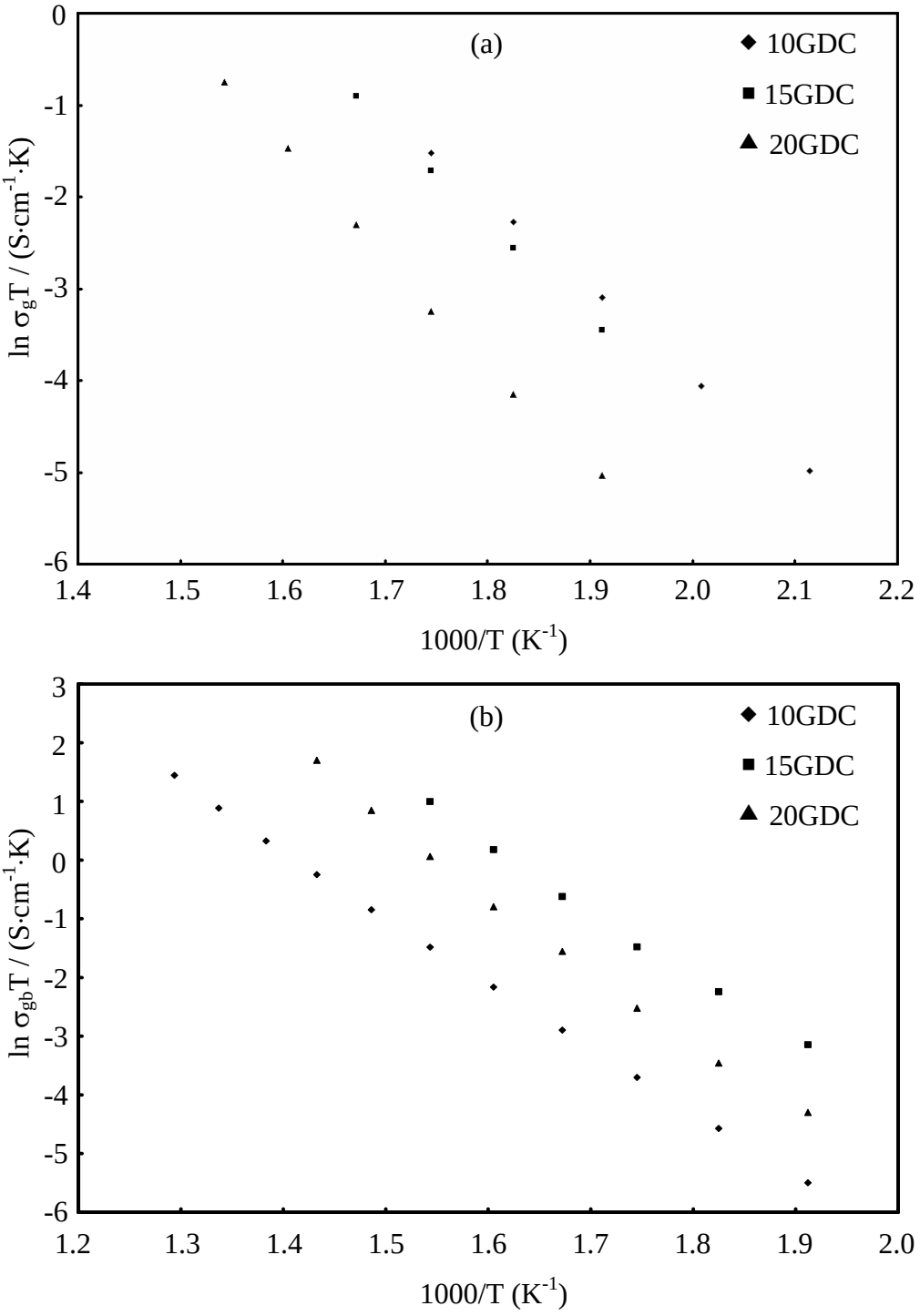


Figure 4.18 Arrhenius plots of the conductivities as a function of temperature for (a) bulk and (b) grain boundary of 10GDC, 15GDC, and 20GDC pellets.

Figures 4.18a and b show the Arrhenius plots of the apparent grain conductivity, $\sigma_g$, and the grain boundary conductivity, $\sigma_{gb}$, respectively, for 10GDC,

15GDC, and 20GDC samples. The values were taken from the impedance measurements. It has been shown that oxygen ionic conductivity in rare earth ($Re^{3+}$) doped ceria can be represented by the following equation.

$$\sigma = (A/T) \exp(-E_a/k_BT)$$

It can be seen from this figure that the bulk conductivity ($\sigma_b$) of the $Ce_{1-x}Gd_xO_{2-\delta}$ samples followed the order: x = 0.1>0.15>0.2, which is in agreement with the reported results [5]. This is expected because the increase in dopant concentration beyond x = 0.1 results in defect association, which in turn results in ionic conductivity decrease. The grain boundary conductivity ($\sigma_{gb}$) of the $Ce_{1-x}Gd_xO_{2-\delta}$ samples followed the order: x = 0.15>0.2>0.1.

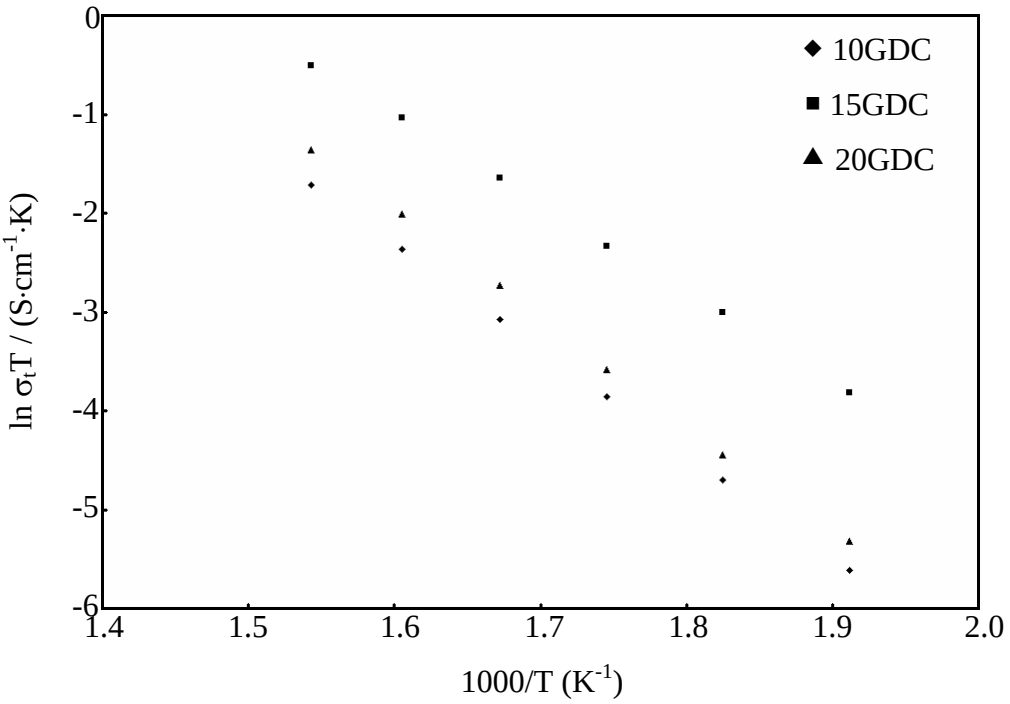


Figure 4.19 Arrhenius plots of the total conductivities as a function of temperature of 10GDC, 15GDC and 20GDC pellets.

Figure 4.19 shows the temperature dependence of the total conductivity, $\sigma_t$, for $Ce_{1-x}Gd_xO_{2-\delta}$ solid solutions. The total conductivity of the $Ce_{1-x}Gd_xO_{2-\delta}$ samples reached a maximum at x = 0.15. Usually, the maximum of the conductivity is believed to result from two opposite effects: (i) gadolinium substitution, which caused a significant increase in oxygen vacancies and thus an increase in the ionic conductivity; (ii) the interaction between dopant cations ($Gd^{3+}$) and oxygen vacancies,

which leads to a decrease in the mobility of vacancies and a subsequent decrease in the ionic conductivity. However, according to our study, it seems that the grain boundary conductivity determined the maximum in the total conductivity at x = 0.15.

Table 4.3 gives the activation energy values of all the samples. It was shown that 15GDC showed the lowest activation energy.

Table 4.3 Activation energies of 0GDC, 10GDC, 15GDC, and 20GDC pellets sintered at 1500°C

| Samples | Activation energy (eV) | | |
|---|---|---|---|
| | Bulk | Grain Boundary | Total Conductivity |
| 10GDC | 0.92 | 0.97 | 0.91 |
| 15GDC | 0.82 | 0.96 | 0.78 |
| 20GDC | 1.02 | 1.08 | 0.94 |

SEM micrographs of gadolinia doped ceria sintered at 1500°C are illustrated in Figure 4.20 (a)-(c). For 15GDCN and 20GDCN, the dense pellet obtained, but 15GDCN showed larger grain sizes corresponding to small areas of grain boundary influence the total conductivity of 15 mol% Gd doped ceria.

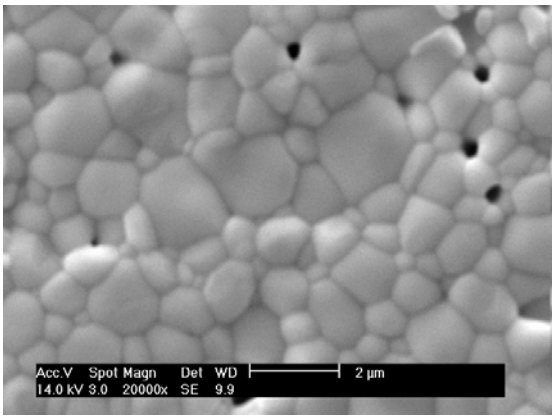


(a)

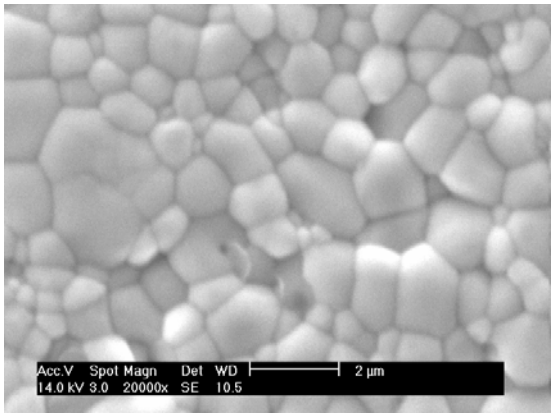


(b)

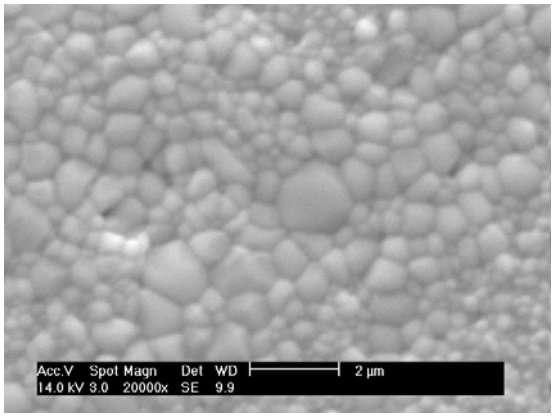


(c)

Figure 4.20 SEM micrographs of (a) 10GDC, (b) 15GDC, and (c) 20GDC pellets sintered at 1500°C for 5h.

## 4.4 Conclusions

$Ce_{1-x}Gd_xO_{2-\delta}$ (x = 0-0.2) solid solutions with the fluorite structure were prepared by the metal organic complex method. Ultrafine particles were formed. Because of the small particle size of the doped ceria, the sintering temperature needed to obtain a dense ceramic pellet was reduced substantially from 1600°C, which is required for the corresponding materials prepared by the conventional solid state methods to 1500°C. The highest conductivity was found for the x = 0.15 Gd substituted ceria ($\sigma_{600°C}$ = 0.025 S/cm).

## References

[1] B.C.H. Steele, J. Mater. Sci. 36 (2001) 1053.

[2] V.V. Kharton, A.P. Viskup, I.P. Marozau, E.N. Naumovich, Mater. Lett. 57 (2003) 3017.

[3] A. Boudgheene, Stambouli, E. Traversa, Renewable Sustainable Energy Rev. 6 (2002) 433.

[4] H.Inaba, H. Tagawa, Solid State Ionics 83 (1996) 1.

[5] B.C.H. Steele, Solid State Ionics 129 (2000) 95.

[6] F.Y. Wang, S. Chen, S. Cheng, Electrochemistry Communications 6 (2004) 743.

[7] J.V. Herle, D. Seneviratne, A.J. McEvoy, J. Eur. Ceram. Soc., 19 (1999) 837.

[8] J.M. Ralph, J. Przydatek, J.A. Kilner, T. Seguelong, Ber. Bunsen-Ges., Phys. Chem. 101 (1997) 1403.

[9] H.Yoshida, T. Inagaki, K. Miura, M. Inaba, Z. Ogumi, Solid State Ionics 160 (2003) 109.

[10] A. Laobuthee, Synthesis of $MgAl_2O_4$ spinel and its application as a humidity sensing element, A thesis submitted in partial fulfillment of requirements for the degree of Master of Science, The Petroleum and Petrochemical College, Chulalongkorn University, 1997.

[11] A. Laobuthee, S. Wongkasemjit, E. Traversa, R. M. Laine, J. Eur. Ceram. Soc., 20, 91-97 (2000).

[12] B. Ksapabutr, E. Gulari, and S. Wongkasemjit, Materials Chemistry and Physics, 83, 34-42 (2004).

[13] G.M. Christie, F.P.F. van Berkel, Solid State Ionics 3 (1996) 17.

[14] J. R. Macdonald, Impedance spectroscopy, Wiley & Sons, New York, USA, 1987.

# CHAPTER V
# NEW ROUTE FOR SAMARIA DOPED CERIA PREPARATION FROM METAL ORGANIC COMPLEX FOR SOLID OXIDE FUEL CELL ELECTROLYTE


## Abstract

Samaria doped ceria (SDC) powders as solid electrolyte ceramics have been successfully prepared using a metal organic complex method with triethanolamine (TEA) as a novel ligand. The SDC powders synthesized with various samaria contents have been characterized by X-ray diffractometry, scanning electron microscopy, and Brunauer-Emmett-Teller analysis (BET). The appropriate temperature for SDC powder calcination was found to be 600 °C. By sintering the SDC powders, highly dense ceramics were obtained at temperatures lower than 1600°C, which is lower than a common sintering temperature. The changes of crystal structure and electrical conductivity with the samaria content were also investigated.


## 5.1 Introduction

Doped ceria can be prepared by a variety of techniques such as the conventional ceramic route, solid-state reaction [1,2], co-precipitation [3,4], sol-gel formation [5], hydrothermal technique [6], and metal organic complex [7]. Among these processes, the metal organic complex method which is a one step process is the simplest method, saving in time and energy consumption. The calcined powders are generally homogeneous, with high purity, and high surface areas.

In the chapter 4, the metal organic complex method was used to prepare gadolinia doped ceria (GDC) powders. Here, we used the same synthesis to prepare samaria doped ceria (SDC) solid solutions. The SDC powders were prepared from the metal organic complexes as starting materials. The effect of dopant contents and calcination temperatures on the physical, chemical, and electrical properties of the SDC powders was investigated.

## 5.2 Experimental procedure

### 5.2.1 Materials synthesis

Cerium(III) nitrate hexahydrate [$Ce(NO_3)_3 \cdot 6H_2O$, 99.50% purity] was purchased from Acros Organics. Samarium(III) nitrate hexahydrate [$Sm(NO_3)_3 \cdot 6H_2O$, 99.9% purity] was purchased from Sigma-Aldrich, Inc. Triethanolamine [TEA, $N(CH_2CH_2OH)_3$, 98% purity] and n-propanol [$CH_3CH_2CH_2OH$, 99.5% purity] were obtained from Carlo Erba (Barcelona). All starting materials were used without further purification.

Samaria doped ceria (SDC) powders, $Ce_{1-x}Sm_xO_{2-\delta/2}$ with x = 0.10 (10SDC), 0.15 (15SDC), and 0.20 (20SDC) were prepared by the thermal decomposition of metal organic complexes. Metal nitrates in the stoichiometric ratios were dissolved in n-propanol. Then, TEA was added in the solution. The molar ratio between total cations and TEA was 1:1. The solutions were distilled for 3 hours until the reaction completed yielding precipitated complexes. The complexes were separated by evaporating n-propanol solvent under vacuum.

### 5.2.2 Materials characterization

Simultaneous thermogravimetric and differential thermal analysis (TG/DTA) was performed on the complexes using TGA/SDTA analyzer (Model TGA/SDTA 851e, Mettler Toledo). The samples, placed in an alumina crucible, were heated under air atmosphere from 50 to 1000°C with a heating rate of 5°C/min. To study the effect of the calcination temperature on the powder morphology, the complexes were then calcined at different temperatures (600, 800, and 1000°C) for 2 hours. X-ray diffraction (XRD) analysis was carried out at room temperature in an X-ray diffractometer (D8 Advance, Bruker-AXS) operating at 40 kV and 40 mA using Ni filter and CuKα radiation. Diffraction patterns were recorded in the 2θ range of 20-90° by step scanning with a step interval of 0.02° and a scanning time of 2 s for each step. The crystallite size (D) of the calcined powders was determined by using the Scherrer equation: $D = 0.9\lambda/\beta\cos\theta$ where λ is the wavelength of the X-rays (1.5406 Å), and β is the corrected peak at full width at half-maximum (FWHM) intensity. The specific surface area ($S_{BET}$) of the calcined powders was measured by using a surface area analyzer (Autosorb 1c, Quantachrome) based on BET (Brunauer-Emmett-Teller) principle with nitrogen adsorption. From the specific surface area analysis, the particle sizes were calculated using the equation: $D_{BET} = 6000/\rho S_{BET}$,

where the $D_{BET}$ is the average particle size in nanometer, ρ is the theoretical density of $CeO_2$ (7.211g/$cm^3$), and $S_{BET}$ is the specific surface area of the powders expressed in $m^2$/g. The morphology of the calcined products was observed by using scanning electron microscope (SEM, JEOL-JSM-6301F). Gold electrodes were coated on both sides of the dense samples and sintered at 1500°C for 5 hours. Impedance spectroscopy (Solartron1260) measurements were carried out in dry air in a temperature range between 250 and 700°C and over a frequency range of 0.1 Hz to 10 MHz.

**5.3 Results and discussion**

The cerium(III) nitrate, samarium(III) nitrate, and TEA are readily dissolved in n-propanol. After the clear solution was distilled for 3 hours, the precipitation of the complexes occurred. The yellowish powders of the complexes were obtained when the solvent was removed.

To obtain the appropriate temperature for calcination, TG/DTA analysis of the complexes was carried out. Figure 5.1 shows simultaneous TGA and DTA curves obtained for the 10SDC complex. The first mass loss around 100°C resulted from the removal of physisorbed moisture and residual solvent. The second weight loss happened in temperatures ranging between 125°C and 350°C. A large weight loss in the TGA curve and a sharp strong exothermic peak in DTA were ascribed to the decomposition of TEA groups. In the third stage, a gradual weight loss process occurred until around 600°C, which possibly resulted from the further release of organic residues or carbon in ceria at high temperatures. The total weight loss was 68.3 wt%. Moreover, 15SDC and 20SDC also showed the same trend. The total weight loss of 15SDC and 20SDC were 67.4 and 67.1 wt%, respectively.

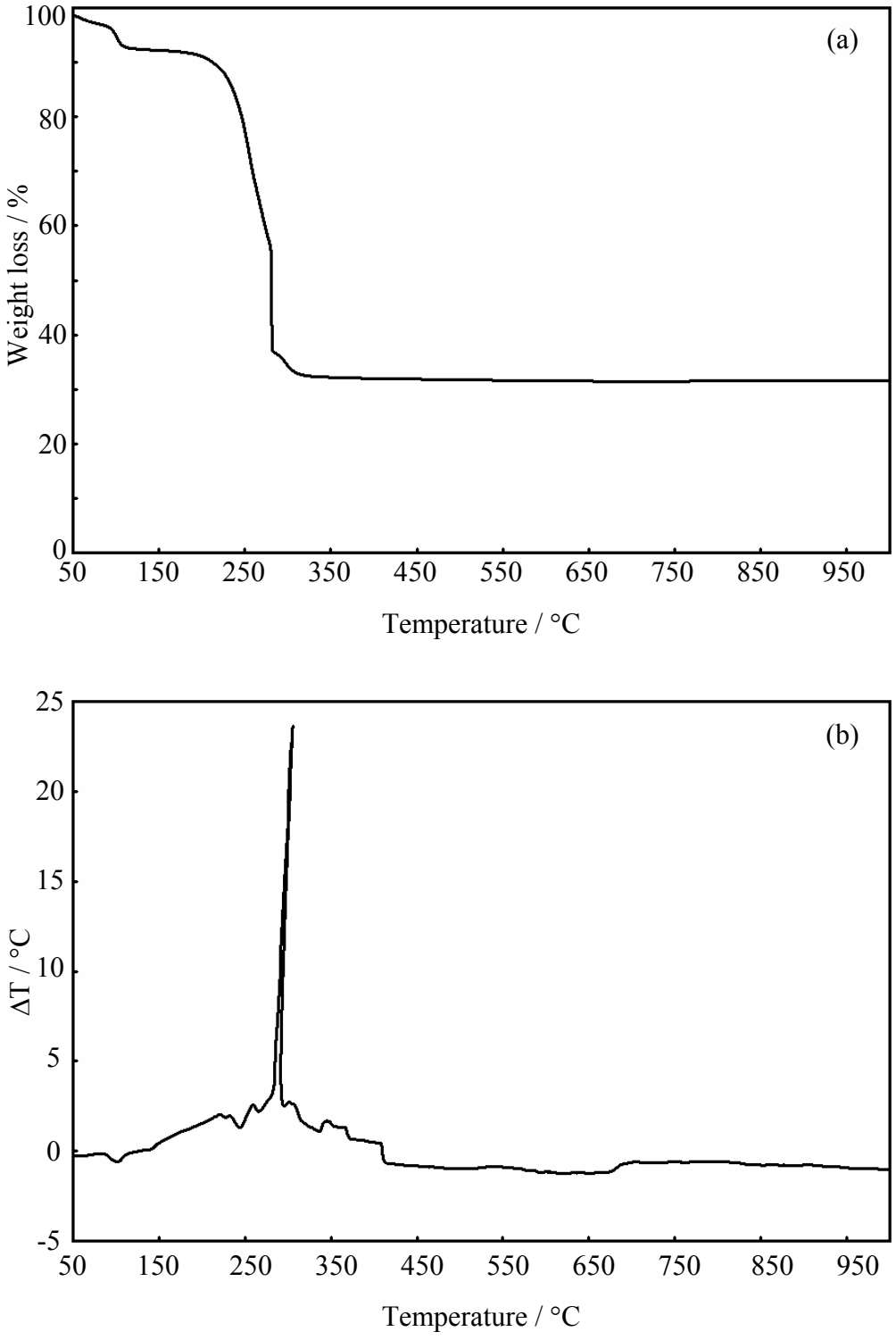


Figure 5.1 TGA curve (a) and DTA curve (b) of a 10 mole% samarium doped $CeO_2$ complex.

Figure 5.2 shows the XRD patterns of the products calcined at 600°C for the different samaria contents. The data show that 10SDC, 15SDC, and 20SDC exhibited the same phase and structure corresponding to the cubic fluorite structure $CeO_2$ (JCPDS. No. 34-0394). Moreover, Figure 5.3 shows the XRD patterns of 10SDC powders obtained by calcining the complex at different temperatures in air for 2 h. The characteristic peaks corresponding to (111), (200), (220), (311), (222), (400), (331), (420), (422) planes located at 2θ = 28.494°, 33.021°, 47.414°, 56.247°, 58.988°, 69.273°, 76.551°, 78.924°, and 88.230°, respectively are very close to the ones of the face-centered cubic $CeO_2$ (JCPDS No. 34-0394), indicating that all the as prepared powders have the cubic fluorite structure. At the same time, all the peaks became stronger and sharper with increasing the calcination temperature. This phenomenon was also observed for 15SDC and 20SDC.

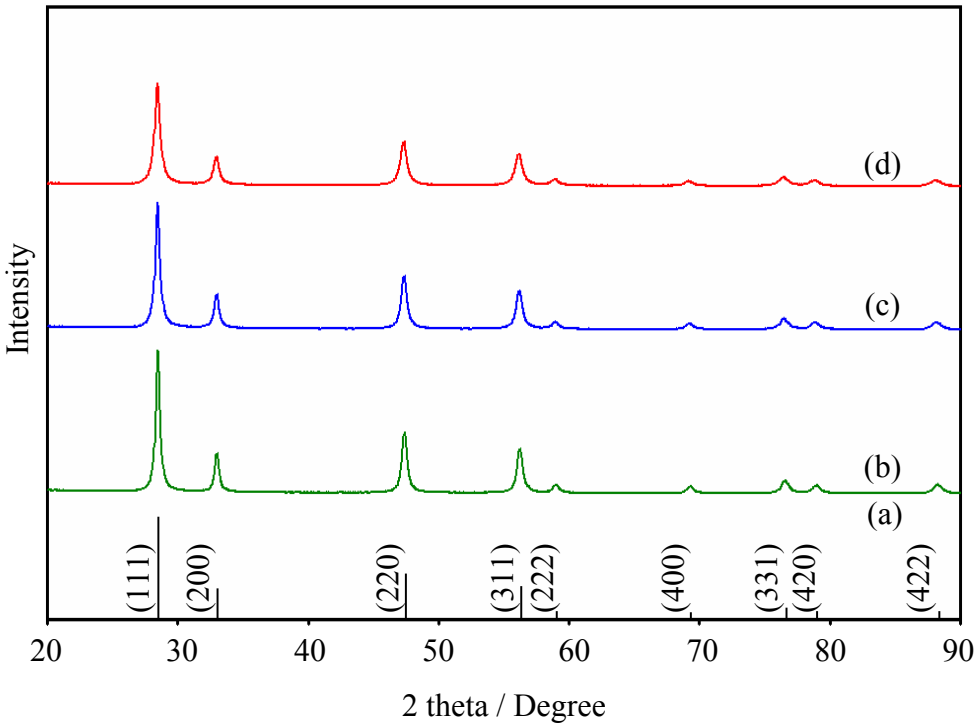


Figure 5.2 XRD patterns of (a) standard $CeO_2$ No. 34-0394 (cubic fluorite structure), and powders obtained from complexes calcined at 600°C, (b) 10SDC, (c) 15SDC, and (d) 20SDC.

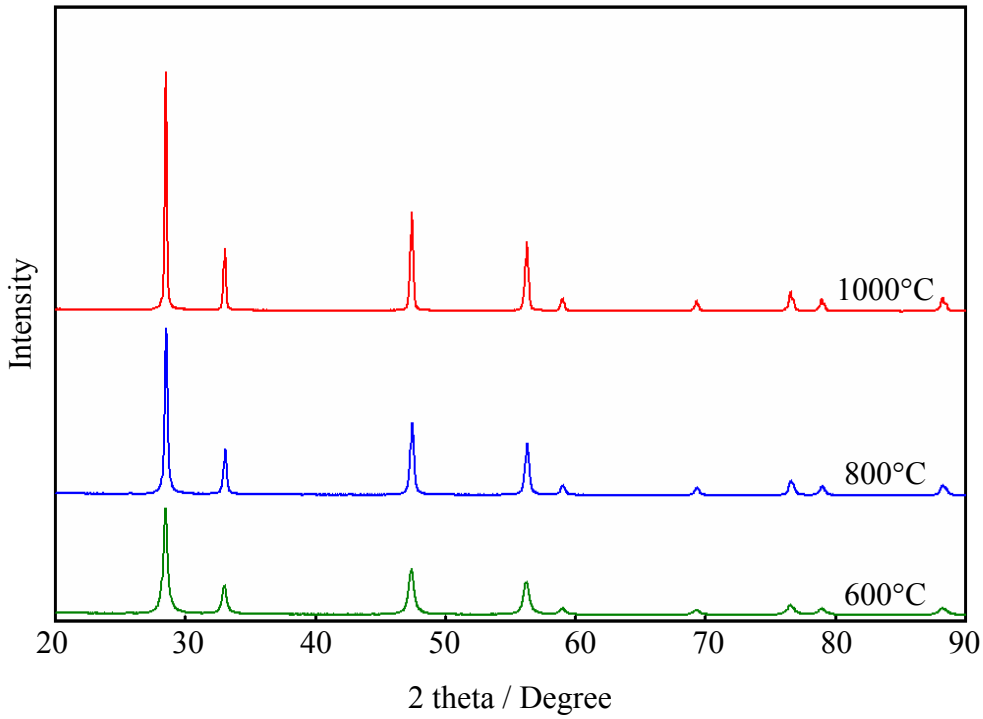


Figure 5.3. XRD patterns of 10SDC powder calcined at 600, 800, and 1000 °C.

Table 5.1 gives some physical characteristics of the 10SDC, 15SDC, and 20SDC powders calcined at 600°, 800°, and 1000°C for 2 h. From the XRD results, it can be concluded that the crystallite size increased with increasing the calcination temperature. Moreover, with increasing the calcination temperature, the specific surface area ($S_{BET}$) decreased and the particle size ($D_{BET}$) increased.

Figure 5.4 shows the SEM micrographs of the 10SDC particles obtained calcining the complex at different temperatures for 2 h. It can be seen that the ceria particles calcined at 600°C and 800°C displayed a foam-like morphology (Fig. 5.4(a and b)), while the ceria calcined at 1000°C (Fig. 5.4(c)) exhibited blocky particles with irregular shape, due to agglomeration and sintering occurring during calcination. In addition, 15SDC and 20SDC powders showed morphologies similar to those observed for 10SDC samples.

Table 5.1 Specific surface areas ($S_{BET}$), average particle sizes ($D_{BET}$) and crystallite size of 10SDC, 15SDC, and 20SDC powders calcined at various temperatures

| Samples | Calcination temperature (°C) | $S_{BET}$ ($m^2/g$) | $D_{BET}$ (nm) | Crystallite size (Å) |
|---|---|---|---|---|
| 10SDC | 600 | 18.3 | 45 | 227 |
| | 800 | 13.5 | 62 | 326 |
| | 1000 | 6.9 | 120 | 505 |
| 15SDC | 600 | 19.6 | 42 | 119 |
| | 800 | 11.1 | 75 | 288 |
| | 1000 | 5.9 | 141 | 462 |
| 20SDC | 600 | 16.8 | 50 | 165 |
| | 800 | 10.0 | 83 | 274 |
| | 1000 | 7.2 | 116 | 687 |

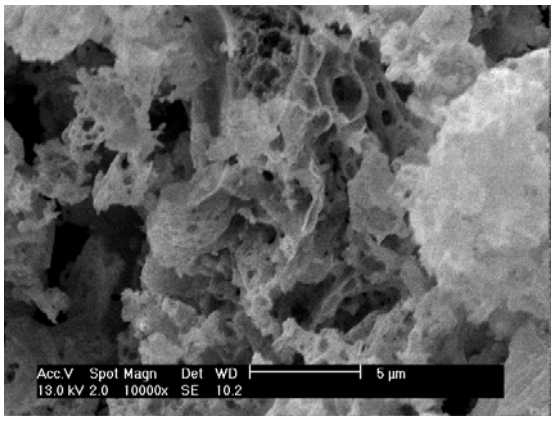


(a)

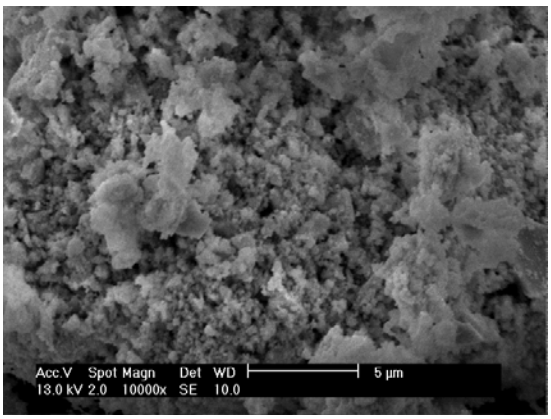


(b)

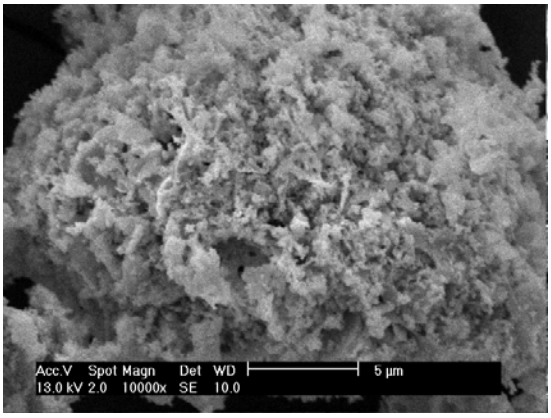


(c)

Figure 5.4 SEM micrographs of 10SDC powder calcined at (a) 600, (b) 800, and (c) 1000°C.

The impedance spectroscopy for pellets with the three compositions $Ce_{1-x}Sm_xO_{2-\delta/2}$ ($0<x<0.2$) were measured in the frequency range between 10 MHz and 0.1 Hz at temperatures between 250 and 700°C.

Figure 5.5 shows the variation of the total specific conductivity ($\sigma_t$) as a function of temperature for sample with different Sm content in $Ce_{1-x}Sm_xO_{2-\delta/2}$. At all the temperatures, the maximum total conductivity was seen for the sample with x = 0.15. The Arrhenius plots of the total conductivity were found to be linear for all the compositions.

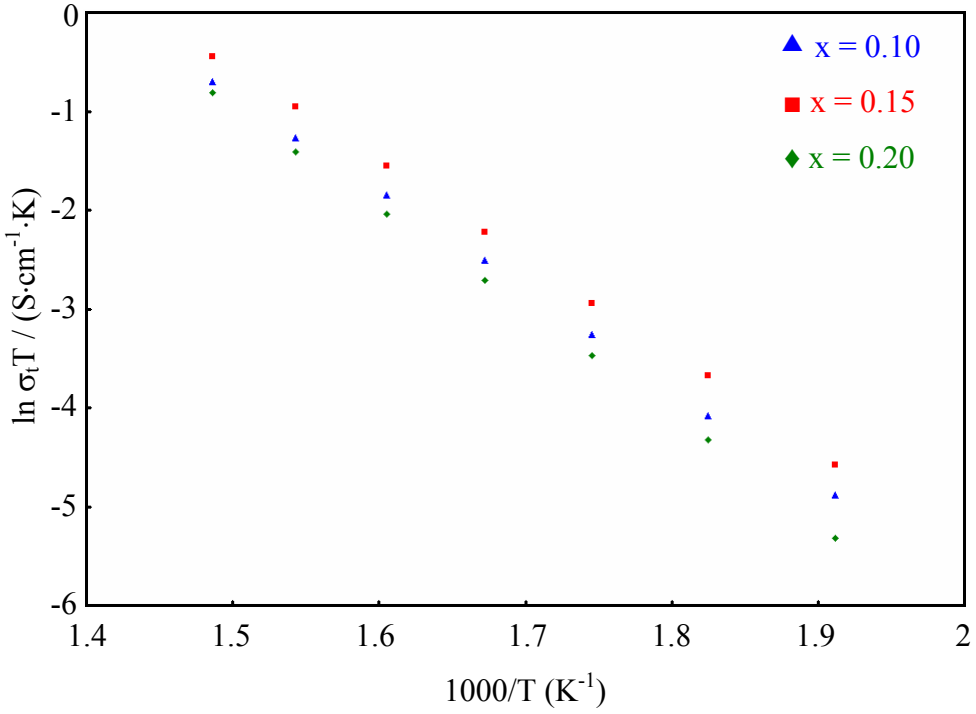


Figure 5.5 Arrhenius plots of the total conductivities as a function of temperature of 10SDC, 15SDC, and 20SDC pellets.

The activation energies for total conduction were found to be 0.85, 0.84, and 0.91 eV for the compositions x = 0.1, 0.15 and 0.2, respectively. The minimum activation energy was observed for the sample with x = 0.15.

### 5.4. Conclusions

Samaria doped ceria powders with nominal composition of $Ce_{1-x}Sm_xO_{2-\delta/2}$ where $0.1\leq x\leq 0.2$ were successfully prepared from the thermal decomposition of metal organic complexes. The crystal structure of all the samples calcined at 600 °C was

fluorite, showing the formation of ceria based solid solutions. The largest conductivity was observed for the $Ce_{0.85}Sm_{0.15}O_{2-\delta/2}$ samples.

**References**

[1] Z. Zhan, T. L. Wen H. Tu, and Z. Y. Lu, J. Electrochem. Soc. 148 (2001) A427.

[2] J. Ma, T.S. Zhang, L.B. Kong, P. Hing, and S.H. Chan, J. Power Sources 132 (2004) 71.

[3] Y.P. Fu, S.B. Wen, and C.H. Lu, J. Am. Ceram. Soc. 91 (2008) 127-131.

[4.] D. Ding B. Liu, Z. Zhu, S. Zhou, and C. Xia, Solid State Ionics (2007).

[5] R.O. Fuentes, and R.T. Baker. Int. J. Hydrogen Energy 33 (2008) 3480.

[6 D. Zhao, E. Han, X. Wu, and H. Guan, Mater. Lett. 60 (2006) 3544.

[7] A. Laobuthee, S. Wongkasemjit, E. Traversa, and R. M. Laine, J. Eur. Ceram. Soc., 20, 91-97 (2000).

# CHAPTER VI
# PREPARATION OF GADOLINIA DOPED CERIA FROM THE THERMAL DECOMPOSITION OF METAL COMPLEXES PREPARED USING CHLORIDES


## Abstract

$Ce_{1-x}Gd_xO_{2-\delta}$ where x = 0, 0.10, 0.15 and 0.20 were prepared from the thermal decomposition of cerium complexes, prepared using chloride as starting materials. The structure of the complexes, such as [Ce(TEA)] and [Ce(TEA)Cl], was determined by FTIR and MS. To prepare gadolinia doped ceria powders, the complexes were calcined at 600, 800, and 1000°C for 2 h in air. The physical properties of the obtained powders were characterized by TGA, XRD, BET, and SEM. The electrical properties of gadolinia doped ceria were studied using impedance spectroscopy measurement. Ceria doped with 15 mol% gadolinium exhibited the largest ionic conductivity ($\sigma_{600°C}$ = 0.030 S/cm).


## 6.1 Experimental procedure

### 6.1.1 Metal complex preparation

The cerium complexes with the composition of $Ce_{1-x}Gd_xO_{2-\delta}$ (x = 0 (0GDCCL), 0.10 (10GDCCL), 0.15 (15GDCCL), and 0.20 (20GDCCL)) were prepared. The stoichiometric ratios of $CeCl_3 \cdot 7H_2O$ (Acros Organics, 99.0% purity) and $GdCl_3 \cdot 6H_2O$ (Acros Organics, 99.0% purity) were mixed in n-propanol (Carlo Erba, 99.5% purity). Triethanolamine (TEA, Carlo Erba, 98% purity) was then added to the chloride solution in the molar ratio of TEA to metal chloride as 1:1. The mixtures were then heated to distill off n-propanol and crystallization water for 3 h. The mixtures were evaporated to remove some organic solvent and obtain the white powder of cerium complexes. The obtained complexes were characterized using fourier transform infrared spectrophotometer (FTIR, Perkin-Elmer system 2000 FTIR) and electrospray ionization mass spectrometer (ESI-MS, Bruker Esquire mass spectrometer) to identify the possible structure of the obtained complexes. The thermal decomposition of the complexes was studied by simultaneous thermogravimetric/differential thermal analysis which carried out with a TGA/SDTA

analyzer (Model TGA/SDTA 851e, Mettler Toledo), at a heating rate of 5°C/min under the air condition and the temperature range 50-1000°C.

6.1.2 Powder preparation and characterization

All the metal complexes were calcined in an alumina crucible at 600, 800, and 1000°C for 2 h to obtain the ceramic powders. Calcined powders were studied by X-ray diffraction (XRD) using a Bruker (Cu-Kα radiation). Diffraction patterns were recorded over a range of 2θ angles from 20 to 90° in a step-scanning mode (0.02° steps with a step-counting time of 2 s). The crystalline phase was identified from the Joint Committee on Powder Diffraction Standard (JCPDS) file No. 34-0394. The crystallite size, D, of the calcined powders was estimated using the Scherrer equation; $D = 0.9\lambda/\beta\cos\theta$, where λ is the wavelength of the X-ray (1.5418 Å), θ is the scattering angle of the main reflection (111) and β is the corrected peak at full width at half-maximum (FWHM) intensity.

Specific surface area measurements were carried out using Brunauer-Emmett-Teller (BET) analysis by nitrogen adsorption isotherms at 77 K using a Micromeritics ASAP 2020 surface analyzer and a value of 0.162 $nm^2$ for the cross-section of the nitrogen molecule. Samples were degassed at 350°C under nitrogen vacuum for 20 h before measurement.

The powder morphology was observed using a scanning electron microscope (SEM, XL30 series, Phillips) operating at an acceleration voltage of 20 KV and magnification values in 10000x to identify the powder microstructures. Samples were mounted on alumina stubs using a carbon tape and then sputter coated with Au to avoid particle charging.

6.1.3 Electrochemical characterization

The powders were uniaxially pressed into pellets under a pressure of 30 MPa, and subsequently isostatistically pressed at 200 MPa. The resulting pellets were sintered in air at 1500°C for 5 h in order to obtain the maximum density. The Archimedes method was used to determine the bulk density of the sintered ceramic pellets. Normally, the pellets were found to have a density above 90% of their theoretically determined density.

The grain size and morphology of the pellets measured were examined using a Phillips XL30 series. The pellets were first polished before thermal etching at 1400°C in air.

The electrical conductivity of the pellets was measured on the sintered ceramic pellets. Gold paste was painted onto two faces of the pellets to act as electrodes. The pellets were then fired at 800°C for 2 h in air. Ac impedance spectra were measured in air with a ZPlot™ (National Instruments) software and a Solartron SI 1260 impedance analyzer. The pellets were heated during the measurement and a thermocouple was placed right next to the samples. The frequency range was measured at 0.1 Hz to 10 MHz.

## 6.2 Results and discussion

### 6.2.1 Metal complex characterization

The stoichiometric ratios of $CeCl_3 \cdot 7H_2O$ and $GdCl_3 \cdot 6H_2O$ were dissolved in n-propanol to obtain a clear solution. TEA was added to form the cerium complexes. After completing the reaction, the homogeneous milky solution of cerium complexes was obtained after distillation. A white powder was obtained after removing the organic solvent.

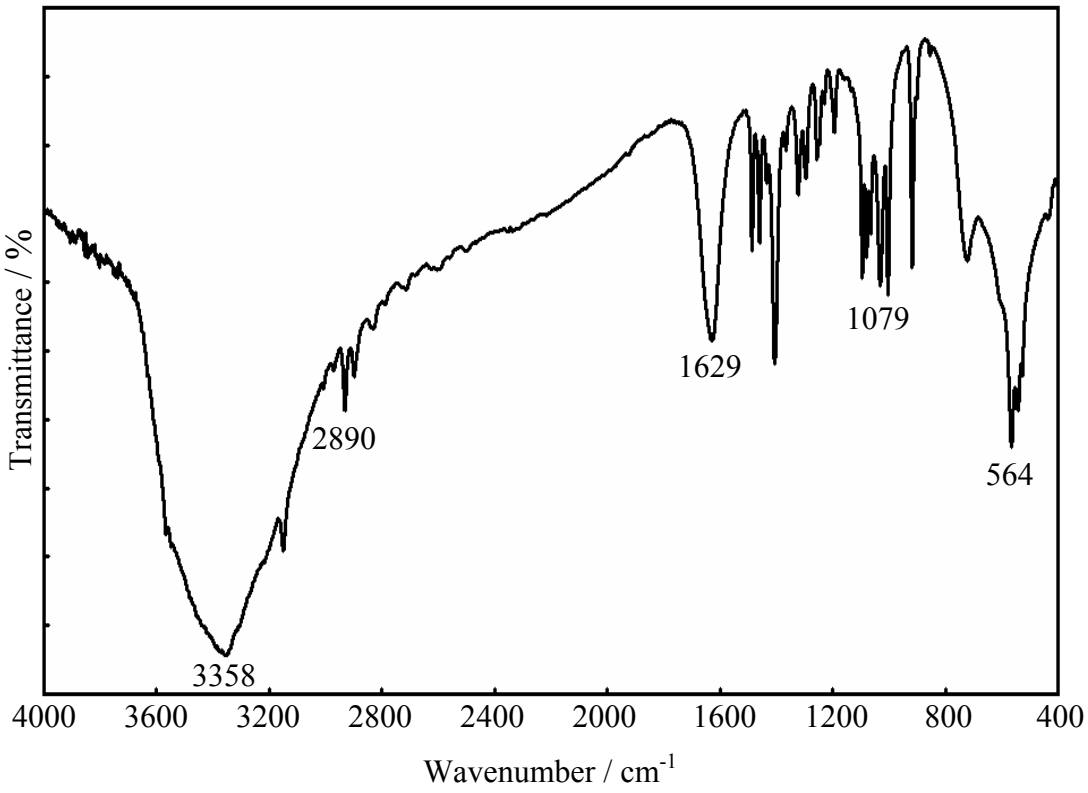


Figure 6.1 FTIR spectrum of cerium complex prepared from chlorides.

The structure of the cerium complexes was characterized by FTIR and the spectrum of the undoped cerium complex is shown in Figure 1. The broad peak located at 3358 $cm^{-1}$ was assigned to the O-H stretching due to the moisture absorption and/or the triethanolamine-residue from the reaction. The C-H stretching bands at 2928 and 2890 $cm^{-1}$ were assigned to -$CH_2$- group. The C-H bending bands were shown in the region of 1450-1200 $cm^{-1}$. The band at 1629 $cm^{-1}$ was attributed to O-H overtone. Moreover, the resonance at 1079 $cm^{-1}$ was ascribed to the Ce-O-C stretching vibration, while the band at 564 $cm^{-1}$ was assigned to the Ce-O stretching. The FTIR spectra of the doped cerium complexes were the same as for the undoped cerium complex.

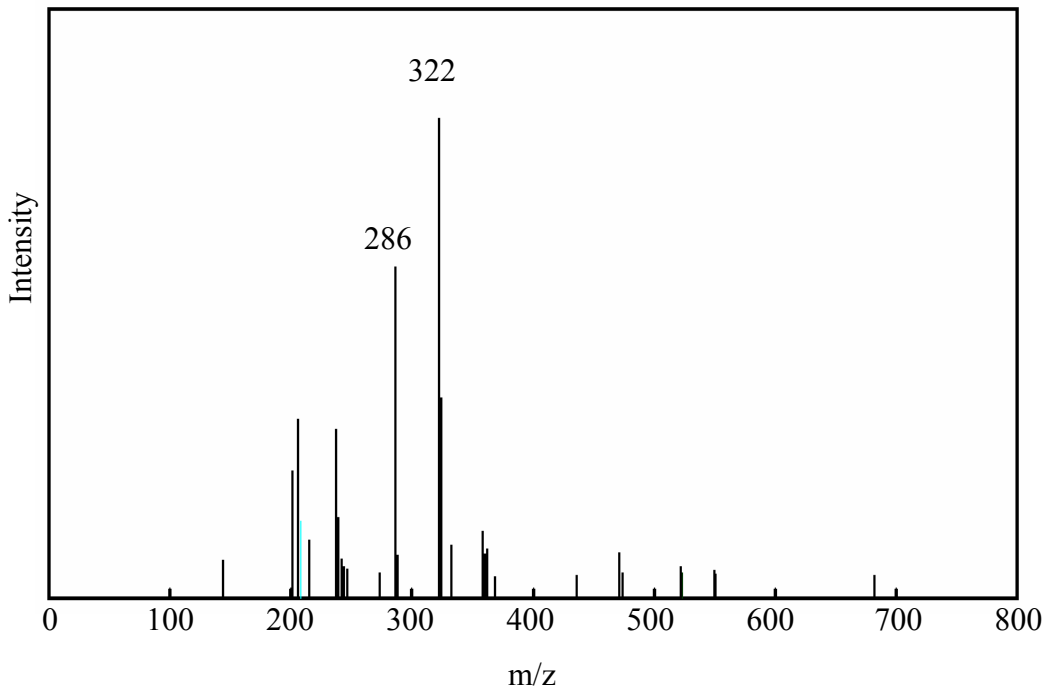


Figure 6.2 Mass spectrum of cerium complex prepared from chlorides.

The product structures were then identified by electrospray ionization mass spectroscopy (ESI-MS). The MS spectrum (Figure 6.2) shows that there are two intense peaks at m/z = 286 and 322 corresponding to [Ce(TEA)] and [Ce(TEA)Cl] complexes, respectively. Based on the results from FTIR and ESI-MS, two possible structures of cerium complexes (Figure 6.3) can be proposed as four coordinated cerium ion binding to one TEA molecule (Structure I) and five coordinated cerium ion with TEA and $Cl^-$ ligands (Structure II).


Figure 6.3 The two possible structures of cerium complexes.

The mass spectra of doped complexes cannot be shown due to the complicated peaks generated from the various types of complexes.

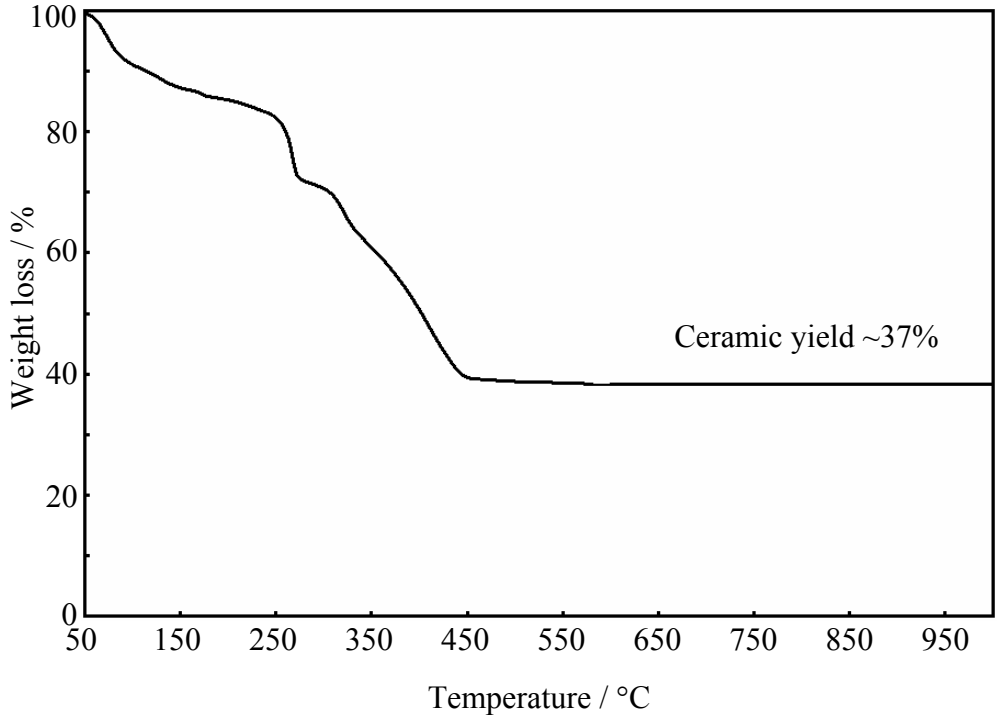


Figure 6.4 TGA curve of cerium complex prepared from chlorides.

All the complexes were converted into ceramic powders by calcination process. The appropriate temperature for calcination was investigated by TGA. The thermogram (Figure 6.4) revealed that the weight loss of pure cerium complex was very close to the weight loss observed for the doped cerium complexes. Three regions of weight loss were observed. The first weight loss occurring between 80-120°C resulted from the removal of organic solvent and physisorbed moisture. The second weight loss observed at temperatures between 250-450°C involved the

decomposition of the organic ligand and generated a char as by-product. The last weight loss occurred at 450-600°C due to the decomposition of carbon residues. The TGA curve of the cerium complex showed that no weight loss occurred above 600°C, demonstrating that the appropriate temperature for calcination was 600°C.

6.2.2 Powder preparation and characterization

All the complexes were calcined at 600, 800 and 1000°C for 2 h in air to obtain light-yellowish colored powders.

Figure 6.5 shows the X-ray diffraction patterns of pure and gadolinia doped ceria powders obtained by calcining the complexes at different temperatures for 2 h in air. It was found that all the compositions used are single phase with a cubic fluorite structure. This may suggest that gadolinium dissolves into ceria lattice with no other secondary phases present. In agreement with the TGA results, the calcined powders of each complex at 600°C for 2 h in air exhibited single phases. Since the calcination temperatures influenced the crystallinity, all the peaks became stronger and sharper with increasing the calcination temperature.

The crystallite size (D), specific surface area ($S_{BET}$), and average particle size ($D_{BET}$) of the calcined powders are presented in Table 6.1. It was found that the crystallite size of all the powders, calculated from the Scherrer equation, increased with increasing the calcination temperature due to the growth of the crystals at high temperature. The specific surface area ($S_{BET}$) trends to increase and average particle sizes are decreased with the increasing of calcination temperatures.

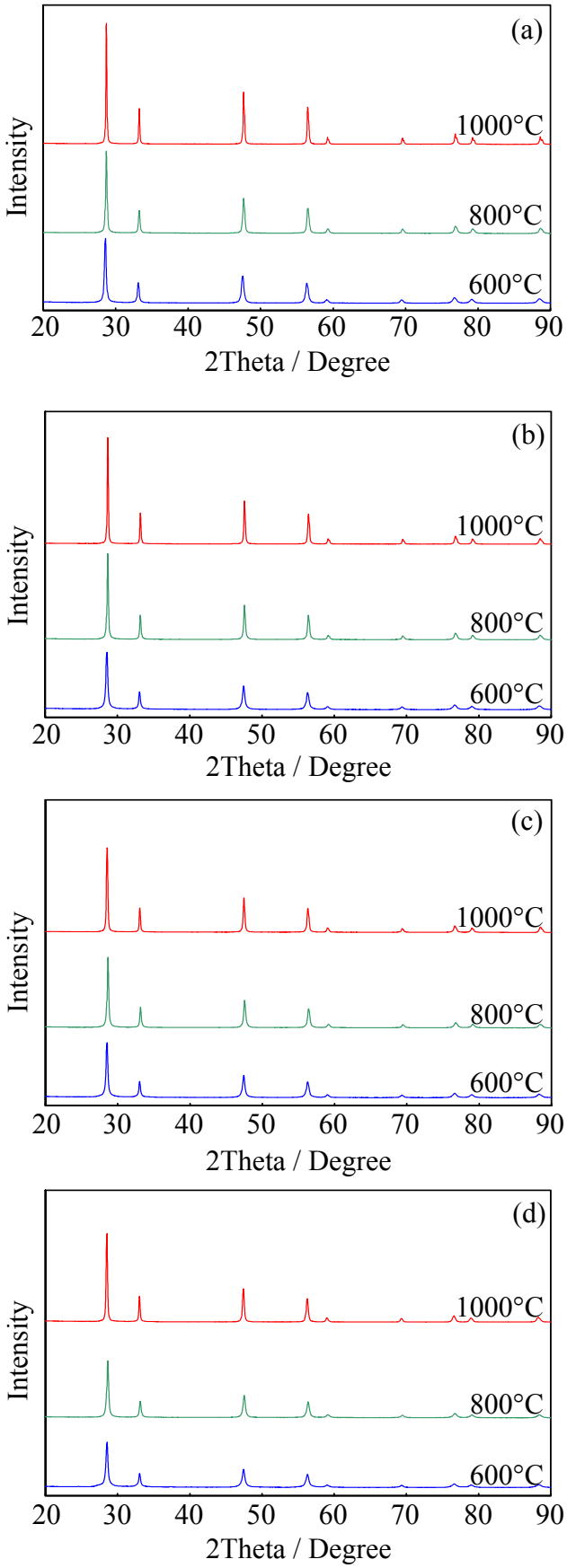


Figure 6.5 XRD patterns of (a) 0, (b) 10, (c) 15, and (d) 20 mole % doped gadolinium $CeO_2$ complexes calcined at various temperatures.

Table 6.1 Crystallite size (D), specific surface area ($S_{BET}$) and average particle size ($D_{BET}$) of ceria powders doped with 0, 10, 15 and 20 mole % Gd calcined at various temperatures

| Gd Substitution (mole %) | Calcination Temperature (°C) | Crystallite Size, D (nm) | Specific Surface Area, $S_{BET}$ ($m^2/g$) | Average Particle Size, $D_{BET}$ (nm) |
|---|---|---|---|---|
| 0 | 600 | 32.4 | 31.3 | 26.1 |
| | 800 | 36.7 | 21.0 | 39.7 |
| | 1000 | 63.2 | 8.3 | 100.3 |
| 10 | 600 | 34.3 | 44.6 | 18.7 |
| | 800 | 47.7 | 22.8 | 36.6 |
| | 1000 | 59.5 | 7.9 | 106.0 |
| 15 | 600 | 35.4 | 46.6 | 17.9 |
| | 800 | 41.3 | 28.3 | 29.4 |
| | 1000 | 47.1 | 12.7 | 65.4 |
| 20 | 600 | 29.1 | 45.3 | 18.4 |
| | 800 | 30.1 | 30.9 | 26.9 |
| | 1000 | 45.5 | 12.00 | 69.3 |

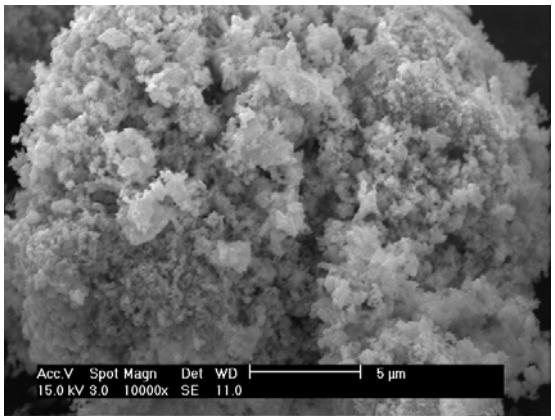


(a)

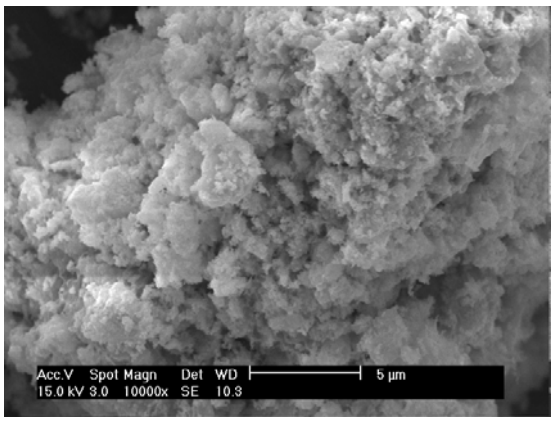


(b)

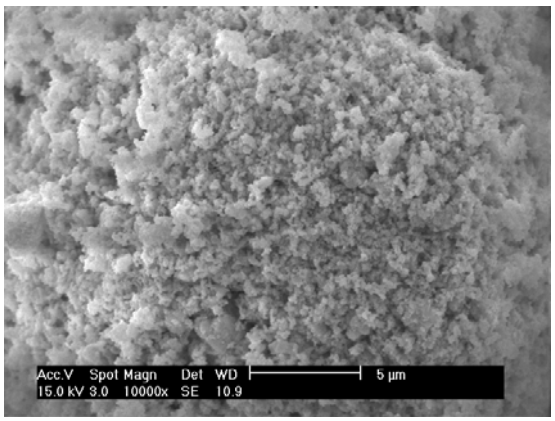


(c)

Figure 6.6 SEM micrographs of 0GDCCL powder calcined at (a) 600, (b) 800, and (c) 1000°C.

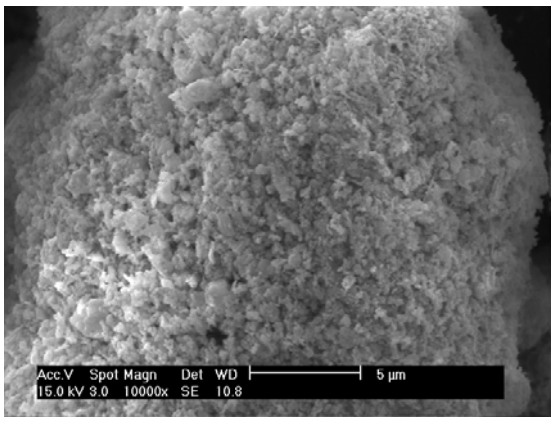


(a)

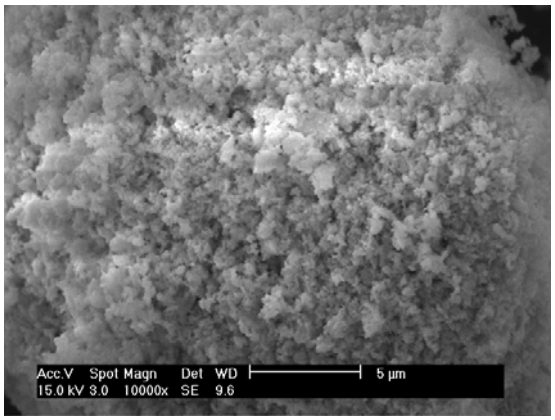


(b)

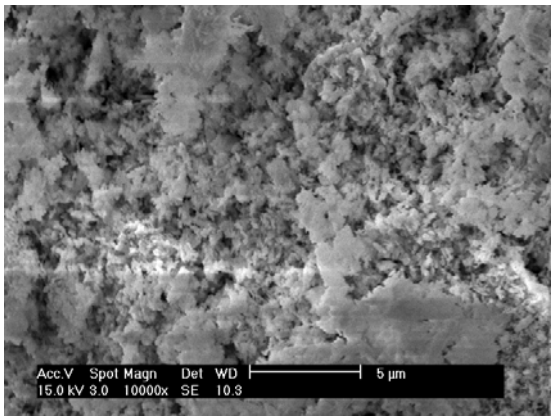


(c)

Figure 6.7 SEM micrographs of 10GDCCL powder calcined at (a) 600, (b) 800, and (c) 1000°C.

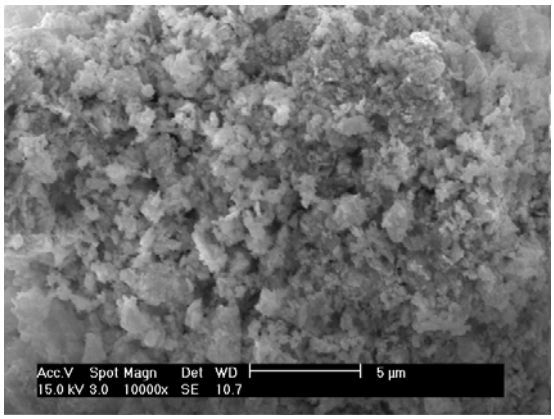


(a)

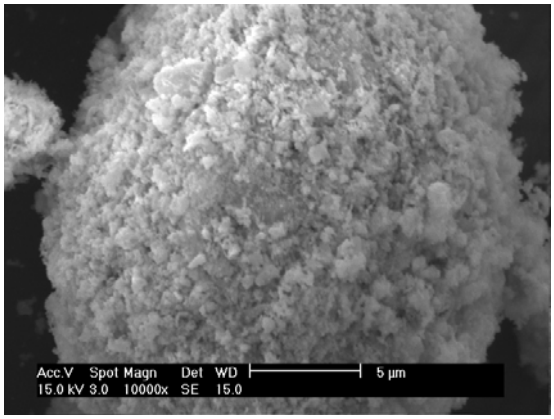


(b)

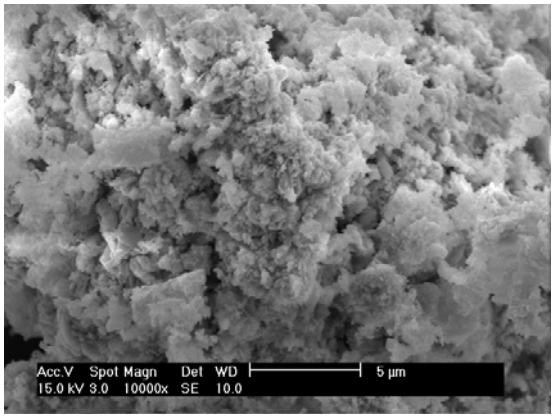


(c)

Figure 6.8 SEM micrographs of 15GDCCL powder calcined at (a) 600, (b) 800, and (c) 1000°C.

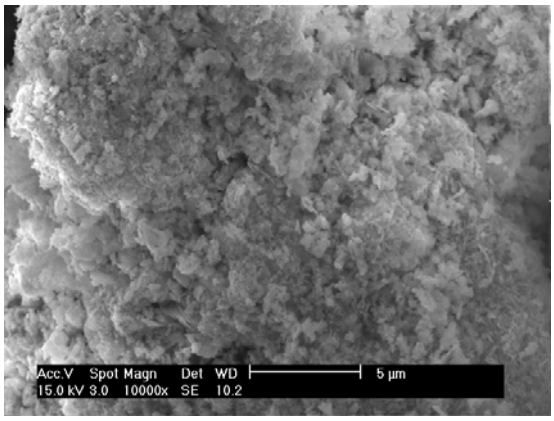


(a)

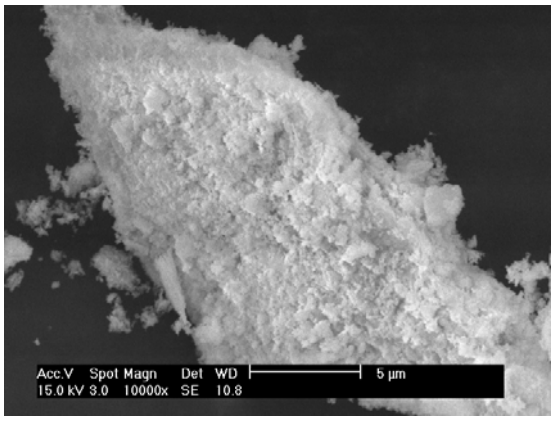


(b)

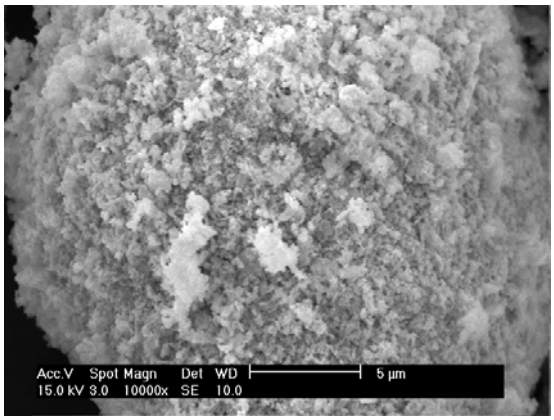


(c)

Figure 6.9 SEM micrographs of 20GDCCL powder calcined at (a) 600, (b) 800, and (c) 1000°C.

The SEM micrographs of the calcined powders are shown in Figures 6.6-6.9. It was found that the calcination temperature affected the microstructure of the powders. The higher the temperature, the denser the powder.

6.2.3 Electrochemical characterization

The obtained powders were prepared as pellets for measuring the ionic conductivity. Figure 6.10 shows the temperature dependence of the total conductivity ($\sigma_t$) for gadolinia doped ceria samples with various amounts of the Gd substitution.

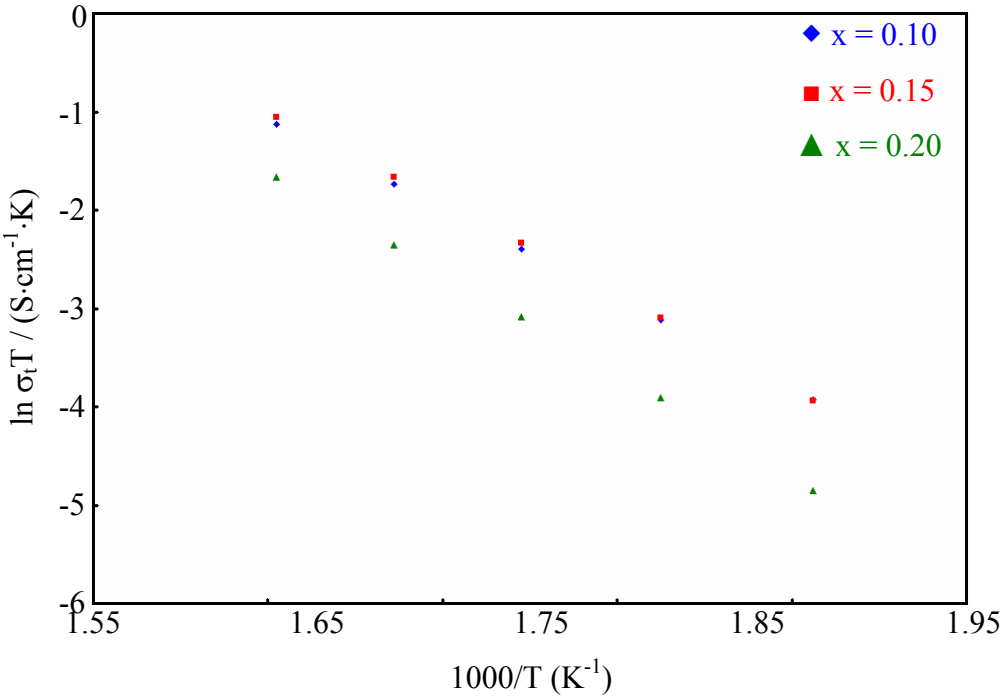


Figure 6.10 Arrhenius plots of the total conductivities as a function of temperature of 10GDCCL, 15GDCCL, and 20GDCCL pellets.

From the data presented in Figure 6.10, ceria doped with 15% Gd showed the largest ionic conductivity. The conductivities at 600°C and the activation energy of the specimens are listed in Table 6.2.

Table 6.2 The ionic conductivities at 600°C and activation energies of $Ce_xGd_{1-x}O_{2-\delta}$

| Substitution (mole%) | Ionic conductivity (S/cm) | Activation energy (eV) |
|---|---|---|
| x = 0.10 | 0.025 | 0.79 |
| x = 0.15 | 0.030 | 0.81 |
| x = 0.20 | 0.026 | 0.90 |

### 6.3 Conclusions

The easy and inexpensive method of metal complex can be used for preparing $Ce_{1-x}Gd_xO_{2-\delta}$ (x = 0, 0.10, 0.15 and 0.20) starting from chlorides. The appropriate temperature for calcination was 600°C. The XRD patterns showed that the obtained powders possessed the expected crystal structure, were single phase with good crystallinity. The effects of calcination temperature were clearly observed from SEM micrographs; the agglomeration and densification increased with increasing the calcination temperature. From the impedance measurements, the largest conductivity was found for the 0.15 mol% Gd substitution ($\sigma_{600°C}$ = 0.030 S/cm).

### References

[1] S.P.S. Badwal and K. Foger, Ceram. Int. 22 (1996) 257-265.

[2] A. Boudghene Stambouli and E. Traversa, Renewable & Sustainable Energy Rev. 6 (2002) 433-455.

[3] G. Bryan Balazs and Robert S. Glass, Solid State Ionics 76 (1995) 155-162.

[4] S. Kuharuangrong, J. Power Sources 171 (2007) 506-510.

[5] R.S. Torrens, N.M. Sammes, and G.A. Tompsett, Solid State Ionics 111 (1998) 9-15.

[6] A.I.Y. Tok, L.H. Luo, and F.Y.C. Boey, Materials Science & Engineering A 383 (2004) 229-234.

[7] Y.P. Fu, S.B. Wen, and C.H. Lu, J. Am. Ceram. Soc. 91 (2008) 127-131.

[8] G. Ruifeng and M. Zongqiang, J. Rare Earths 25 (2007) 364-367.

[9] S. Dikmen, P. Shuk, M. Greenblatt, and H. Gocmez, Solid State Sciences 4 (2002) 585-590.

[10] R.O. Fuentes and R.T. Baker, Int. J. Hydrogen Energy 33 (2008) 3480-3484.

[11] A. Laobuthee, S. Wongkasemjit, E. Traversa, and R.M. Laine, J. Eur. Ceram. Soc. 20 (2000) 90-91.

[12] T. Mahata, G. Das, R.K. Mishra, and B.P. Sharma, J. Alloys and Compounds 391 (2005) 129-135.

[13] Ifan E.L. Stephens and John A. Kilner, Solid State Ionics 177 (2006) 669-676.

[14] N. Sakai, Y.P. Xiong, K. Yamajai, H. Yokokawa, Y. Terashi, and H. Seno, Solid State Ionics 177 (2006) 2503-2507.

[15] J. Hu, Y. Li, X. Zhou, and M. Cai, Mat. Lett. 61 (2007) 4989-4992.

[16] E.R. Trejo, J.S. Salazar, R.V. Morales, A.B. Rico, F.G. Garcia, C.F. Morales, J.C. Carvayar, and T. Gustavo, J. Solid State Chem. 180 (2007) 3093-3100.

[17] S.H. Jo, P. Muralidharan, and D.K. Kim, Solid State Ionics 178 (2008) 1990-1997.

# CHAPTER VII
# CONCLUSIONS

Metal organic complexes are simple and effective precursors for the synthesis of metal oxide compounds. This method offers many advantages, such as easy, straightforward, and low temperature reaction. Ceria and doped ceria were successfully prepared via cerium organic complex by using triethanolamine as the ligand.

Firstly, the Ce-TEA complexes can be synthesized. The effect of anions, $NO_3^-$ and $Cl^-$, on the physical properties of ceria products was studied by using cerium nitrate, and cerium chloride as starting materials for synthesizing cerium-TEA complexes. Based on FTIR and MS identification, the possible structures of synthesized cerium–TEA complexes were proposed as a monometallic species consisting of one TEA ligand binding to the cerium ion with an addition of one nitrate group (from cerium nitrate), or one chloride group (from cerium chloride). Calcination process was carried out to convert the Ce-TEA complexes to oxide powders. The suitable calcination temperature for all the complexes determined by thermal analysis was 600°C. After the calcination process, the obtained products were characterized by XRD, SEM, and BET. Based on the XRD analysis, the obtained powders exhibited the cubic fluorite structure of cerium oxide ($CeO_2$). Moreover, with increasing the calcination temperature, the crystallite size based on the XRD pattern and $D_{BET}$ calculated from BET results of ceria became larger. On the other hand, the specific surface area decreased. However, the calcined powders from cerium nitrate had lower specific surface areas than the powders from cerium chlorides. In addition, the morphology of the calcined powders at 600°C for 2 h exhibited a foam-like structure as shown in SEM micrographs. The AC impedance measurement of pure ceria is difficult to perform due to its low ionic conductivity.

In order to improve the ionic conductivity, doped ceria such as $Ce_{1-x}Gd_xO_{2-\delta}$ (x = 0.10, 0.15 and 0.20) and $Ce_{1-x}Sm_xO_{2-\delta}$ (x = 0.10, 0.15 and 0.20) were synthesized by metal organic complex method. The mixed oxide ceramic powders were prepared by calcining the complexes at 600°C for 2 h, based on TG/DTA analysis. The phase identification of all calcined powders was not significantly changed or distorted from cubic fluorite structure of pure ceria. Similar to the pure ceria, as increasing

calcination temperature, the crystallite size and $D_{BET}$ increased. On the other hand, the specific surface area decreased. The AC impedance measurement of dense doped ceria pellets was investigated. $Ce_{0.85}Gd_{0.15}O_{2-\delta}$ and $Ce_{0.85}Sm_{0.15}O_{2-\delta}$ exhibited the largest ionic conductivity compared to each corresponding dopant. The largest ionic conductivity was observed for doped samples prepared from the thermal decomposition of the complexes prepared using the chlorides. This can be ascribed to the better morphology of the calcined powders that will lead to a better sintered ability of the ceramic pellet.

## REFERENCES

Balazs, G.B.; and Glass R.S. Solid State Ionics, 1995, 76, 155-162.

Bošković, S. B.; Matovic, B. Z.; Vlajić, M.D.; and Kristić, V.D. Ceram. Int., 2007, 33, 89-93.

Cai, W.; Zhang, B.; Li, Y.; Xu, Y.; and Shen, W. Catal. Commun., 2007, 8, 1588-1594.

Chen, W.; Li, F.; and Yu, J. Mat. Lett., 2006, 60, 57-62.

Cheng, J.G.; Zha, S.W.; Huang, J.; Liu, X.Q.; and Meng, G.Y. Materials Chemistry and Physics, 2003, 78, 791-795.

Chinarro, E.; Jurado, J.R.; and Colomer, M.T. J. Eur. Ceram. Soc., 2007, 27, 3619-3623.

Chourashiya, M.G.; Patil, J.Y.; Pawar, S.H.; and Jadhav, L.D. Materials Chemistry and Physics, 2008, 109, 39-44.

Dikmen, S.; Shuk, P.;Greenblatt, M.; and Gocmez, H. Solid State Sciences, 2002, 4, 585-590.

Ding, D.; Liu, B.; Zhu, Z.; Zhou, S.; and Xia, C. Solid State Ionics, 2008, 179, 896-899.

Dudek, M. J. Eur. Ceram. Society., 2008, 28, 965-971.

Dudek, M.; Bogusz, W.; Zych, L.; and Trybalska, B. Solid State Ionics, 2008, 179, 164-167.

Fu, Y.P.; Wen, S.B.; and Lu, C.H. J. Am. Ceram. Soc. 2008, 91, 127-131.

Fuentes, R.O.; and Baker, R.T. Int. J. Hydrogen Energy, 2008, 33, 3480-3484.

Gandhi, H.S.; Graham, G.W.; and McCabe, R.W. J. Catal., 2003, 216, 433-442.

Godinho, M.J.; Goncalves, R.F.; Santos, L.P.S.; Varela, J.A.; Longo, E.; and Leite, E.R. Mat. Lett., 2007, 61, 1904-1907.

Grover, V.; and Tyagi, A.K. Material Research Bulletin, 2004, 39, 859-866.

Guan, X.; Zhou, H.; Liu, Z.; Wang, Y.; and Zhang, J. Materials Research Bulletin, 2008, 43, 1046-1054.

Hayre, R.O.; Cha, S.K.; Colella, W.; and Prinz, F.B., Fuel Cell Fundamentals, John Wiley & Sons, Inc., 2006.

Hennings, U.; and Reimert, R. Appl. Catal. A, 2007, 325, 41-49.

Hu, J.D.; Li, Y.X.,; Zhou, X.Z.; and Cai, M.X. Mat. Lett., 2007, 61, 4989-4992.

Im, J.M.; You, H.J.; Yoon, Y.S.; and Shin, D.W. Ceram. Int., 2008, 34, 877-881.

Im, J.M.; You, H.J.; Yoon, Y.S.; and Shin, D.W. J. Eur. Ceram. Society., 2007, 27, 3671-3675.

Jasper, A.; Kilner, J.A.; and Mccomb, D.W. Solid State Ionics, 2008, 179, 904-908.

Ji, Y.; Liu, J.; He, T.; Cong, L.; Wang, J.; Su, W. J. Alloys and Compounds, 2003, 353, 257-262.

Jo, S.H.; Muralidharan, P.; and Kim, D.K. Solid State Ionics, 2008, 178, 1990-1997.

Kim, N.; Kim, B.H.; and Lee, D. J. Power Sources, 2000, 90, 139-143.

Kuharuangrong, S. J. Power Sources, 2007, 171, 506-510.

Kumar, V.P.; Reddy, Y.S.; Kistaiah, P.; Prasad, G.; and Reddy, C.V. Materials Chemistry and Physics, 2008, 112, 711-718.

Laobuthee, A.; Wongkasemjit, S.; Traversa, E.; and Laine, R.M. J. Eur. Ceram. Soc., 2000, 20, 91-97.

Laobuthee, A. Synthesis of $MgAl_2O_4$ Spinel and its Applications as a Humidity Sensing Element; Master's Thesis in Polymer Science, The Petroleum and Petrochemical College, Chulalongkorn University, 1997.

Lee, J.S.; and Choi, S.C. Mat. Lett., 2004, 58, 390-393.

Lee, J.S.; Lee, J.S.; and Choi, S.C. Mat. Lett., 2005, 59, 395-398.

Lenka, R.K.; Mahata, T.; Sinha, P.K.; and Tyagi, A.K. J. Alloys and Compounds, 2008, 466, 326-329.

Lenka, R.K.; Mahata, T.; Sinha, P.K.; and Sharma, B.P. J. Am. Ceram. Soc., 2006, 89, 3871-3873.

Li, J.G.; Ikegami, T.; and Mori, T. Acta Materialia, 2004, 52, 2221-2228.

Macdonald, J.R., Impedance spectroscopy: Emphasizing solid materials and systems, John Wiley & Sons, Inc., 1987.

Mahata, T.; Das, G.; Mishra, R.K.; and Sharma, B.P., J. Alloys and Compounds, 2005, 391, 129-135.

Ma, J.; Zhang, T.S.; Kong, L.B.; Hing, P.; and Chan, S.H. J. Power Sources, 2004, 132, 71-76.

Minh, N.Q. J. Am. Ceram. Soc., 1993, 76, 563-588.

Omar, S.; Wachsman, E.D.; and Nino, J.C. Solid State Ionics, 2008, 178, 1890-1897.

Peng, C.;and Zhang, Z. Ceram. Int., 2007, 33, 1133-1136.

Peng, R.; Xia, C.; Fu, Q.; Meng, G.; and Peng, D. Mat. Lett., 2002, 56, 1043-1047.

Perez-Coll, D.; Nunez, P.; Frade, J.R.; and Abrantes, J.C.C. Electrochimica Acta, 2003, 48, 1551-1557.

Purohit, R.D.; Sharma, B.P.; Pillai, K.T.; and Tyagi, A.K. Materials Research Bulletin, 2001, 36, 2711-2721.

Ragsapram, S. Characteristics of Lanthanum Aluminate as an Electrolyte in Solid Oxide Fuel Cell; Master's Thesis in Ceramic Technology, Chulalongkorn University, 2000.

Riess, I.; Godickemeier M.; and Gauckler L.J. Solid State Ionics, 1996, 90, 91-104.

Ramirez-Cabrera, E.; Atkinson, A.; and Chadwick, D. Appl. Catal. B, 2004, 47, 127-131.

Ruifeng, G.; and Zongqiang, M. Journal of rare earths, 2007, 25, 364-367.

Ruiz-Trejo, E. ; Santoyo-Salazar, J. ; Vilchis-Morales, R.; Benítez-Rico, A.; Gómez-García, F.; Flores-Morales, C.; Chávez-Carvayar, J.; and Tavizón, G. J. Solid State. Chem., 2007,180, 3093-3100.

Santos, M.L.D.; Lima, R.C.; Riccardi, C.S.; Tranquilin, R.L.; Bueno, P.R.; Varela, J.A.; and Longo, E. Mat. Lett., 2008, 62, 4509-4511.

Sakai, N.; Xiong, Y.P.; Yamajai, K.; Yokokawa, H.; Terashi, Y.; and Seno, H. Solid State Ionics, 2006, 177, 2503-2507.

Sha, X.; Lu, Z.; Huang, X.; Miao, J.; Liu, Z.;Xin, X.; Zhang, Y.; and Su, W. J. Alloys and Compounds, 2007, 433, 274-278.

Steele, B.C.H. and Heinzel A. Nature, 2001, 44, 345-352.

Stephens, I.E.L.; and Kilner, J.A. Solid State Ionics, 2006, 177, 669-676.

Trejo, E.R.; Salazar, J.S.; Morales, R.V.; Rico, A.B.; Garcia, F.G.; Morales, C.F.; Carvayar, J.C.; and Gustavo, T. J. Solid State Chem., 2007, 180, 3093-3100.

Thangadurai, V.; and Kopp, P. J. Power Sources, 2007, 168, 178-183.

Tok, A.I.Y.; Luo, L.H.; and Boey, F.Y.C. Materials Science and Engineering A, 2004, 383, 229-234.

Torrens, R.S.; Sammes, N.M.; and Tompsett, G.A. Solid State Ionics, 1998, 111, 9-15.

Trovarelli, A., Catalysis by ceria and related materials, Imperial College Press, 2001.

Wang, F.Y.; Chen, S.; and Cheng, S. Electrochemistry Communications, 2004, 6, 743-746.

Wang, F.Y.; Cheng, S.; Wan, B.Z.; Chung, C.H.; and Chen, M.J. Ceram. Int., 2008, 34, 1989-1992.

Wang, L.; Zhang, K.; Song, Z.; and Feng, S. Appl. Surf. Sci., 2007, 253, 4951-4954.

Wang, Y.; Mori, T.; Li, J.G.; and Ikegami, T. J. Am. Ceram. Soc., 2002, 85, 3105-3107.

Zha, S.; Xia, C.; and Meng, G. J. Power Sources, 2003, 115, 44-48.

Zhan, Z.; Wen, T.L.; Tu, H.; and Lu Z.Y. J. Electrochem. Soc., 2001, 148, A427-A432.

Zhang, D.; Liu, Z.; Yue, H.; and Yao, K. Physica B, 2004, 344, 265-270.

Zhang, T.S.; Ma, J.; Cheng, H.; and Chan, S.H. Materials Research Bulletin, 2006, 41, 563-568.

Zhang, T.; Peter, H.; Huang, H.; and Kilner, J. Solid State Ionics, 2002, 148, 567-573.

Zhen, Y.D.; Tok, A.I.Y.; Jiang, S.P.; and Boey, F.Y.C. J. Power Sources, 2008, 178, 69-74.

Zheng, X.; Wang, S.; Wang, X.; Wang, S.; Wang, X.; and Wu, S. Mat. Lett., 2005, 59, 2769-2773.

# CURRICULUM VITAE

Name: Chatchai Veranitisagul

Date of Birth: March 13, 1979

Nationality: Thai

University Education:

| | |
|---|---|
| 1996-2000 | Master Degree of Science in Polymer Science, The Petroleum and Petrochemical College, Chulalongkorn University, Bangkok, Thailand. |
| 2000-2002 | Bachelor Degree of Science in Materials Science (Polymer and Textile), Chulalongkorn University, Bangkok, Thailand. |

Working Experience:

| | | |
|---|---|---|
| 2003 | Position: | Lecturer |
| | University: | Phranakorn Rajabhat University |

## List of Publications

### Articles published on Conference Proceedings with refereeing

1. C. Veranitisagul, N. Koonsaeng, B. Ksapabutr, E. Traversa, and A. Laobuthee
Synthesis of Ceria Powder from Organometallic Complex via One Pot Process for an Application as an Electrolyte Membrane in Solid Oxide Fuel Cell
Accepted for publications on 32nd Congress on Science and Technology of Thailand, Bangkok, Thailand, October 10-12, 2006.

2. C. Veranitisagul, A. Laobuthee, E. Traversa, and N. Koonsaeng
Preparation of Gadolinia Doped Ceria (GDC) Powder from Metal-Organic Complex Method for Electrolyte Membrane in Solid Oxide Fuel Cell
Accepted for publications on PACCON Proceedings Pure and Applied Chemistry International Conference 2008, Bangkok, Thailand, January 30-February 1, 2008.

3. T. Rakthin, C. Veranitisagul, N. Koonsaeng, E. Traversa, and A. Laobuthee
Preparation of Ceria Powder via Metal-Organic Complex Method
Accepted for publications on PACCON Proceedings Pure and Applied Chemistry International Conference 2008, Bangkok, Thailand, January 30-February 1, 2008.

4. 1. T. Rakthin, C. Veranitisagul, N. Koonsaeng, E. Traversa, and A. Laobuthee
A Cerium Complex for Ceria Powder Preparation

Accepted for publications on 34th Congress on Science and Technology of Thailand, Bangkok, Thailand, October 31-November 2, 2008.